UNIVERSITY OF COPENHAGEN

Master's Thesis

Fidelity characterization of spin-photon entangled states

Pol Llopart Mirambell

Supervisor: Anders Søndberg Sørensen

July 2019

Abstract

In this thesis a study on the characterization of the fidelity of spin-photon entangled GHZ states is presented. The presence of an extra, far-detuned energy level is explained and a time optimization for two shapes (square and Gaussian) of the input laser field is presented. Analytical and numerical results of the conditional fidelity of the system with the far-detuned transition and the addition of inhomogeneous broadening are computed. Finally, a formalism for second-order emissions of photons is used to derive analytical expressions for both, the square-shaped and the Gaussian-shaped pulses. A final derivation of the conditional fidelity taking into account all the described inconsistencies is presented and the numerical and analytical results with realistic experimental parameters are presented.

To my grandparents

Acknowledgements

First of all, I want to thank my supervisor, Anders Søndberg Sørensen for teaching me the fundamental concepts of Quantum Information, and his help by introducing and explaining to me many concepts of quantum optics. I would like to thank Martin Appel for his feedback with realistic experimental parameters and explaining to me the experimental techniques implemented in the laboratory.

I would also like to thank everyone in the Theoretical Quantum Optics group, for the interesting and fruitful conversations in the literature club and the group meetings.

Last but not least, I want to thank my family and friends for their emotional support through the thesis.

Contents

1. Introduction **1**

2. Preliminaries **3**
2.1. Basic Quantum mechanics . . . 3
2.2. Statistical ensembles . . . 5
2.3. Entanglement and bipartite systems . . . 6
2.4. Basic Quantum Optics . . . 7
2.4.1. Semiclassical approach . . . 7
2.4.2. Full quantum approach . . . 9

3. Far-detuned transition **12**
3.1. Protocol description . . . 12
3.2. Stric definition of Fidelity . . . 14
3.3. Time optimization of the Square pulse . . . 14
3.3.1. Strict fidelity and numerical comparison . . . 16
3.4. Time optimization of the Gaussian pulse . . . 18
3.4.1. Strict fidelity and numerical comparison . . . 24

4. Inhomogeneous broadening and relaxation of the far-detuned transition **27**
4.1. Description of the inconsistencies . . . 27
4.2. System wave-function . . . 28
4.3. Conditional Fidelity . . . 29
4.3.1. Conditional fidelity without filter . . . 29
4.3.2. Conditional fidelity with filter and experimental efficiency . . . 32
4.4. Square-shaped pulse coefficients . . . 35
4.5. Gaussian-shaped pulse coefficients . . . 40
4.6. Analytical expansion of the fidelity . . . 42
4.7. Numerical and Analytical results . . . 44

5. Second-order emissions **46**
5.1. Formalism description . . . 46
5.2. System wave-function . . . 50
5.3. Conditional fidelity with second-order emissions . . . 53
5.4. Second-order coefficients of the square pulse . . . 57
5.5. Second-order coefficients of the Gaussian pulse . . . 59
5.6. Analytical expansion of the conditional Fidelity . . . 63
5.7. Numerical and Analytical results . . . 65

6. Conclusions and Outlook **70**
6.1. Conclusions . . . 70
6.2. Outlook . . . 70

A. Analytical computations **72**
A.1. Solution of the 1-2 transition . . . 72
A.2. Interaction picture transformation . . . 72

B. Comparison between Numerical and Analytical results **74**
B.1. Stric fidelity 74
B.2. Conditional fidelity with broadening 75
B.3. Conditional fidelity with second-order emissions 75

1. Introduction

The first quantum revolution occurred at the turn of the last century, motivated by the theoretical attempts to explain blackbody radiation. Quantum mechanics questioned big part of the fundamental knowledge we had on the world and challenged the scientific community with its counterintuitive description of the reality. By the end of the 20th century, all the novel concepts that arose from this first revolution allowed the creation of many core technologies present in the modern society.

At the present moment, we are at the beginning of the second quantum revolution [1]. We are trying to actively control quantum states to our liking, in order to exploit their properties and overcome the limitations of classical systems. This new revolution is expected to permanently change many fields of society. Some examples are the secure key distribution [2], the promising quantum algorithms for database search [3] or integer factorization [4].

For this second revolution to be completely exploited, the improvement and research on quantum communications and quantum networks will be crucial [5]. One of the most important resources for quantum communication is entanglement. For the creation of fault-tolerant communication protocols, it will be necessary to be able to master the generation of entangled photons.

In this thesis we will characterize the fidelity of the generation of spin-photon entangled GHZ states. The protocol that will be used [6], generates a state of entangled photons in the time-bin encoding [7, 8].

We will take into account the presence of a far-detuned transition and consider square and Gaussian shapes of the input field. We will use experimental parameters for quantum-dots embedded in waveguides [9, 10]. We will also take into consideration inhomogeneous broadening, produced by fluctuations on the laser frequency or fluctuations of the excited states [11, 12].

The outline of this thesis is as follows:

- **Chapter 02:** The main concepts of quantum mechanics, statistical ensembles and entanglement are introduced. Also, fundamental concepts of quantum optics are introduced, putting emphasis on the semi-classical solution of a two-level system with a classical monochromatic field. Finally, the quantization of the electromagnetic field and the full-quantum Hamiltonian is explained.

- **Chapter 03:** The protocol used to create multi-photon GHZ states is presented. The presence of a far-detuned energy level is introduced and an optimization of the length of the pulse is performed for the square-shaped and Gaussian-shaped pulses.

- **Chapter 04:** Inhomogeneous broadening and spontaneous emission from the far-detuned transition are introduced. The system wave-function and the conditional fidelity, taking these inconsistencies into account, are derived. The analytical and numerical results are presented and discussed.

- **Chapter 05:** Second-order photon emissions are introduced and the formalism is explained. The computation of the wave-function and the conditional fidelity with these new phenomenon is performed. The two-photon analytical coefficients for the square and Gaussian pulses are derived. The analytical and numerical results are presented and discussed.
- **Chapter 06:** The conclusions and outlook of this work are provided.

2. Preliminaries

In this chapter the basic theory necessary to follow the work of the thesis is presented. We start by reviewing the fundamental concepts of quantum mechanics, then we will talk about statistical ensembles, entanglement and we will end by explaining the basic concepts of quantum optics.

2.1. Basic Quantum mechanics

State vectors

Quantum mechanics is a mathematical model of the physical world. According to quantum mechanics, every isolated system is corresponded by a Hilbert space $\mathscr{H}$, also called state space [13]. The state of the physical system is completely described by a state vector, which corresponds to a "ray" in the Hilbert space [14].

A Hilbert space is a vector space spanned over the complex numbers $\mathbb{C}$. We will use the Dirac bra-ket $|\Psi\rangle$ ($\langle\Psi|$) notation to represent states of the Hilbert space. An inner product between states $\langle\Phi|\Psi\rangle$ is defined and maps any pair of vectors from $\mathscr{H}$ to the complex numbers $\mathbb{C}$. The inner product has the following properties:

- Positivity: $\forall\, |\Psi\rangle \in \mathscr{H}$, $\langle\Phi|\Psi\rangle \geq 1$
- Linearity: $\langle\Phi| (a\,|\Psi_1\rangle + b\,|\Psi_2\rangle) = a\,\langle\Phi|\Psi_1\rangle + b\,\langle\Phi|\Psi_2\rangle$
- Skew symmetry: $\langle\Phi|\Psi\rangle = \langle\Psi|\Phi\rangle^*$
- Completeness: $||\Psi||^2 = \langle\Psi|\Psi\rangle$

Notice that we can span the state vector $|\Psi\rangle$ into any orthonormal basis of the Hilbert space [15]:

$$|\Psi\rangle = \sum_n |n\rangle\,\langle n|\Psi\rangle \tag{2.1}$$

By the definition of orthonormality, $\langle n|n\rangle = 1$ and $\langle n|n'\rangle = 0$. And since the set of $|n\rangle$ form a complete basis, $\sum_n |n\rangle\,\langle n| = \mathbb{1}$

Observables

In quantum mechanics observables are represented by Hermitian operators acting on Hilbert spaces. An observable is a property of a physical system that can be measured. Hermitian operators fulfill $\langle\Psi|\,\hat{O}\,|\Phi\rangle = (\langle\Phi|\,\hat{O}\,|\Psi\rangle)^\dagger$.

According to the spectral theorem [13] an Hermitian operator can be spectrally decomposed:

$$\hat{O} = \sum_i O_i\,|i\rangle\,\langle i| = \sum_i O_i P_i \tag{2.2}$$

Where $O_i \in R$ (eigenvalues), P_i is the orthogonal projector operator onto the subspace spanned by the eigenvector $|i\rangle$ with eigenvalue i.

The expected value of the Hermitian operator $\hat{O}$ with respect to the state of the system $|\Psi\rangle$ is:

$$\langle \hat{O} \rangle = \langle \Psi | \hat{O} | \Psi \rangle = \sum_i O_i |\langle \Psi | i \rangle|^2 \tag{2.3}$$

Measurement

When measuring an observable $\hat{O}$, one can only obtain as outcome one of the eigenvalues from $\hat{O}$. Since the eigenvectors of $\hat{O}$ form a complete basis in the Hilbert space $\mathscr{H}$, we can decompose the state of the system as $|\Psi\rangle = \sum_i \langle \Psi | i \rangle |i\rangle = \sum_i \psi_i |i\rangle$.

The probability of measuring the eigenvalue O_i corresponds to:

$$p(i|\Psi) = ||P_i |\Psi\rangle ||^2 = |\psi_i|^2 \tag{2.4}$$

Right after the measurement, If O_i has been the outcome of the system measurement, the post-measurement state becomes:

$$|\Psi\rangle \xrightarrow{measurement} \frac{P_i |\Psi\rangle}{||P_i |\Psi\rangle ||^2} = \frac{P_i |\Psi\rangle}{\sqrt{p(i|\Psi)}} = |i\rangle \tag{2.5}$$

Time evolution

Time evolution of an isolated quantum system is unitary $|\Psi(t)\rangle = U(t', t) |\Psi(t')\rangle$. The generator of the unitary transformation is a self-adjoint operator called the Hamiltonian of the system. In the Schrödinger picture the operators do not evolve in time and the state vectors evolve in time following the Schrödinger equation:

$$i\hbar \frac{d}{dt} |\Psi\rangle = \hat{H} |\Psi\rangle \tag{2.6}$$

In the case when the Hamiltonian $\hat{H}$ is time-independent, the unitary transformation that describes the dynamics of the system is $U(t', t) = e^{-i(t'-t)\hat{H}/\hbar}$.

Notice that the temporal evolution of the system is deterministic and reversible, since it is governed by an unitary operation. On the other hand, the measurement and collapse of the wave-function is not deterministic, since quantum mechanics only gives us the probabilities to obtain the possible outcomes of the measurement.

Interaction picture

Many quantum mechanical systems in nature have time-dependent Hamiltonians [16]. We will explain how to deal with this type of Hamiltonians. We consider a Hamiltonian that can be split into two parts $\hat{H} = \hat{H}_0 + \hat{V}(t)$.

Where $\hat{H}_0$ does not depend on time explicitly and we assume that we know the solution for the system when $\hat{V}(t) = 0$, with the eigenkets and eigenvalues of $\hat{H}_0$ being:

$$\hat{H}_0 |n\rangle = E_n |n\rangle \tag{2.7}$$

Assume that at time $t = 0$ the general state ket of the system in the Schrödinger picture $|\Psi\rangle_S$ can be represented as

$$|\Psi\rangle_S = \sum_n c_n(0) |n\rangle \tag{2.8}$$

For $t > 0$ the state ket in the Schrödinger picture will be

$$|\Psi(t)\rangle_S = \sum_n c_n(t) e^{-iE_n t/\hbar} |n\rangle \tag{2.9}$$

Where we have encoded the effect of the time-dependent part of the Hamiltonian $\hat{V}(t)$ in the time evolution of the coefficients $c_n(t)$. Now we are interested in the transformation:

$$\begin{aligned} |\Psi(t)\rangle_I &= e^{i\hat{H}_0 t/\hbar} |\Psi(t)\rangle_S \\ V_I &= e^{i\hat{H}_0 t/\hbar} \hat{V} e^{-i\hat{H}_0 t/\hbar} \end{aligned} \tag{2.10}$$

Where the subscript I corresponds to the interaction picture. Notice that by performing this transformation, we are going to a rotation frame where the time-evolution of the sate ket $|\Psi\rangle_I$ only depends on the time-dependent potential $\hat{V}(t)$. Also, the time evolution of the operators in the interaction picture, $\hat{A}_I$, is generated by $\hat{H}_0$. In the interaction picture the "interesting dynamics" of the system (coming from $\hat{V}(t)$) are encoded on the state kets and the already known dynamics (produced by $\hat{H}_0$) are encoded on the operators.

The fundamental equation that describes the time evolution of state kets in the interaction picture is:

$$i\hbar \frac{d}{dt} |\Psi(t)\rangle_I = V_I |\Psi(t)\rangle_I \tag{2.11}$$

Which corresponds to the Schrödinger equation in the interaction picture.

2.2. Statistical ensembles

Despite the fact that the state of a quantum mechanical system is fully described by $|\Psi\rangle$, in many practical situations it is not useful to work with it. In most of the situations, the knowledge that we have of the system preparation is partial. This can be due to the inherent imperfections of the measurement apparatus to the coupling of the system we want to study to the environment. In that case, we can only talk about the possible states in which our system may have been prepared $|\Psi_i\rangle$ and their probabilities p_i. In this case, we have to describe our system with the density matrix operator:

$$\hat{\rho} = \sum_i pi |\Psi_i\rangle \langle\Psi_i| \tag{2.12}$$

The density matrix contains all the information accessible for us of the system. Any positive (and hence Hermitian) operator fulfilling $tr(\hat{\rho}) = 1$ is a density operator. If there exists a basis where $\hat{\rho} = |\Phi\rangle \langle\Phi|$, the system is said to be in a pure state and we can access to all the information of the system (we can describe the system using the formalism explained in 2.1). If does not exist such basis, we say that the system is in a mixed state.

It is possible to reformulate the postulates of quantum mechanics in terms of the density matrix operator. When measuring an observable $\hat{O} = \sum_i O_i P_i$, the probability for the outcome of the measurement to be O_i is

$$p(i|\hat{\rho}) = tr\,(P_i \hat{\rho}) \tag{2.13}$$

And the outcome of the measurement

$$\hat{\rho} \xrightarrow{measurement} \frac{P_i \hat{\rho} P_i}{tr\left(P_i \hat{\rho}\right)} \tag{2.14}$$

For simplicity we have only considered orthogonal measurements. Expectation values of observables can also be calculated with the denisty matrix formalism

$$\langle \hat{O} \rangle = \sum_i p_i \langle \Psi_i | \hat{O} | \Psi_i \rangle = \sum_n \langle n | \left(\sum_i p_i | \Psi_i \rangle \langle \Psi_i | \right) \hat{O} | n \rangle = tr\left(\hat{\rho}\hat{O}\right) \tag{2.15}$$

Finally, If the temporal evolution of the system can be described with a unitary matrix $U(t',t)$, the density operator of the system at time t will be

$$\hat{\rho}(t) = \sum_i p_i U(t',t) |\Psi_i(t')\rangle \langle \Psi_i(t')| U(t',t)^\dagger = U(t',t)\hat{\rho}(t')U(t',t)^\dagger \tag{2.16}$$

2.3. Entanglement and bipartite systems

Assume that our system is composed by two parts, subsystem A and subsystem B. A bipartite pure state $|\Psi\rangle_{AB} \in \mathscr{H}_A \otimes \mathscr{H}_B$ can be expressed in the standard form (Schmidt decomposition)

$$|\Psi\rangle_{AB} = \sum_i \lambda_i |\alpha_i\rangle_A |\beta_i\rangle_B \tag{2.17}$$

Where $\{|\alpha_i\rangle_A\}$ and $\{|\beta_i\rangle_B\}$ are orthonormal basis for $\mathscr{H}_A$ and $\mathscr{H}_B$, respectively [13]. The coefficients λ_i are called Schmidt coefficients and fulfill $\lambda_i \geq 1$ and $\sum_i \lambda_i^2 = 1$.

The Schmidt number of a bipartite pure state $|\Psi\rangle_{AB}$ is defined as the number of nonzero eigenvalues in $\hat{\rho}_A$ or $\hat{\rho}_B$, therefore, the number of terms in the Schmidt decomposition of $|\Psi\rangle_{AB}$ [17].

Mathematically, we say that a bipartite system is entangled (non separable) when its Schmidt number is greater than 1, otherwise we say that the system is unentangled (or separable). For an entangled system, we can not represent its wave-function as a product of the wave-functions of each subsystem . For a bipartite system with two subsystems A and B, we say that they are entangled if

$$|\Psi\rangle_{AB} \neq |\Psi\rangle_A |\Psi\rangle_B \tag{2.18}$$

Entanglement is one of the most interesting resources of quantum mechanics. It is a purely quantum mechanical property where entangled states exhibit correlations that have no classical analog. This resource can be exploited to design quantum protocols that outperform the classical ones or arise new features (e.g. to teleport information between two distant systems [18]). Entanglement can also be exploited to create secure key distribution protocols [2]. And it can be exploited to locally perform one-way quantum computing by using single qubit measurements on cluster states [19].

In many situations, we can think of our system to be part of a bigger system $|\Psi\rangle_{AB}$, and we only have access to the subspace A. This may be due to the fact that the subsystem B is very far away, or maybe the subsystem B corresponds to the environment, which we can not control. If all the measurements that we can perform are on the subsystem A, it makes sense to work with the density matrix $\hat{\rho}_A \in \mathscr{H}_A$, that acts only on the subspace A. The density operator $\hat{\rho}_A$ can be obtained by performing the partial trace over the subsystem B

$$\hat{\rho}_A = tr_B \left(|\Psi\rangle_{AB} \langle\Psi|_{AB} \right) \tag{2.19}$$

We say that a bipartite state is maximally entangled when $tr_B(\hat{\rho}_{AB}) = \mathbb{1}/2$. This means that all information of the system is found in the correlations between subsystem A and B, and it is impossible to retrieve any information by performing local measurements on subsystem A.

There is one basis of four mutually orthogonal states, which all are maximally entangled:

$$\begin{aligned} |\phi^{\pm}\rangle &= \frac{1}{\sqrt{2}} \left(|00\rangle \pm |11\rangle \right) \\ |\psi^{\pm}\rangle &= \frac{1}{\sqrt{2}} \left(|01\rangle \pm |10\rangle \right) \end{aligned} \tag{2.20}$$

For example, Imagine that we only have access to the subsystem A of the state $|\psi^{+}\rangle$, from 2.20. By performing the partial trace over B system we will end up wit the identity operator (no information):

$$\hat{\rho}_A = tr_B(|\phi^+\rangle \langle\phi^+|) = \frac{1}{2} \sum_i \langle i|_B \left(|00\rangle + |11\rangle \right) \left(\langle 00| + \langle 11| \right) |i\rangle_B = \frac{1}{2} \left(|0\rangle \langle 0| + |1\rangle \langle 1| \right) = \frac{\mathbb{1}}{2} \tag{2.21}$$

In fact, in this thesis we will try to characterize the fidelity of the generation of the state $|\psi^{+}\rangle$ but with an arbitrary number of qubits N, called Greenberger–Horne–Zeilinger (GHZ) state

$$|\Psi\rangle_{GHZ} = \frac{1}{\sqrt{2}} \left(|0\rangle^{\otimes N} + |1\rangle^{\otimes N} \right) \tag{2.22}$$

Originally, a three-particle GHZ state was proposed to find a conflict with local realism for predictions of quantum mechanics [20] [21].

2.4. Basic Quantum Optics

In this section we will work with the simplest atom-field transition, with only two energy states interacting with one applied laser field.

2.4.1. Semiclassical approach

We will start by treating the two level system quantum mechanically and our input laser field classically. We will label the ground state of the two level system as $|g\rangle$ and the excited state $|e\rangle$, with an energy difference of $\hbar\omega_0$.
We assume that our two-level system is illuminated by a classical monochromatic electromagnetic field [15]:

$$\vec{E}(\vec{r}, t) = \frac{\vec{\varepsilon}(\vec{r}, t)}{2} e^{-i\nu t - \vec{k}\vec{r}} + \frac{\vec{\varepsilon}(\vec{r}, t)^*}{2} e^{i\nu t - \vec{k}\vec{r}} \tag{2.23}$$

Where we will assume that $\vec{\varepsilon}(\vec{r}, t)$ varies in a time-scale much longer than the optical frequency ν and a length scale much larger than the optical length. In the presence of an static electric field, neutral atoms do get an electric dipole moment $\hat{d}$ which can interact with the electric field $\vec{E}$. The energy of the interaction is $\hat{U} = -\hat{d}\vec{E}$.

When selection rules do only allow transitions between two energy levels, we can express the dipole operator in the atomic (or quantum dot) eigenstates:

$$\hat{d} = |g\rangle \langle e| \mu_{ge} + |e\rangle \langle g| \mu_{eg} \tag{2.24}$$

Where $\mu_{ge} = \langle g| \hat{d} |e\rangle$ and we have assumed that $\langle g| \hat{d} |g\rangle = \langle e| \hat{d} |e\rangle = 0$, the eigenstates do not have associated permanent dipole.

The Hamiltonian of the two-level system with the classical field is:

$$H = \hbar\omega_0 |e\rangle \langle e| - (\hat{\sigma}_{ge}\mu_{ge} + \hat{\sigma}_{eg}\mu_{eg})(\frac{\vec{\varepsilon}}{2}e^{-i\nu t} + \frac{\vec{\varepsilon}^*}{2}e^{i\nu t}) \tag{2.25}$$

Where we have used the notation $\hat{\sigma}_{ge} = |g\rangle \langle e|$ and $\hat{\sigma}_{eg} = |e\rangle \langle g|$. To solve the dynamics of the state we propose a time-dependent wavefunction $|\Psi\rangle = c_g(t) |g\rangle + c_e(t) |e\rangle$. We can describe the dynamics of the system with the Hamiltonian from 2.25 by using the Schrödinger equation (2.6):

$$\begin{aligned} i\hbar \langle e| \frac{d}{dt} |\Psi\rangle = \langle e| \hat{H} |\Psi\rangle \Rightarrow \dot{c}_e(t) = -i\omega_0 c_e(t) + \frac{i}{\hbar}(\vec{\varepsilon}e^{-i\nu t} + \vec{\varepsilon}^* e^{i\nu t})\mu_{eg}c_g(t) \\ i\hbar \langle g| \frac{d}{dt} |\Psi\rangle = \langle g| \hat{H} |\Psi\rangle \Rightarrow \dot{c}_g(t) = +\frac{i}{\hbar}(\vec{\varepsilon}e^{-i\nu t} + \vec{\varepsilon}^* e^{i\nu t})\mu_{ge}c_e(t) \end{aligned} \tag{2.26}$$

We will perform the transformation $c_e(t) = \tilde{c}_e(t)e^{-i\nu t}$, which is equivalent to going to the rotating frame. In the rotating frame we will be able to spot the fast-oscillating terms and the slow varying terms in the differential equations.

$$\begin{aligned} \dot{\tilde{c}}_e(t) &= -i\Delta c_e(t) + \frac{i}{\hbar}(\frac{\vec{\varepsilon}}{2} + \frac{\vec{\varepsilon}^*}{2}e^{2i\nu t})\mu_{eg}c_g(t) \\ \dot{c}_g(t) &= +\frac{i}{\hbar}(\frac{\vec{\varepsilon}}{2}e^{-2i\nu t} + \frac{\vec{\varepsilon}^*}{2})\mu_{ge}c_e(t) \end{aligned} \tag{2.27}$$

Where $\Delta = \omega_0 - \nu$. The relevant dynamics occur at frequencies proportional to $\Omega = \frac{\varepsilon\mu_{eg}}{\hbar}$ We will neglect the terms $\propto e^{2i\nu t}$ under the assumptions that $\Delta << \nu, \omega_0$ and $\Omega << \nu$ (Rotating Wave Approximation). The equations of motion under these considerations becomes:

$$\begin{aligned} \dot{\tilde{c}}_e(t) &= -i\Delta c_e(t) + i\frac{\Omega}{2}c_g(t) \\ \dot{c}_g(t) &= i\frac{\Omega^*}{2}c_e(t) \end{aligned} \tag{2.28}$$

In equations 2.28, spontaneous emission is not taken into account. The process of spontaneous emission can not be explained with the semi-classical model that we are using, since it arises from the coupling of the system to the vacuum modes of the electromagnetic field. If we do treat the field classically, this behavior does not appear. We will include "by hand" the effect of spontaneous emission by adding the factor $-\frac{c_e(\tau)}{2}$.

From now on, for simplicity, we will omit the tilde in $\tilde{c}_e(t)$. For convenience we will work with the dimensionless time $\tau = \gamma t$.

$$\begin{aligned} \dot{c}_e(\tau) &= -(i\tilde{\Delta} + \frac{1}{2})c_e(\tau) + i\frac{\tilde{\Omega}}{2}c_g(\tau) \\ \dot{c}_g(t\tau) &= i\frac{\tilde{\Omega}^*}{2}c_e(\tau) \end{aligned} \tag{2.29}$$

Where $\tilde{\Delta} = \frac{\Delta}{\gamma}$ and $\tilde{\Omega} = \frac{\Omega}{\gamma}$. If we assume that the input field is constant in time (square-shaped) and that the initial conditions are: $c_e(0) = 0$ and $c_g(0) = 1$, we can solve 2.29 exactly:

$$
\begin{aligned}
c_e(\tau) &= i\frac{\tilde{\Omega}}{\hat{\Omega}} e^{i\frac{\tau}{2}(\frac{i}{2}-\tilde{\Delta})} sin\left(\frac{\tau\hat{\Omega}}{2}\right) \\
c_g(\tau) &= e^{i\frac{\tau}{2}(\frac{i}{2}-\tilde{\Delta})}\left[cos\left(\frac{\tau\hat{\Omega}}{2}\right) + \frac{1+2i\tilde{\Delta}}{2\hat{\Omega}} sin\left(\frac{\tau\hat{\Omega}}{2}\right)\right]
\end{aligned}
\tag{2.30}
$$

With $\hat{\Omega} = \sqrt{\tilde{\Omega}^2 + (\tilde{\Delta} - \frac{i}{2})^2}$

2.4.2. Full quantum approach

So far, we have been treating the atom-field interaction assuming that the field is classical. In this subsection we will approach the problem by assuming that both the field and the atom behave quantum mechanically [22]. This way, we will be able to explain spontaneous emission, result of the atom interacting with the vacuum modes of the electromagnetic field, and the Rotation Wave Approximation will appear more naturally, without the necessity to go to a rotating frame.

Quantization of the Electromagnetic field

For a large cavity with volume V and legth L, by assuming vanishing electric field at the boundaries and satisfying Maxwell's equations, the electric and magnetic fields can be expanded as a set of sinusoidal modes:

$$E_x(z,t) = \sum_j \sqrt{\frac{2\nu_j}{\epsilon_0 V}} q_j sin(k_j z)$$

$$B_y(z,t) = \frac{1}{c^2}\sum_j \frac{\dot{q}_j}{k_j}\sqrt{\frac{2\nu_j}{\epsilon_0 V}} q_j cos(k_j z)$$

Where ν_j is the mode frequency, $k = \frac{c}{\nu_j}$ is the mode wavenumber and ϵ_0 (μ_0) are the permittivity and permeability of free space. We will define $A_j = \sqrt{\frac{2\nu_j}{\epsilon_0 V}}$, q_j and $\dot{q}_j$ are coefficients that correspond to the canonical position and canonical momentum, respectively.

The quantum mechanical Hamiltonian (eq. 2.31) will correspond to the classical energy within de cavity.

$$H = \sum_j \frac{\nu_j^2 q_j^2}{2} + \frac{\dot{q}_j^2}{2} \tag{2.31}$$

This Hamiltonian is analogous to the Hamiltonian for a set of unit mass harmonic oscillators with position q_j and frequency ν_j. For this reason, we will use the same quantization procedure as the harmonic oscillator quantization. We define q_j and $\dot{q}_j$ as operators

$$q_j \rightarrow \hat{q}_j \qquad \dot{q}_j \rightarrow \hat{p}_j$$

That fulfill the canonical commutation relation:

$$[\hat{q}_j, \hat{p}_{j'}] = i\hbar\delta_{j,j'}$$

Creation and annihilation operators for the excitation of each mode can be defined as follows:

$$\hat{a}_j = \frac{1}{\sqrt{2\hbar\nu_j}}(\nu_j\hat{q}_j + i\hat{p}_j) \qquad \hat{a}_j^\dagger = \frac{1}{\sqrt{2\hbar\nu_j}}(\nu_j\hat{q}_j - i\hat{p}_j)$$

That fulfill the bosonic commutation relations:

$$[\hat{a}_j, \hat{a}_{j'}] = 0 \qquad [\hat{a}_j, \hat{a}_{j'}^\dagger] = \delta_{j,j'}$$

And the electric field with polarization vector ε_α will be given by:

$$\hat{E}_\alpha = \varepsilon_\alpha \sum_j \varepsilon_j (\hat{a}_j + \hat{a}_j^\dagger) sin(k_j z)$$

With $\varepsilon_j = \sqrt{\frac{\hbar\nu_j}{\epsilon_0 V}}$, the electric field associated with a single photon with frequency ν_j. The Hamiltonian is given by:

$$\hat{H} = \sum_j \hbar\nu_j \left(\hat{a}_j^\dagger\hat{a}_j + \frac{1}{2}\right)$$

We denote $|n\rangle_j$ the eigenstates of the Hamiltonian. $E_{n_j} = \hbar\nu_j\left(n + \frac{1}{2}\right)$, where n describes the number of photons with frequency ν_j.

$$\hat{H}\,|n\rangle_j = E_{n_j}\,|n\rangle_j$$

Notice that annihilation ($\hat{a}_j$) and creation ($\hat{a}_j^\dagger$) operators act on the eigenstates of the Hamiltonian as:

$$\hat{a}_j\,|n\rangle_j = \sqrt{n}\,|n-1\rangle_j \qquad \hat{a}_j^\dagger\,|n\rangle_j = \sqrt{n+1}\,|n+1\rangle_j$$

They annihilate (create) one photon of frequency ν_j. Also, the photon number operator can be defined as $\hat{n}_j = \hat{a}_j^\dagger\hat{a}_j$.

Jaynes-Cummings model

The Jaynes-Cummings model describes the system of a two-level atom(with the ground state $|g\rangle$ and excited state$|e\rangle$) interacting with a quantized mode of an optical cavity. The full system is described with the Hamiltonian:

$$\hat{H} = \hat{H}_A + \hat{H}_F + \hat{H}_I$$

Where $\hat{H}_A$ is the bare atomic Hamiltonian (eq. 2.32), with transition frequency ω_0 between the two energy levels. $\hat{H}_F$ corresponds to the free field Hamiltonian (eq. 2.33).

$$\hat{H}_A = \hbar\omega_0\,|e\rangle\langle e| \tag{2.32}$$

$$\hat{H}_F = \hbar\nu\left(\hat{a}^\dagger\hat{a} + \frac{1}{2}\right) \tag{2.33}$$

$\hat{H}_I$ is the interaction Hamiltonian, described in a similar way to the semi-classical approach, but this time with the quantized electric field.

$$\hat{H}_I = -\hat{d}\hat{E} = -\hbar g\left(\hat{\sigma}_{eg} + \hat{\sigma}_{ge}\right)\left(\hat{a} + \hat{a}^\dagger\right) \tag{2.34}$$

With $g = \frac{\mu_{eg}}{\hbar}\sqrt{\frac{\hbar\nu_j}{2\epsilon_0 V}}$ corresponds to the coupling constant. Notice that in equation 2.34 we have four terms in the Hamiltonian. Performing the Rotating Wave Approximation corresponds to getting rid of the terms $\hat{\sigma}_{eg}\hat{a}^\dagger$ and $\hat{\sigma}_{ge}\hat{a}$. The first term corresponds to having a transition from ground state to excited state while emitting a photon and the second term corresponds to having a transition from excited state to ground state while absorbing one photon. These terms do not fulfill energy conservation and they can be neglected.

$$\hat{H}_I = -\hbar g \left(\hat{\sigma}_{eg}\hat{a} + \hat{\sigma}_{ge}\hat{a}^\dagger\right)$$

3. Far-detuned transition

In this chapter we will introduce the protocol used to generate the spin-photon entangled GHZ states. We will discuss the behavior of the system when taking into account the main inconsistency that we will study in this thesis, the presence of a far-detuned transition, and we will find the optimal pulse duration for the square and Gaussian-shaped pulses, only taking into account the presence of this extra energy-level.

3.1. Protocol description

The protocol uses a three-level state (fig. 3.1) to generate the time-bin encoded GHZ state [6].

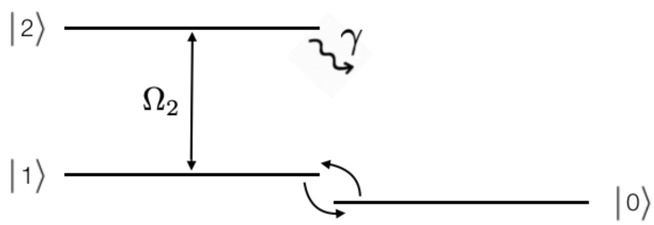

Figure 3.1.: Scheme of the 3-level system used to generate the spin-photon GHZ entangled state.

The protocol starts with a superposition of the two ground sates $\frac{1}{\sqrt{2}}(|0\rangle + |1\rangle)$. From here, a π_{1-2} y-rotation of the spin is applied on the transition $|1\rangle - |2\rangle$ and we wait for the excited state to relax.

$$\frac{1}{\sqrt{2}}(|0\rangle + |1\rangle) \xrightarrow{\pi_{1-2}} \frac{1}{\sqrt{2}}(|0\rangle + |2\rangle) \xrightarrow{s.e.} \frac{1}{\sqrt{2}}(|0\rangle + |e_1, 1\rangle) \tag{3.1}$$

The label (e) has been used for the emission of the photon, since it has been emitted in the early time-bin. From here, we apply a π_{0-1} y-rotation between the transition $|0\rangle - |1\rangle$ to flip the coefficients.

$$\xrightarrow{\pi_{0-1}} \frac{1}{\sqrt{2}}(|1\rangle - |e_1, 0\rangle) \tag{3.2}$$

Now, we repeat the π_{1-2} y-rotation and wait for the relaxation from the excited state (late part) and finally we flip the two ground states

$$\begin{aligned} &\xrightarrow{\pi_{1-2}} \frac{1}{\sqrt{2}}(|2\rangle - |e_1, 0\rangle) \xrightarrow{s.e.} \frac{1}{\sqrt{2}}(|L_1, 1\rangle - |e_1, 0\rangle) \\ &\xrightarrow{\pi_{0-1}} \frac{-1}{\sqrt{2}}(|L_1, 0\rangle + |e_1, 1\rangle) \equiv M\,|\Psi\rangle \end{aligned} \tag{3.3}$$

After applying this sequence of pulses and relaxation times, we end up with the superposition of one early photon and one late photon, which they are also entangled with the spins. Applying $M\,|\Psi\rangle$ corresponds to one cycle of the protocol, and only one photon is generated. If we apply M, N times, we would end with a GHZ state made of N entangled photons:

$$\frac{1}{\sqrt{2}}(|0\rangle + |1\rangle) \xrightarrow{(M)^N} \frac{(-1)^N}{\sqrt{2}}(|L_1, L_2, ..., L_N, 0\rangle + |e_1, e_2, ..., e_N, 1\rangle) = \\ \frac{(-1)^N}{\sqrt{2}}(|L\rangle^{\otimes N}|0\rangle + |e\rangle^{\otimes N}|1\rangle) \tag{3.4}$$

In figure 3.2 a scheme of the protocol is shown. As we can see, each round (or cycle) of the protocol is symmetric between the early the late time-bins. We will exploit this symmetry in later chapters to compute the conditional fidelity of the system.

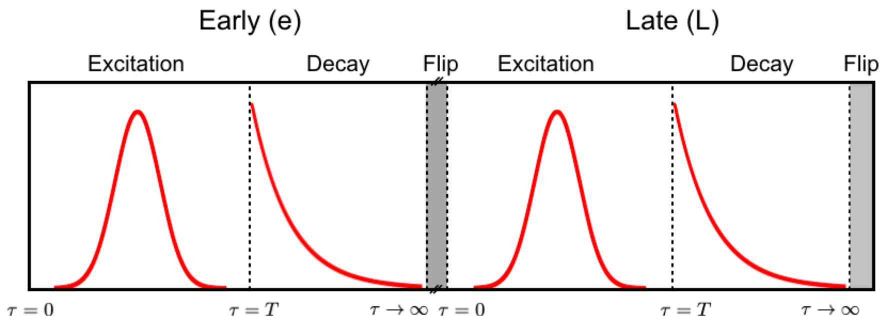

Figure 3.2.: Scheme of one cycle of the protocol used to generate the GHZ state.

It is important to point out that by using a $\left(\frac{\pi}{2}\right)_{0-1}$ y-rotation of the spin between each generated late photon, one would be able to create a linear cluster state instead of the GHZ state [23].

It is unnecessary to include the imperfections of the detector for time-bin entangled states when the time-bin is much larger than the uncertainty in the detection time [24, 25].

In the scheme described above we considered the ideal three-level state without any imperfections. Realistically, when performing the protocol on the laboratory, there are many imperfections that should be taken into account. One of them is the presence of a far-detuned energy level. For the realization of this protocol with quantum dots in the Voigt geometry magnetic field [6], it is clear that the Zeeman-spliting of the excited states will contain this additional energy level that we want to study.

In figure 3.3 an scheme of the system with the far-detuned energy level is presented. Ω_2 corresponds to the Rabi frequency of the resonant transition, Ω_3 corresponds to the Rabi frequency of the off-resonant transition. Notice that since we are driving both transitions with the same laser pulse, $\frac{\Omega_2}{\Omega_3} = \frac{\mu_{12}}{\mu_{03}} \equiv R$. For simplicity, we will assume that $R = 1$. While resonantly driving the transition $|1\rangle - |2\rangle$, it may be possible to drive some population to the far-detuned state $|3\rangle$, compromising the protocol.

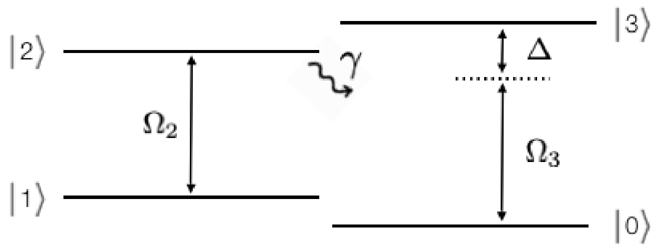

Figure 3.3.: Scheme of the 3-level system used to generate the spin-photon GHZ entangled state with the addition of the far-detuned energy level.

3.2. Stric definition of Fidelity

The fidelity is a measurement of the "closeness" between two quantum states. It expresses the probability for one state to pass a test to be identified as the other. The most used definition of fidelity is the squared overlap between two systems:

$$F = |\langle \Psi_{ideal} | \Psi_{experimental} \rangle|^2 \tag{3.5}$$

With $F \leq 1$, and $F = 1$ when the two states are exactly the same.

If we take into account the presence of the far-detuned transition $|3\rangle$ when trying to drive the transition $|1\rangle - |2\rangle$, we can assume that the action of the laser pulse will create a superposition of the ground and excited states:

$$\begin{aligned} |1\rangle &\rightarrow c_1 |1\rangle + c_2 |2\rangle \\ |0\rangle &\rightarrow c_0 |0\rangle + c_3 |3\rangle \end{aligned} \tag{3.6}$$

In this case, the fidelity of the system after applying one cycle of the protocol would be:

$$F = |c_0 c_2|^2 \tag{3.7}$$

Which corresponds to the ground state $|0\rangle$ not being driven by the π_{1-2} rotation, and the state $|1\rangle$ being driven by the π_{1-2} rotation (as expected). For N cycles of the protocol we would have the same expression to the power of N.

This definition of fidelity will be a good starting point to understand the system dynamics and spot the the compromises between some parameters of the system. In next chapters we will introduce a more experimentally realistic definition of the fidelity.

3.3. Time optimization of the Square pulse

In this section we will solve the dynamics of our four-level system described in section 3.1 assuming that the shape of the input laser pulse is square (constant in time), taking into account the presence of the extra energy level $|3\rangle$. Our goal is to be able to derive an analytical expression for the optimal length of the pulse T. Before jumping into the equations, we can already guess that there will be a compromise between the spontaneous emission form the main transition (between $|1\rangle - |2\rangle$) and the excitation of $|3\rangle$. On one hand, if the pulse is too short, the intensity of the pulse will be high enough to drive the off-resonant transition between $|0\rangle - |3\rangle$. On the other hand, If the pulse is too long, the spontaneous emission from

$|2\rangle$ will become relevant.

In section 2.4.1 we derived and solved the differential equations that govern the dynamics of a two-level system with a time-independent pulse. Due to the fact that in our model we are not considering the cross-terms $|2\rangle \to |0\rangle$ and $|3\rangle \to |1\rangle$, we can treat our four-level system as a two two-level systems separately. The analytical solutions for the $|1\rangle - |2\rangle$ transition, resonant with the input laser and governed by spontaneous emission are:

$$c_2(T) = i\frac{\tilde{\Omega}_2}{\hat{\Omega}_2}e^{-\frac{T}{4}} sin\left(\frac{T\hat{\Omega}_2}{2}\right)$$
$$c_1(T) = e^{-\frac{T}{4}}\left[cos\left(\frac{T\hat{\Omega}_2}{2}\right) + \frac{1}{2\hat{\Omega}_2} sin\left(\frac{T\hat{\Omega}_2}{2}\right)\right]$$

And the analytical solutions for the far off-resonant transition $|0\rangle - |3\rangle$ are:

$$c_3(T) = i\frac{\tilde{\Omega}_3}{\hat{\Omega}_3}e^{-\frac{iT\tilde{\Delta}}{2}} sin\left(\frac{T\hat{\Omega}_3}{2}\right)$$
$$c_0(T) = e^{-\frac{iT\tilde{\Delta}}{2}}\left[cos\left(\frac{T\hat{\Omega}_3}{2}\right) + i\frac{\tilde{\Delta}}{\hat{\Omega}_3} sin\left(\frac{T\hat{\Omega}_3}{2}\right)\right]$$

Where $\hat{\Omega}_3 \equiv \sqrt{\tilde{\Delta}^2 + |\tilde{\Omega}_3|^2}$ and $\hat{\Omega}_2 \equiv \sqrt{-\frac{1}{4} + |\tilde{\Omega}_2|^2}$.

In order to find the optimal time T from these equations, we want to impose the maximum population to be in $|2\rangle$ and the least amount of population to be found in the excited state of the far-detuned energy level $|3\rangle$. For these conditions to be fulfilled we have to impose the following restrictions:

$$\begin{aligned} |c_2|^2 = 1 &\Rightarrow \frac{T\hat{\Omega}_2}{2} = \frac{\pi}{2} \\ |c_0|^2 = 0 &\Rightarrow \frac{T\hat{\Omega}_3}{2} = \pi(n+1) \end{aligned} \tag{3.8}$$

Where $n = 0, 1, 2, ...$

With these restrictions (eq. 3.8) and assuming $R = 1$, we are able to solve the optimal Rabi frequency $\tilde{\Omega}_2$:

$$\frac{\hat{\Omega}_3}{\hat{\Omega}_2} = 2(n+1) \Rightarrow \tilde{\Omega}_2^2 = \frac{(n+1)^2 + \tilde{\Delta}^2}{4(n+1)^2 - 1}$$

With this result we can solve $\hat{\Omega}_2$, $\hat{\Omega}_3$ and T:

$$\hat{\Omega}_2 = \sqrt{\frac{\tilde{\Delta}^2 - 1}{4(n+1)^2 - 1}} \simeq \frac{\tilde{\Delta}}{\sqrt{4(n+1)^2 - 1}}$$
$$\hat{\Omega}_3 = \sqrt{\frac{(n+1)^2(1 + 4\tilde{\Delta}^2)}{4(n+1)^2 - 1}} \simeq \frac{2\tilde{\Delta}(n+1)}{\sqrt{4(n+1)^2 - 1}}$$
$$T = \pi\sqrt{\frac{4(n+1)^2 - 1}{\tilde{\Delta}^2 - 1}} \simeq \frac{\pi\sqrt{4(n+1)^2 - 1}}{\tilde{\Delta}}$$

For generality, we have computed the solutions for all n. In eq. 3.9 we have set $n = 0$, targeting the first maximum.

$$\hat{\Omega}_2 \simeq \frac{\tilde{\Delta}}{\sqrt{3}} \qquad \hat{\Omega}_3 \simeq \frac{2\tilde{\Delta}}{\sqrt{3}} \tag{3.9}$$

$$\boxed{T \simeq \frac{\sqrt{3}\pi}{\tilde{\Delta}}}$$

By substituting the expressions from eq. 3.9 into the analytical expressions of $\{c_2, c_1, c_3, c_0\}$ and computing the their modulus square, we end up with the populations of the four transitions in the optimal time:

$$\boxed{|c_3(T)|^2 = 0 \qquad |c_0(T)|^2 \approx 1 \qquad |c_2(T)|^2 \approx 1 - \frac{\sqrt{3}\pi}{2\tilde{\Delta}} \qquad |c_1(T)|^2 \approx \frac{\sqrt{3}}{2\tilde{\Delta}}}$$

3.3.1. Strict fidelity and numerical comparison

With the square pulse populations for the optimal time, we can use the strict definition of fidelity explained in section 3.2 to derive an analytical expression:

$$F = |c_0 c_2|^{2N} \approx 1 - N\frac{\sqrt{3}\pi}{2\tilde{\Delta}}$$

In appendix B.1 the comparison between the analytical and numerical results for the optimal fidelity is shown. Notice that for this fidelity we are only targeting the first maximum (shortest T). Because of experimental reasons, we are interested in this regime, since realistic pulse durations are approximately $T \approx 0.01 - 0.1$ [10]. Achieving the first maximum is already a challenge. This restriction arises from the grading monochromator used to generate the monochromatic laser pulses [26]. The longer the length of the pulse, the less accurate discrimination of the laser frequency is made.

If the pulse durations could be experimentally increased, it may be interesting to lie in the regime where $n = 2, 3, 4$. As we will see and discuss in the following chapters, this regime, despite not containing the highest fidelities, it is less dependent on oscillations.

Now that we have been able to obtain an analytical expression for the optimal duration of the pulse T and the mathematical fidelity F, we will compare them with the numerical results.

As one can see in figure 3.5, the fidelity does highly depend on the length of the pulse T. This behavior arises from the constructive and destructive interference of the fast oscillations from the far-detuned transition ($|0\rangle - |3\rangle$) and the Rabi oscillations from the main transition ($|1\rangle - |2\rangle$).

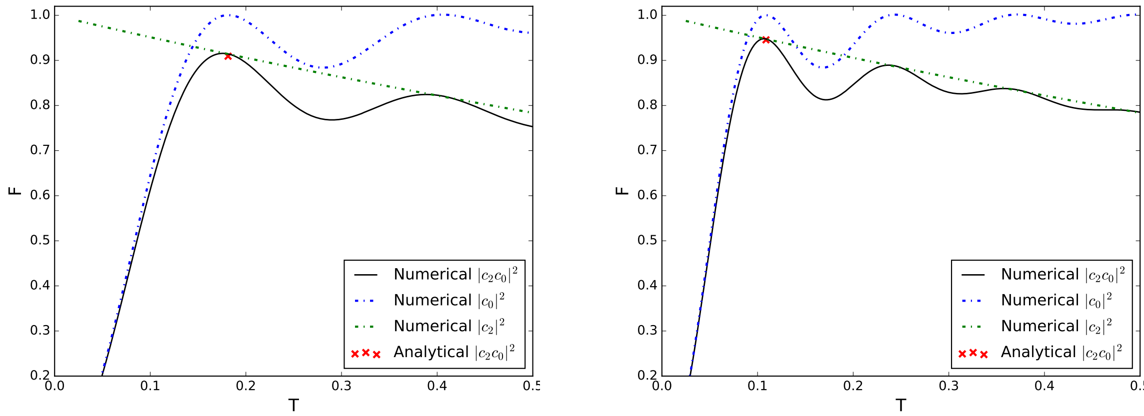

Figure 3.4.: Plots of the strict fidelity as a function of the length of the pulse T, with $\tilde{\Delta} = 30$ (left) and $\tilde{\Delta} = 50$ (right).

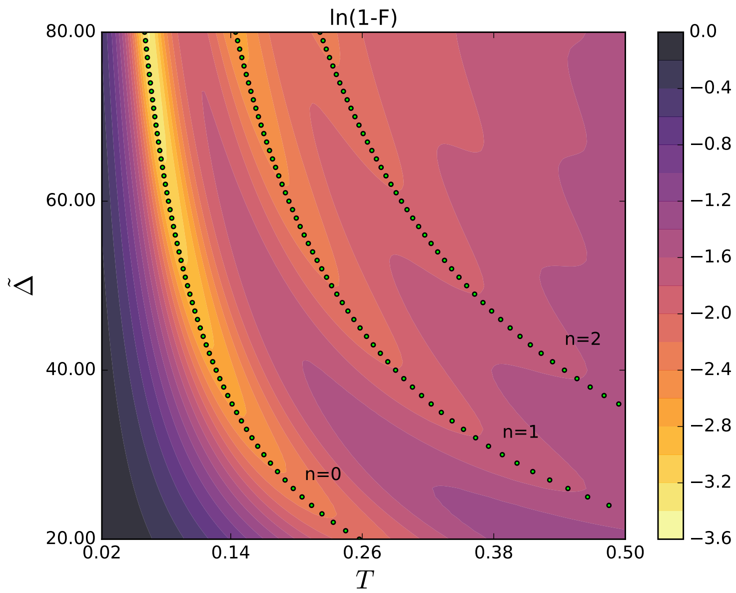

Figure 3.5.: 2D colormap of the numerical results for $ln(1-F)$ as a function of the length of the pulse T (x axis) and the dimensionless detuning $\tilde{\Delta}$ (y axis). The green-dotted lines correspond to the analytical optimal times for $n = \{0, 1, 2\}$.

In figure 3.4 we can also see that the optimal time T does decrease as the dimensionless detuning $\tilde{\Delta}$ increases. This phenomenon is produced due to the fact that for larger values of $\tilde{\Delta}$, the extra energy level $|3\rangle$ is more off-resonant. The shorter the pulse, the more intensity, and more easily is to drive the far off-resonant transition.

3.4. Time optimization of the Gaussian pulse

In this section we will derive the optimal time T for a Guassian-shaped pulse. From 2.4.1 we know that the equations of motion for our system are:

$$\dot{c}_3(\tau) = -i\tilde{\Delta}c_3(\tau) + i\frac{\tilde{\Omega}_3(\tau)_3}{2}c_0(\tau) \qquad \dot{c}_0(\tau) = i\frac{\tilde{\Omega}_3(\tau)_3^*}{2}c_3(\tau)$$

And:

$$\dot{c}_2(\tau) = i\frac{\tilde{\Omega}_2(\tau)_2}{2}c_1(\tau) - \frac{1}{2}c_2(\tau) \qquad \dot{c}_1(\tau) = i\frac{\tilde{\Omega}_2(\tau)_2^*}{2}c_2(\tau)$$

Notice that in this case the Rabi frequency $\tilde{\Omega}(\tau)$ does depend on time (eq. 3.10). Due to this reason, we will no longer be able to solve these differential equations exactly, as we did with the square-shaped pulse. We will proceed by performing perturbation theory on the equations and find their solutions up to the order where the relevant dynamics appear.

It is important to point out that we can't apply perturbation theory around the same parameters for each pair of differential equations. The dynamics of each transition are different. On one hand, the transition $|1\rangle - |2\rangle$ is resonant and is governed by spontaneous emission. On the other hand, the $|0\rangle - |3\rangle$ transition is governed by the large detuning $\tilde{\Delta}$.

The Gaussian-shaped pulse Ω_2 is defined as:

$$|\tilde{\Omega}_2(\tau)| = \frac{\alpha}{\sqrt{2\pi}\sigma}e^{\left(\frac{\tau-\mu}{\sqrt{2}\sigma}\right)^2} \tag{3.10}$$

Where α is a normalization constant that will be fixed by imposing that we want to drive the maximum amount of population from $|1\rangle$ to $|2\rangle$ (eq. 3.14). Since we assume that the pulse starts at time ($\tau = 0$) and finishes at ($\tau = T$), then $\mu = \frac{T}{2}$. Also, $\sigma = \frac{T}{\beta}$. Notice that the β factor defines the width of the pulse. If $\beta >> 1$, the pulse will be very narrow and almost all the area of the Gaussian will lie inside time-window between $\tau = 0$ and $\tau = T$. On the other hand, if $\beta << 1$, the pulse will be so wide that its power will remain approximately constant, resembling to the square pulse. Since we have already explored the square pulse dynamics in this section we will explore the regime where $\beta >> 1$.

Resonant transition $|1\rangle - |2\rangle$

We will proceed to solve the following system of coupled linear differential equations:

$$\dot{c}_2(\tau) = i\frac{\tilde{\Omega}_2}{2}c_1(\tau) - \frac{1}{2}c_2(\tau) \qquad \dot{c}_1(\tau) = i\frac{\tilde{\Omega}_2^*}{2}c_2(\tau) \tag{3.11}$$

Due to the fact that $\frac{1}{2} << \frac{\tilde{\Omega}_2}{2}$ we can perform perturbation theory around $\epsilon = -\frac{1}{2}$, where ϵ is the perturvative coefficient. We expand c_1 and c_2 as follows:

$$c_2(\tau) = c_2^{(0)}(\tau) + c_2^{(1)}(\tau)\epsilon + c_2^{(2)}(\tau)\epsilon^2 + ...$$
$$c_1(\tau) = c_1^{(0)}(\tau) + c_1^{(1)}(\tau)\epsilon + c_1^{(2)}(\tau)\epsilon^2 + ...$$

Plugging this into the differential equations from eq. 3.11 we obtain:

$$\left[\dot{c}_2^{(0)}(\tau) + \dot{c}_2^{(1)}(\tau)\epsilon + \dot{c}_2^{(2)}(\tau)\epsilon^2 + ...\right] = \left[c_2^{(0)}(\tau)\epsilon + c_2^{(1)}(\tau)\epsilon^2 + c_2^{(2)}(\tau)\epsilon^3 + ...\right]$$
$$+ i\frac{\tilde{\Omega}_2}{2}\left[c_1^{(0)}(\tau) + c_1^{(1)}(\tau)\epsilon + c_1^{(2)}(\tau)\epsilon^2 + ...\right]$$
$$\left[\dot{c}_1^{(0)}(\tau) + \dot{c}_1^{(1)}(\tau)\epsilon + \dot{c}_1^{(2)}(\tau)\epsilon^2 + ...\right] = i\frac{\tilde{\Omega}_2^*}{2}\left[c_2^{(0)}(\tau) + c_2^{(1)}(\tau)\epsilon + c_2^{(2)}(\tau)\epsilon^2 + ...\right]$$

By grouping the terms with the same powers of ϵ we find the recursive relationship (eq. 3.12):

$$\begin{aligned} \dot{c}_2^{(N)}(\tau) &= c_2^{(N-1)}(\tau) + i\frac{\tilde{\Omega}_2}{2}c_1^{(N)}(\tau) \\ \dot{c}_1^{(N)}(\tau) &= i\frac{\tilde{\Omega}_2^*}{2}c_2^{(N)}(\tau) \end{aligned} \tag{3.12}$$

Where N corresponds to the order of the perturvative expansion. For the zeroth order ($N = 0$) we find the following equations:

$$\begin{aligned} \dot{c}_2^{(0)}(\tau) &= i\frac{\tilde{\Omega}_2(\tau)}{2}c_1^{(0)}(\tau) \\ \dot{c}_1^{(0)}(\tau) &= i\frac{\tilde{\Omega}_2^*(\tau)}{2}c_2^{(0)}(\tau) \end{aligned}$$

In appendix A.1 we derive the solutions for these coupled differential equations assuming the initial conditions to be $c_1^{(0)}(0) = 1$ and $c_2^{(0)}(0) = 0$. In eq. 3.13 the solutions are presented.

$$\begin{aligned} c_2^{(0)}(T) &= i\frac{\tilde{\Omega}}{|\tilde{\Omega}_2|}sin\left(\frac{1}{2}\int_0^T |\tilde{\Omega}_2| d\tau'\right) \\ c_1^{(0)}(T) &= cos\left(\frac{1}{2}\int_0^T |\tilde{\Omega}_2| d\tau\right) \end{aligned} \tag{3.13}$$

Where we have set $\tau = T$. Notice that the zeroth order term corresponds to the free dynamics of the system without spontaneous emission. We will use the zeroth order solutions from eq. 3.13 to derive the normalizing factor α for the Gaussian pulse by imposing:

$$|c_2^{(0)}(T)|^2 = 1 \Rightarrow \frac{\pi}{2} = \frac{1}{2}\frac{\alpha}{\sqrt{2\pi}\sigma}\int_0^T e^{\left(\frac{\tau'-\mu}{\sqrt{2}\sigma}\right)^2} d\tau' \tag{3.14}$$

Now, we will expand 3.14 by using the property: $erf(x) = \frac{2}{\sqrt{\pi}}\int_0^x e^{-z^2}dz$.

$$\alpha = \pi\left[erf\left(\frac{T-\mu}{\sqrt{2}\sigma}\right) + erf\left(\frac{\mu}{\sqrt{2}\sigma}\right)\right]^{-1} \Rightarrow \tag{3.15}$$

$$\alpha = \pi\left[erf(\frac{\beta}{2\sqrt{2}})\right]^{-1} \tag{3.16}$$

Notice that in the regime that we are interested to explore ($\frac{\beta}{2\sqrt{2}} > 1$), due to this reason we can expand the error function:

$$erf(z) \approx 1 - \frac{e^{-z^2}}{\sqrt{\pi}z}$$

Plugging this expression into equation 3.16 we obtain:

$$\alpha \approx \pi\left[1 - \frac{2\sqrt{2}}{\sqrt{\pi}\beta}e^{-\frac{\beta^2}{8}}\right]^{-1} \approx \pi$$

We have been able to study the free dynamics of the transition and fix the normalization constant for the Gaussian pulse. With the zeroth order solved, now we will move to the first order differential equations (eq. 3.17).

$$\begin{aligned} \dot{c}_2^{(1)}(\tau) &= i\frac{\tilde{\Omega}_2}{|\tilde{\Omega}_2|} sin\left(\frac{1}{2}\int_0^{\tau}|\tilde{\Omega}_2|d\tau'\right) + i\frac{\tilde{\Omega}_2}{2}c_1^{(1)}(\tau) \\ \dot{c}_1^{(1)}(\tau) &= i\frac{\tilde{\Omega}_2^*}{2}c_2^{(1)}(\tau) \end{aligned} \tag{3.17}$$

In order to be able to solve this system of equations we will apply the guess function (Ansatz) described in equations 3.18, obtained by using the Green's function method [27] .

$$\begin{aligned} c_2^{(1)}(\tau) &= \int_0^{\tau} cos\left(\frac{1}{2}\int_{\tau'}^{\tau}|\tilde{\Omega}_2|d\tau''\right)c_2^{(0)}(\tau')d\tau' \\ c_1^{(1)}(\tau) &= i\frac{\tilde{\Omega}_2^*}{|\tilde{\Omega}_2|}\int_0^{\tau} sin\left(\frac{1}{2}\int_{\tau'}^{\tau}|\tilde{\Omega}_2|d\tau''\right)c_2^{(0)}(\tau')d\tau' \end{aligned} \tag{3.18}$$

We will begin by computing the $c_2^{(1)}(T)$ coefficient:

$$\begin{aligned} c_2^{(1)}(T) &= i\frac{\tilde{\Omega}_2}{|\tilde{\Omega}_2|}\int_0^{T} cos\left(\frac{1}{2}\int_{\tau'}^{T}|\tilde{\Omega}_2|d\tau''\right) sin\left(\frac{1}{2}\int_0^{\tau'}|\tilde{\Omega}_2|d\tau''\right)d\tau' \\ &= \frac{i}{2}\frac{\tilde{\Omega}_2}{|\tilde{\Omega}_2|}\int_0^{T}\left[sin\left(\frac{1}{2}\int_{\tau'}^{T}|\tilde{\Omega}_2|d\tau'' + \frac{1}{2}\int_0^{\tau'}|\tilde{\Omega}_2|d\tau''\right) - sin\left(\frac{1}{2}\int_{\tau'}^{T}|\tilde{\Omega}_2|d\tau'' - \frac{1}{2}\int_0^{\tau'}|\tilde{\Omega}_2|d\tau''\right)\right]d\tau' \\ &= \frac{i}{2}\frac{\tilde{\Omega}_2}{|\tilde{\Omega}_2|}\int_0^{T}\left[sin\left(\frac{1}{2}\int_0^{T}|\tilde{\Omega}_2|d\tau''\right) - sin\left(\frac{1}{2}\int_0^{T}|\tilde{\Omega}_2|d\tau'' - \int_0^{\tau'}|\tilde{\Omega}_2|d\tau''\right)\right]d\tau' \end{aligned} \tag{3.19}$$

In the first step of eq.3.19 I have used the relationship $cos(A)sin(B) = \frac{sin(A+B)-sin(A-B)}{2}$. Now, by using the restriction on the pulse derived in 3.14 we obtain:

$$\begin{aligned} c_2^{(1)}(T) &= \frac{i}{2}\frac{\tilde{\Omega}_2}{|\tilde{\Omega}_2|}\int_0^{T}\left[sin\left(\frac{\pi}{2}\right) - sin\left(\frac{\pi}{2} - \int_0^{\tau'}|\tilde{\Omega}_2|d\tau''\right)\right]d\tau' \\ &= \frac{i}{2}\frac{\tilde{\Omega}_2}{|\tilde{\Omega}_2|}\int_0^{T}\left[1 - cos\left(\int_0^{\tau'}|\tilde{\Omega}_2|d\tau''\right)\right]d\tau' \\ &\approx i\frac{\tilde{\Omega}_2}{|\tilde{\Omega}_2|}\frac{T}{2} - \frac{i}{2}\frac{\tilde{\Omega}_2}{|\tilde{\Omega}_2|}\int_0^{T} cos\left(\frac{\pi}{2}\left(erf\left(\frac{\tau'-\mu}{\sqrt{2}\sigma}\right) + erf\left(\frac{\beta}{2\sqrt{2}}\right)\right)\right)d\tau' \end{aligned} \tag{3.20}$$

In the regime where we are working $erf\left(\frac{\beta}{2\sqrt{2}}\right) \approx 1$:

$$\begin{aligned} c_2^{(1)}(T) &\approx i\frac{\tilde{\Omega}_2}{|\tilde{\Omega}_2|}\frac{T}{2} - \frac{i}{2}\frac{\tilde{\Omega}_2}{|\tilde{\Omega}_2|}\int_0^{T} sin\left(\frac{\pi}{2}\left(erf\left(\frac{\tau'-\mu}{\sqrt{2}\sigma}\right)\right)\right)d\tau' \\ &= i\frac{\tilde{\Omega}_2}{|\tilde{\Omega}_2|}\frac{T}{2} \end{aligned} \tag{3.21}$$

Notice that in the last step of eq. 3.21, we have used that $\int_0^T erf\left(\frac{\tau'-\mu}{\sqrt{2}\sigma}\right)d\tau' = 0$ because the function is odd with respect to $\tau' = \frac{T}{2}$, for this reason, the sine integral will vanish.

Now we are able to compute $c_2(\tau)$ up to first order:

$$c_2(T) \simeq c_2^{(0)}(T) + \epsilon c_2^{(1)}(T) \simeq i\frac{\tilde{\Omega}_2}{|\tilde{\Omega}_2|} sin\left(\frac{1}{2}\int_0^T |\tilde{\Omega}_2| d\tau'\right) - i\frac{\tilde{\Omega}_2}{|\tilde{\Omega}_2|}\frac{T}{4}$$

And the modulus square is:

$$|c_2(\tau)|^2 \simeq \left(1 - \frac{T}{4}\right)^2 \simeq 1 - \frac{T}{2}$$

For the $c_1^{(1)}$ coefficient we will have:

$$\begin{aligned}
&c_1^{(1)}(T) = -\int_0^T sin\left(\frac{1}{2}\int_{\tau'}^T |\tilde{\Omega}_2| d\tau''\right) sin\left(\frac{1}{2}\int_0^{\tau'} |\tilde{\Omega}_2| d\tau''\right) d\tau' \\
&= \frac{1}{2}\int_0^T \left[cos\left(\frac{1}{2}\int_{\tau'}^T |\tilde{\Omega}_2| d\tau'' + \frac{1}{2}\int_0^{\tau'} |\tilde{\Omega}_2| d\tau''\right) - cos\left(\frac{1}{2}\int_{\tau'}^T |\tilde{\Omega}_2| d\tau'' - \frac{1}{2}\int_0^{\tau'} |\tilde{\Omega}_2| d\tau''\right)\right] d\tau' \\
&= \frac{1}{2}\int_0^T \left[cos\left(\frac{1}{2}\int_0^T |\tilde{\Omega}_2| d\tau''\right) - cos\left(\frac{1}{2}\int_0^T |\tilde{\Omega}_2| d\tau'' - \int_0^{\tau'} |\tilde{\Omega}_2| d\tau''\right)\right] d\tau' \\
&= \frac{1}{2}\int_0^T \left[cos\left(\frac{\pi}{2}\right) - cos\left(\frac{\pi}{2} - \int_0^{\tau'} |\tilde{\Omega}_2| d\tau''\right)\right] d\tau' \\
&= \frac{-1}{2}\int_0^T sin\left(\int_0^{\tau'} |\tilde{\Omega}_2| d\tau''\right) d\tau' \approx 0
\end{aligned} \tag{3.22}$$

In this case, the sine integral does not vanish but its contribution is negligible. As we will see in next chapters, the coefficient $|c_1|^2$ will appear in the conditional fidelities together with terms that are already very small, and there is no need to expand the calculation to higher orders.

Far-detuned transition $|0\rangle - |3\rangle$

In this part we are interested in looking at the dynamics of the $|0\rangle - |3\rangle$ transition. We start with the differential equations:

$$\dot{c}_3(\tau) = -i\tilde{\Delta} c_3(\tau) + i\frac{\tilde{\Omega}_3(\tau)}{2} c_0(\tau) \qquad \dot{c}_0(\tau) = i\frac{\tilde{\Omega}_3^*(\tau)}{2} c_3(\tau) \tag{3.23}$$

Notice that the dominant term (in eq 3.23) is the one containing $\tilde{\Delta}$ (we are in the far-detuned regime). Before expanding these differential equations perturbatively, first we will perform the change of variable $d\xi = |\tilde{\Omega}_3| d\tau$. This way, we will be able to remove the time-dependency from the perturbation term. In equation 3.24 one can see the coupled differential equations after the change of variable.

$$\dot{c}_3(\xi) = -i\frac{\tilde{\Delta}}{|\tilde{\Omega}_3|} c_3(\xi) + \frac{i}{2}\frac{\tilde{\Omega}_3}{|\tilde{\Omega}_3|} c_0(\xi) \qquad \dot{c}_0(\xi) = \frac{i}{2}\frac{\tilde{\Omega}_3^*}{|\tilde{\Omega}_3|} c_3(\xi) \tag{3.24}$$

Now, we can use perturbation theory and expand the coefficients around $\epsilon = \frac{i}{2}\frac{\tilde{\Omega}_3}{|\tilde{\Omega}_3|}$:

$$c_3(\xi) = c_3^{(0)}(\xi) + c_3^{(1)}(\xi)\epsilon + c_3^{(2)}(\xi)\epsilon^2 + ...$$
$$c_0(\xi) = c_0^{(0)}(\xi) + c_0^{(1)}(\xi)\epsilon + c_0^{(2)}(\xi)\epsilon^2 + ...$$

By plugging in again the expansion into equation 3.24, we get N differential equations for each term of the expansion. In our case, we will see that we only have to go to the first order. These differential equations are:

$$\dot{c}_3^{(N)}(\xi) = -i\frac{\tilde{\Delta}}{|\tilde{\Omega}_3|}c_3^{(N)}(\xi) + c_0^{(N-1)}(\xi) \qquad \dot{c}_0^{(N)}(\xi) = \frac{\tilde{\Omega}_3^{*2}}{|\tilde{\Omega}_3|^2}c_3^{(N-1)}(\xi) \tag{3.25}$$

First, from equation 3.25 we set $N = 0$ to obtain the zeroth order system of coupled differential equations:

$$\dot{c}_3^{(0)}(\xi) = -i\frac{\tilde{\Delta}}{|\tilde{\Omega}_3|}c_3^{(0)}(\xi) \qquad \dot{c}_0^{(0)}(\xi) = 0$$

By setting the initial conditions to $c_0^{(0)}(0) = 1$ and $c_3^{(0)}(0) = 0$, we obtain the zeroth order solutions:

$$c_3^{(0)}(\xi) = 0 \qquad c_0^{(0)}(\xi) = 1$$

Since we are trying to solve the dynamics of a far-detuned transition, up to zeroth order, the population of the ground state $|0\rangle$ remain unchanged. This is a good approximation for long enough times T. In our case, In order to find the interesting dynamics we will have to compute the first order coefficients. There, we will see that for short times T, the intensity of the laser will be high enough to drive population to the excited state $|3\rangle$.

By setting $N = 1$ (in eq. 3.25) we find the first order system of differential equations:

$$\dot{c}_3^{(1)}(\xi) = -i\frac{\tilde{\Delta}}{|\tilde{\Omega}_3|}c_3^{(1)}(\xi) + c_0^{(0)}(\xi) \qquad \dot{c}_0^{(1)}(\xi) = \frac{\tilde{\Omega}_3^{*2}}{|\tilde{\Omega}_3|^2}c_3^{(0)}(\xi) \tag{3.26}$$

Notice that the initial conditions for the first order differential equations are $c_0^{(1)}(0) = 0$ and $c_3^{(1)}(0) = 0$. From equation 3.26 we find that:

$$c_0^{(1)}(\xi) = 0$$

To solve the differential equation of $c_3^{(1)}(\xi)$ we will use the method of integrating factor [27]:

$$\begin{aligned} c_3^{(1)}(\xi) &= e^{-i\int \frac{\tilde{\Delta}}{|\tilde{\Omega}_3|}d\xi'} \int e^{i\int \frac{\tilde{\Delta}}{|\tilde{\Omega}_3|}d\xi''} d\xi' \\ \Rightarrow c_3^{(1)}(T) &= e^{-i\tilde{\Delta}T} \int_0^T e^{i\tilde{\Delta}\tau'}|\tilde{\Omega}_3| d\tau' \end{aligned} \tag{3.27}$$

Where (in eq.3.27) we have undone the change of variable of the time. Now, we will solve the integrals by using the definition of the Gaussian pulse in 3.10:

$$\begin{aligned} c_3^{(1)}(T) &= \frac{\alpha R}{\sqrt{2\pi}\sigma}e^{-i\tilde{\Delta}T}\int_0^T e^{i\tilde{\Delta}\tau'}e^{-\left(\frac{\tau'-\mu}{\sqrt{2}\sigma}\right)^2}d\tau' \\ &= \frac{\alpha R}{\sqrt{2\pi}\sigma}e^{-i\tilde{\Delta}\frac{T}{2}}e^{-\frac{\tilde{\Delta}^2T^2}{2\beta^2}}\int_0^T e^{-\left(\frac{\tau-\mu}{\sqrt{2}\sigma}-i\frac{\tilde{\Delta}}{\sqrt{2}}\sigma\right)^2}d\tau' \end{aligned} \tag{3.28}$$

We will proceed by making a change of variable $u(\tau) = \frac{\tau-\mu}{\sqrt{2}\sigma} - i\frac{\tilde{\Delta}}{\sqrt{2}}\sigma$ and expanding the Gaussian integral as error functions:

$$
\begin{aligned}
c_3^{(1)}(T) &= \frac{\alpha R}{\sqrt{\pi}} e^{-i\tilde{\Delta}\frac{T}{2}} e^{-\frac{\tilde{\Delta}^2 T^2}{2\beta^2}} \int_{u(0)}^{u(T)} e^{-u^2} du \\
&= \frac{\alpha R}{2} e^{-i\tilde{\Delta}\frac{T}{2}} e^{-\frac{\tilde{\Delta}^2 T^2}{2\beta^2}} \left[erf\left(\frac{\beta}{2\sqrt{2}} - i\frac{\tilde{\Delta}T}{\sqrt{2}\beta}\right) + erf\left(\frac{\beta}{2\sqrt{2}} + i\frac{\tilde{\Delta}T}{\sqrt{2}\beta}\right)\right] \\
&\approx \alpha R e^{-i\tilde{\Delta}\frac{T}{2}} e^{-\frac{\tilde{\Delta}^2 T^2}{2\beta^2}} erf\left(\frac{\beta}{2\sqrt{2}}\right)
\end{aligned}
\tag{3.29}
$$

Where we have assumed that $\frac{\tilde{\Delta}T}{\sqrt{2}\beta} << 1$, which is fulfilled in the regime where $\beta >> 1$. Now we will use the value of the normalization constant that we found from 3.16 into 3.29:

$$
c_3^{(1)}(T) \approx \pi R e^{-i\tilde{\Delta}\frac{T}{2}} e^{-\frac{\tilde{\Delta}^2 T^2}{2\beta^2}}
$$

We have derived $c_3(T)$ up to first order:

$$
c_3(T) \simeq c_3^{(0)}(T) + \epsilon c_3^{(1)}(T) \simeq i\frac{\pi R}{2}\frac{\tilde{\Omega}_3}{|\tilde{\Omega}_3|} e^{-i\tilde{\Delta}\frac{T}{2}} e^{-\frac{\tilde{\Delta}^2 T^2}{2\beta^2}} \tag{3.30}
$$

We can compute $|c_0|^2$ by using $|c_0|^2 = 1 - |c_3|^2$, with the coefficients derived from equation 3.30 and assuming that $R = 1$.

$$
|c_0(T)|^2 \approx 1 - \frac{\pi^2}{4} e^{-\frac{\tilde{\Delta}^2 T^2}{\beta^2}} \tag{3.31}
$$

Unfortunately, when comparing the analytical results for $|c_0|^2$ and $|c_3|^2$ with the numerical results, we see that there is not a good agreement. In order to understand why the analytical expansion failed to capture properly the dynamics of the system, we have investigated the time evolution of $|c_0|^2$ and $|c_3|^2$ coefficients during the pulse (fig. 3.6 left).

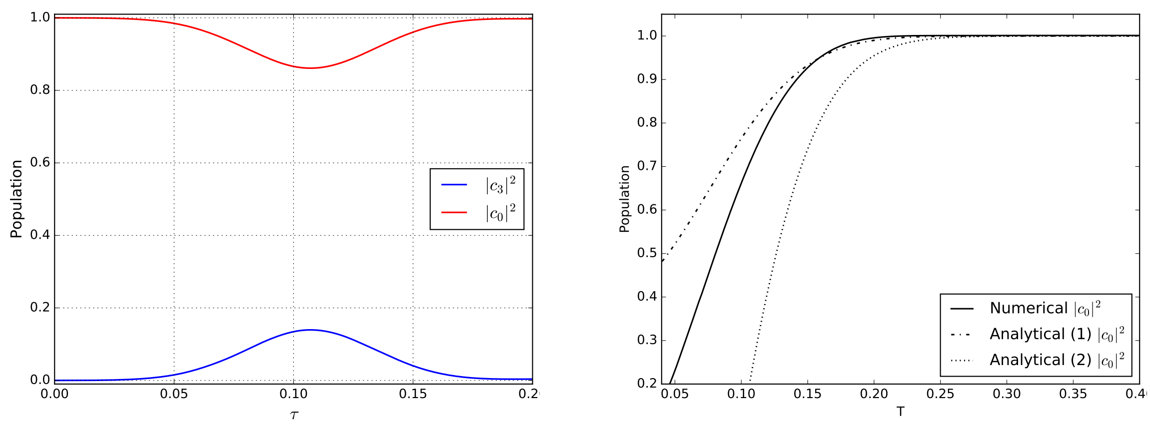

Figure 3.6.: (Left) Plot of the evolution of $|c_0|^2$ and $|c_3|^2$ during the pulse, with the legth of the pulse T being the optimal to maximize the strict fidelity. (Right): Plot of the analytical and numerical $|c_0|^2$. Analytical (2) corresponds to the derived analytical expression. Analytical (1) corresponds tot the analytical expression with an extra $\frac{1}{4}$ factor.

As one can see (fig. 3.6 (left)), the coefficients are far from remaining constant during their evolution. For this reason, the perturbative approximation that we have used to describe them is expected to fail in the optimal time regime. In figure 3.6 (right) one can see the numerical evolution of $|c_0|^2$, the plot of eq. 3.31 and the plot of eq. 3.31 with an extra $\frac{1}{4}$ factor. The analytical expression that we have obtained only converges with the numerics for long pulses T. In the regime we are interested, the approximation is not good. By comparing the numerical and analytical results we have noticed that by adding a factor $\frac{1}{4}$, the analytical expression approximates much better the numerical results. For this reason, we will use the analytical result with this extra factor:

$$|c_0(T)|^2 \approx 1 - \frac{\pi^2}{16} e^{-\frac{\tilde{\Delta}^2 T^2}{\beta^2}} \tag{3.32}$$

3.4.1. Strict fidelity and numerical comparison

Now we are able to compute the mathematical fidelity $F = |c_2 c_0|^2$.

$$F = |c_2 c_0|^2 \simeq \left(1 - \frac{T}{2}\right)\left(1 - \frac{\pi^2}{16} e^{-\frac{\tilde{\Delta}^2 T^2}{\beta^2}}\right) \tag{3.33}$$

Our goal in this section is to find the optimal duration of the pulse T. As we can see, the fidelity does depend on the duration of the pulse T. We will find the optimal T by performing the derivative of the fidelity, and solving the equation:

$$\begin{aligned} \frac{dF}{dT} &= \frac{\pi^2}{8} e^{-\frac{\tilde{\Delta}^2 T^2}{\beta^2}} \left[\frac{1}{4} + \frac{\tilde{\Delta}^2 T}{\beta^2} - \frac{\tilde{\Delta}^2 T^2}{2\beta^2}\right] - \frac{1}{2} = 0 \\ \Rightarrow T &= \frac{\beta}{\tilde{\Delta}} \sqrt{ln\left[\frac{\pi^2}{4}\left(\frac{1}{4} + \frac{\tilde{\Delta}^2 T}{\beta^2} - \frac{\tilde{\Delta}^2 T^2}{2\beta^2}\right)\right]} \end{aligned} \tag{3.34}$$

The solution for the optimal time (eq. 3.34) does depend upon itself . Here we will perform the approximation $T \approx \frac{2\beta}{\tilde{\Delta}}$ and we will get rid of the small terms to end with:

$$\boxed{T \simeq \frac{\beta}{\tilde{\Delta}} \sqrt{ln\left(\frac{\pi^2}{2}\frac{\tilde{\Delta}}{\beta}\right)}}$$

With the optimal time, we can compute the analytical fidelity:

$$F \simeq 1 - \frac{\beta}{2\tilde{\Delta}}\left(\frac{1}{4} + \sqrt{ln\left(\frac{\pi^2}{2}\frac{\tilde{\Delta}}{\beta}\right)}\right) + \frac{\beta^2}{16\tilde{\Delta}^2}\sqrt{ln\left(\frac{\pi^2}{2}\frac{\tilde{\Delta}}{\beta}\right)} \tag{3.35}$$

In appendix B.1 one can find the comparison between the numerical and the analytical strict fidelities.

As one can see in figure 3.7, the oscillations that were present in the square regime do not appear in the Gaussian regime. It is also important to notice that the optimal time T is longer. This is produced due to the fact that the Gaussian pulse achieves a higher peak of intensity, which drives population to the far-detuned transition more easily.

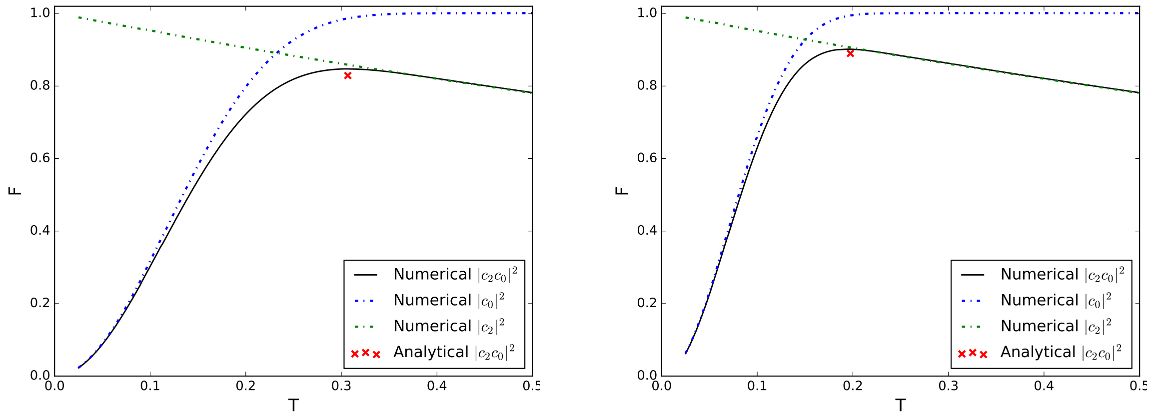

Figure 3.7.: Plots of the strict fidelity as a function of the length of the pulse T, with $\tilde{\Delta} = 30$ (left) and $\tilde{\Delta} = 50$ (right), with $\beta = 5$

In figure 3.8 we can see a 2D map of the $ln(1 - F)$ as a function of $\tilde{\Delta}$ and T, for $\beta = 5$. As expected, the optimal time shrinks as $\tilde{\Delta}$ increases. In this plot it can clearly be seen that fluctuations present in the square pulse do not appear in this regime. There is only one global maximum.

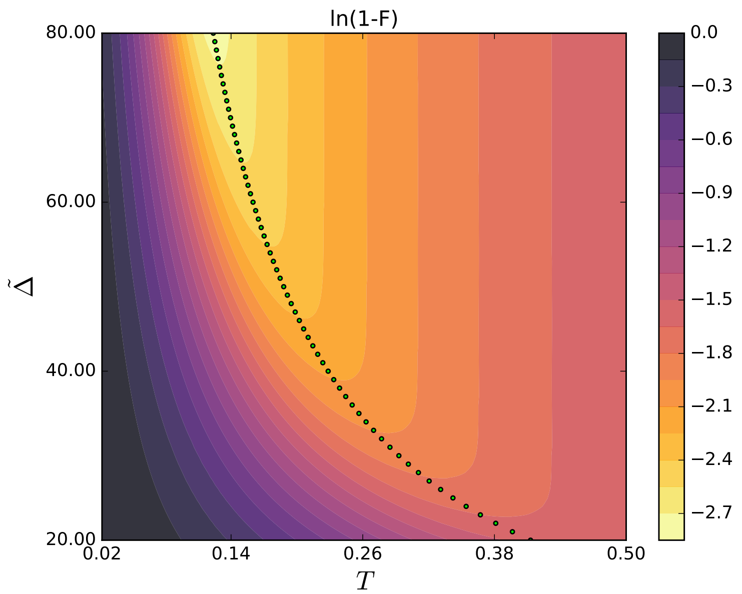

Figure 3.8.: 2D colormap of the numerical results for the $ln(1 - F)$ as a function of the length of the pulse T (x axis) and the normalized detuning $\tilde{\Delta}$ (y axis), with $\beta = 5$. The green-dotted line corresponds to the analytical optimal time for the Gaussian pulse

Finally, figure 3.9 contains the same 2D colormap but for a Gaussian-shaped pulse with $\beta = 0.5$. In this regime we can see that the behavior resembles very much the constant pulse. For this reason, even if the shape of the pulse is Gaussian, depending on the width of the pulse, it may be interesting to use the analytical results found in the previous section.

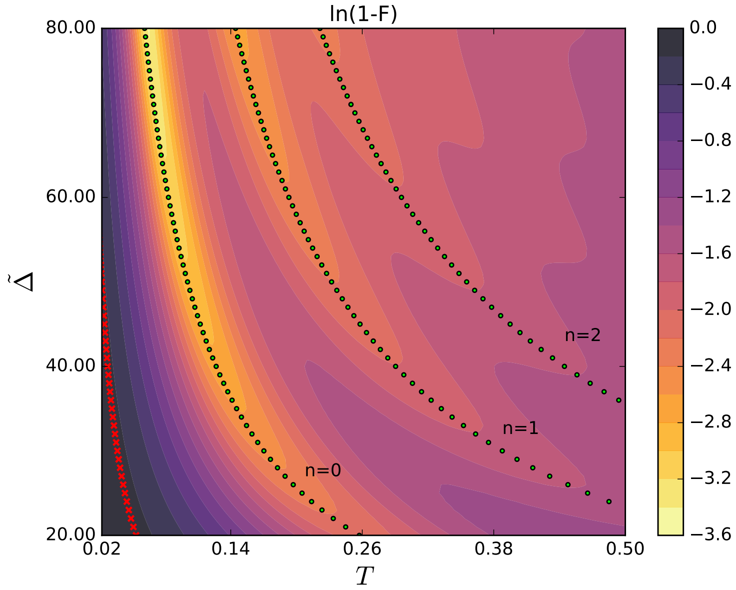

Figure 3.9.: 2D colormap of the numerical reluslts for the $ln(1-F)$ as a function of the length pulse T (x axis) and the normalized detuning $\tilde{\Delta}$ (y axis), with $\beta = 0.5$. The green-dotted lines corresponds to the analytical optimal times $n = \{0, 1, 2\}$ for the square pulse. The red dotted line correspond to the analytical optimal time for the Gaussian pulse.

4. Inhomogeneous broadening and relaxation of the far-detuned transition

4.1. Description of the inconsistencies

Now that we have solved the dynamics of the system just with the extra energy level, we will start adding more inconsistencies in order to build up the final system. In the previous chapter, we have optimized the length of the pulse T for the square and for the Gaussian pulses. In this section we will add inhomogeneous broadening and spontaneous emission from the excited state $|3\rangle$. In figure 4.1 one can see a graphical representation of our system with these features added.

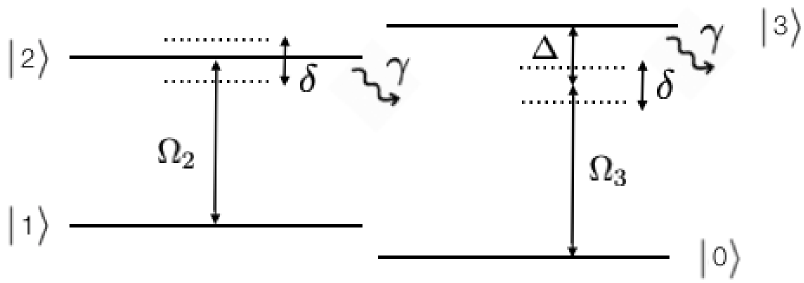

Figure 4.1.: Scheme of the 3-level system used to generate the spin-photon GHZ entangled state with the addition of the far-detuned energy level with inhomogeneous broadening and spontaneous emission.

As we will see, both the spontaneous emission from the far-detuned transition and the inhomogeneous broadening will affect the fidelities weakly, they will appear on the second order $\tilde{\Delta}^{-2}$ in the series expansion. Due to this reason, up to first order in $\tilde{\Delta}$, the optimal times found in the previous chapter will still be valid.

Taking into account the spontaneous emission from the extra energy level is a realistic approach because, unless this transition is shielded from decay, it will relax. Also, as we will se in the next section, taking into account spontaneous emission form both excited states will considerably simplify the wave-function expression, allowing us to exploit its symmetry in the conditional fidelity computation. In our case, we will assume that the spontaneous emission from both excites states is the same $\gamma_{12} = \gamma_{03} = \gamma$, which is a reasonable approximation for the realization of the protocol with quantum dots [10, 28].

Inhomogeneous broadening consists on fluctuations of the laser frequency or the energy states [11, 12]. We will assume that the inhomogeneous broadening is constant for each realization, but it will change from one experiment to the next one. We will assume that for each realization the broadening $\tilde{\delta}$ will be drawn from a Gaussian distribution (eq. 4.2). For this reason, we will have to convolute the density matrix of the system with the inhomogeneous broadening distribution:

$$
\begin{aligned}
\hat{\rho}(T) &= \int_{-\infty}^{\infty} \hat{\rho}(T,\tilde{\delta})p(\tilde{\delta})d\tilde{\delta} \\
&= \int_{-\infty}^{\infty} |e\rangle\langle e| \, |c_e|^2(T,\tilde{\delta})p(\tilde{\delta})d\tilde{\delta} + \int_{-\infty}^{\infty} |g\rangle\langle g| \, |c_g|^2(T,\tilde{\delta})p(\tilde{\delta})d\tilde{\delta} \\
&+ \int_{-\infty}^{\infty} |e\rangle\langle g| \, c_e c_g^*(T,\tilde{\delta})p(\tilde{\delta})d\tilde{\delta} + \int_{-\infty}^{\infty} |g\rangle\langle e| \, c_g c_e^*(T,\tilde{\delta})p(\tilde{\delta})d\tilde{\delta}
\end{aligned}
\tag{4.1}
$$

From equation 4.1 we see that the convoluted populations of the energy levels, $|c_i|^2$ are:

$$
|c_i(T)|^2 = \int_{-\infty}^{\infty} |c_i(T,\tilde{\delta})|^2 p(\tilde{\delta})d\tilde{\delta} \qquad p(\tilde{\delta}) = \frac{1}{\sqrt{2\pi}\sigma_b} e^{-\left(\frac{\tilde{\delta}^2}{\sqrt{2}\sigma_b}\right)^2}
\tag{4.2}
$$

4.2. System wave-function

As described in section 3.1, the protocol starts with the superposition $|\Psi\rangle = \frac{1}{\sqrt{2}}(|0\rangle + |1\rangle)$. From this initial state, a sequence of pulses and relaxation times is applied. Now, we will work out the final state $M|\Psi\rangle$, taking into account inhomogeneous broadening and spontaneous emission. For the early part of the protocol, consisting on one π_{1-2} pulse and a relaxation time window, the wave-function of the system will become:

$$
\begin{aligned}
&\frac{1}{\sqrt{2}}(|0,\emptyset\rangle + |1,\emptyset\rangle) \xrightarrow{\pi_{1-2}} \frac{1}{\sqrt{2}}(c_0|0,\emptyset\rangle + c_3|3,\emptyset\rangle + c_1|1,\emptyset\rangle + c_2|2,\emptyset\rangle) \\
&\xrightarrow{s.e.} \frac{1}{\sqrt{2}}\left(c_0|0,\emptyset\rangle + c_3\hat{B}_0^{\dagger,e}|0,\emptyset\rangle + c_1|1,\emptyset\rangle + c_2\hat{A}_0^{\dagger,e}|1,\emptyset\rangle\right) \\
&= \frac{1}{\sqrt{2}}\left(c_0 + c_3\hat{B}_0^{\dagger,e}\right)|0,\emptyset\rangle + \frac{1}{\sqrt{2}}\left(c_1 + c_2\hat{A}_0^{\dagger,e}\right)|1,\emptyset\rangle \\
&= \frac{1}{\sqrt{2}}(Q_0^e|0,\emptyset\rangle + Q_1^e|1,\emptyset\rangle)
\end{aligned}
$$

Where operators $\{\hat{A}_0^\dagger, \hat{B}_0^\dagger\}$ are formally derived in section 5.2. The action of the early part of the protocol can be encoded into two operators, Q_0^e and Q_1^e. At this point, to finish the protocol, one would need to flip the ground states by applying a π_{0-1} pulse, apply the exact same procedure as in the early part and flip again the two ground states.

Due to the symmetry of the system, the late part of the protocol can be described by the action of the operator Q_1^L onto $|0,\emptyset\rangle$ and the operator Q_0^L onto $|1,\emptyset\rangle$. The resulting state after generating one qubit (one cycle of the protocol) is:

$$
\begin{aligned}
M|\Psi\rangle &= \frac{-1}{\sqrt{2}}\left(Q_1^L Q_0^e|0,\emptyset\rangle + Q_0^L Q_1^e|1,\emptyset\rangle\right) \\
&= \frac{-1}{\sqrt{2}}\left(Q_{10}^{Le}|0,\emptyset\rangle + Q_{01}^{Le}|1,\emptyset\rangle\right)
\end{aligned}
\tag{4.3}
$$

Notice that $Q_0^e(Q_1^L)$ contains the coefficients and creation operators for the early (late) part of the protocol from the $|0\rangle - |3\rangle$ ($|1\rangle - |2\rangle$) transition. Also, $Q_{10}^{Le} \equiv Q_1^L Q_0^e$ and $Q_{10}^{Le} \equiv Q_0^L Q_1^e$.

For the generation of N entangled photons, the same operators will be applied N times:

$$
M^N|\Psi\rangle = \frac{(-1)^N}{\sqrt{2}}\left(\prod_{k=1}^{N} Q_{10}^{Le,k}|0,\emptyset\rangle + \prod_{k=1}^{N} Q_{01}^{Le,k}|1,\emptyset\rangle\right)
\tag{4.4}
$$

Where k corresponds to the cycle from which the photons have been generated.

4.3. Conditional Fidelity

In Chapter 3 we have been using the most strict expression of the fidelity, where we only consider a success when we end up in the exact ideal state, any variation from it is considered as an unsuccessful result.

This definition of fidelity is not experimentally realistic because generally, all the experimental realizations containing lost photons are discarded and not taken into account. Due to this fact, we are interested in computing the fidelity conditioned on the fact that our detector has measured something ("clicked") on every cycle.

Notice that this new definition of fidelity is less restrictive . On the contrary, since we will only take into account experimental realizations with nonzero measurements on each cycle of the protocol, the probability to accept an experimental realization will decrease, hence decreasing the protocol's probability of success.

By using the density matrix formalism explained in section 2.2, the expression for the conditional fidelity is:

$$F = \frac{\langle\Psi_{id}|\, P_{N\geq1}\rho P_{N\geq1}\,|\Psi_{id}\rangle}{tr(P_{N\geq1}\rho)}$$

Where $P_{N\geq1}$ is the projector onto the subspace where there has been at least one photon detected on each cycle of the protocol. In eq. 4.5 we have rewritten the conditional fidelity by using $\hat{\rho} = |\Psi_{re}\rangle\langle\Psi_{re}|$.

$$F = \frac{|\langle\Psi_{id}|\, P_{N\geq1}\,|\Psi_{re}\rangle|^2}{tr(P_{N\geq1}\hat{\rho})} \tag{4.5}$$

For the ideal state $|\Psi_{id}\rangle$ we will assume it to be:

$$|\Psi_{id}\rangle = \frac{1}{\sqrt{2}}\left(\hat{A}_0^{\dagger,L}\,|0,\emptyset\rangle + \hat{A}_0^{\dagger,e}\,|1,\emptyset\rangle\right) \equiv \frac{1}{\sqrt{2}}\left(|0,L\rangle + |1,e\rangle\right) \tag{4.6}$$

We can use this definition because we assume that all the photons that arrive at the detector will be emitted during the relaxation window. There will not be any photon detected outside the time windows where the main excited state $|2\rangle$ is expected to relax. For this reason, it will not be necessary to take into account any overlap between photonic wavefunctions.

4.3.1. Conditional fidelity without filter

We will start by computing the conditional fidelity for one qubit ($N = 1$). Once we understand the conditional fidelity for one qubit we will generalize it and compute the expression for N qubits. Finally, the presence of frequency filters and the system efficiency will be taken into account.

From equation 4.3, we know that the wavefunction of the system, after one cycle of the protocol, can be expressed as:

$$|\Psi\rangle = \frac{1}{\sqrt{2}}\left(Q_{01}^{eL}\,|0,\emptyset\rangle + Q_{10}^{eL}\,|1,\emptyset\rangle\right)$$

Where

$$\begin{aligned}Q_{01}^{eL} = Q_0^e Q_1^L = \left(c_0 + c_3 \hat{B}_0^{\dagger,e}\right)\left(c_1 + c_2 \hat{A}_0^{\dagger,L}\right) \\ = c_0c_1 + c_0c_2\hat{A}_0^{\dagger,L} + c_3c_1\hat{B}_0^{\dagger,e} + c_3c_2\hat{B}_0^{\dagger,e}\hat{A}_0^{\dagger,L}\end{aligned}$$

Now we will apply the projection onto the subspace where at least one photon has been detected on each round of the protocol. This corresponds experimentally to discard all the events where there was no photon detected on every cycle.

$$P_{N\geq 1}Q_{01}^{eL} = \tilde{Q}_{01}^{eL} = c_0c_2\hat{A}_0^{\dagger,L} + c_3c_1\hat{B}_0^{\dagger,e} + c_3c_2\hat{B}_0^{\dagger,e}\hat{A}_0^{\dagger,L}$$

Notice that we are keeping the term $c_3c_2\hat{B}_0^{\dagger,e}\hat{A}_0^{\dagger,L}$, from $\tilde{Q}_{01}^{eL}$. This term corresponds to the generation of one photon in the first part of the cycle (early) and another in the late part of the cycle (late). It should be possible to detect and discard these events if are measured on the $\hat{z}$ basis. In order to experimentally characterize the generation of GHZ states, measurements on the $\hat{x}$ and $\hat{z}$ basis are necessary to be performed [29] [30]. When the generated state is measured on the $\hat{x}$ basis, the two photons arriving early and late will no longer arrive on separate time bins, and therefore, will not be distinguishable. For this reason, we will keep these terms in the computation of the fidelity.

For $N = 1$, the overlap between $|\langle\Psi_{id}| P_{N\geq 1} |\Psi_{re}\rangle|^2$ can be expanded as:

$$\begin{aligned}
&|\langle\Psi_{id}| P_{N\geq1} |\Psi_{re}\rangle|^2 = \langle\Psi_{id}| P_{N\geq1} |\Psi_{re}\rangle (h.c.) = \\
&\frac{1}{4}\left[(\langle 0,L| + \langle 1,e|)\left(\tilde{Q}_{01}^{eL}|0,\emptyset\rangle + \tilde{Q}_{10}^{eL}|1,\emptyset\rangle\right)\right](h.c.) \\
&= \frac{1}{4}\left[\langle 0,L|\tilde{Q}_{01}^{eL}|0,\emptyset\rangle + \langle 1,e|\tilde{Q}_{10}^{eL}|1,\emptyset\rangle\right](h.c.) \\
&= \frac{1}{4}\left[\langle 0,L|\left(c_0c_2\hat{A}_0^{\dagger,L} + c_3c_1\hat{B}_0^{\dagger,e} + c_3c_2\hat{B}_0^{\dagger,e}\hat{A}_0^{\dagger,L}\right)|0,\emptyset\rangle\right. \\
&\left. + \langle 1,e|\left(c_1c_3\hat{B}_0^{\dagger,L} + c_2c_0\hat{A}_0^{\dagger,e} + c_2c_3\hat{A}_0^{\dagger,e}\hat{B}_0^{\dagger,L}\right)|1,\emptyset\rangle\right](h.c.) \\
&= \frac{1}{4}[c_0c_2 + c_0c_2](h.c.) = |c_0c_2|^2
\end{aligned} \tag{4.7}$$

For the denominator part of the conditional fidelity we will have the trace over S, all combinations of photonic modes $\{\hat{A}_0^{\dagger,L}, \hat{A}_0^{\dagger,e}, \hat{B}_0^{\dagger,L}, \hat{B}_0^{\dagger,e}\}$ that can get to the detector.

$$\begin{aligned}
tr[\hat{\rho}] &= \frac{1}{2}tr\left[\left(\tilde{Q}_{01}^{eL}|0,\emptyset\rangle + \tilde{Q}_{10}^{eL}|1,\emptyset\rangle\right)(h.c.)\right] = \\
&= \frac{1}{2}\sum_S\left(\langle 0,S|\tilde{Q}_{01}^{eL}|0,\emptyset\rangle + \langle 1,S|\tilde{Q}_{10}^{eL}|1,\emptyset\rangle\right)(h.c.) \\
&= \frac{1}{2}\sum_S\langle 0,S|\left(c_0c_2\hat{A}_0^{\dagger,L} + c_3c_1\hat{B}_0^{\dagger,e} + c_3c_2\hat{B}_0^{\dagger,e}\hat{A}_0^{\dagger,L}\right)|0,\emptyset\rangle(h.c.) \\
&+ \frac{1}{2}\sum_S\langle 1,S|\left(c_1c_3\hat{B}_0^{\dagger,L} + c_2c_0\hat{A}_0^{\dagger,e} + c_2c_3\hat{A}_0^{\dagger,e}\hat{B}_0^{\dagger,L}\right)|1,\emptyset\rangle(h.c.) \\
&= |c_0c_2|^2 + |c_3c_1|^2 + |c_3c_2|^2 \equiv P_s
\end{aligned}$$

Inside the trace, the only terms that survive are the ones that connect with themselves. For this reason, we only end up with the modulus square of each coefficient in $\tilde{Q}_{01}^{eL}$. The denominator of the conditional fidelity is the probability of success, in other words, the probability of detecting photons on each round, therefore, not discarding the realization.

By getting together the nominator and the denominator parts of the fidelity, we obtain:

$$F = \frac{|c_0c_2|^2}{|c_0c_2|^2+|c_3c_1|^2+|c_3c_2|^2} \tag{4.8}$$

The probability of ending in the right state $|c_0c_2|^2$ (nominator) is the strict fidelity. But it is normalized with the probability of measuring at least one photon (denominator). Because of this reason, the two terms that play an important role in the conditional fidelity are $|c_3c_1|^2$ and $|c_3c_2|^2$. The first one consists on getting one photon from the off-resonant transition and the second one consists on getting two photons, one from the main transition and another from the off.resonant one.

Now that we have computed the conditional fidelity for one qubit (N=1), we will derive the general expression for N qubits (performing N cycles). Remember that the state of the system for N qubits is:

$$|\Psi_{re}\rangle = \frac{(-1)^N}{\sqrt{2}} \left[\prod_{k=1}^{N} Q_0^{e,k} Q_1^{L,k} |0, \emptyset\rangle + \prod_{k=1}^{N} Q_1^{e,k} Q_0^{L,k} |1, \emptyset\rangle \right]$$

Where k corresponds to photons produced in the k'th cycle. The ideal state (GHZ state with N qubits) is defined as:

$$|\Psi_{re}\rangle = \frac{1}{\sqrt{2}} \left(|0, L^{\otimes N}\rangle + |1, e^{\otimes N}\rangle \right)$$

Now we will proceed by computing the overlap of the ideal state with the system state projected onto $P_{N\geq 1}$:

$$\begin{aligned}
\langle\Psi_{id}| P_N |\Psi_{re}\rangle &= \frac{(-1)^N}{2} \left[\langle 0, L^{\otimes N}| + \langle 1, e^{\otimes N}| \right] \left[\prod_{k=1}^{N} \tilde{Q}_{01}^{eL,k} |0, \emptyset\rangle + \prod_{k=1}^{N} \tilde{Q}_{10}^{eL,k} |1, \emptyset\rangle \right] \\
&= \frac{(-1)^N}{2} \left[\langle L^{\otimes N}| \prod_{k=1}^{N} \tilde{Q}_{01}^{eL,k} |\emptyset\rangle + \langle e^{\otimes N}| \prod_{k=1}^{N} \tilde{Q}_{10}^{eL,k} |\emptyset\rangle \right] \\
&= (-1)^N \langle L^{\otimes N}| \prod_{k=1}^{N} \tilde{Q}_{01}^{eL,k} |\emptyset\rangle
\end{aligned}$$

Where in the last step we have used the symmetry of the $\hat{Q}_{01}^{eL}$ and $\hat{Q}_{10}^{eL}$ operators. As previously explained, the early part of $\hat{Q}_{01}^{eL}$ operator does only contain coefficients involved with the $|0\rangle \leftrightarrow |3\rangle$ transition and the late part only contains coefficients from $|1\rangle \leftrightarrow |2\rangle$. The operator $\hat{Q}_{10}^{eL}$ contains the same coefficients but chaning (e) by (L). For this reason:

$$\langle L^{\otimes N}| \prod_{k=1}^{N} \tilde{Q}_{01}^{eL,k} |\emptyset\rangle = \langle e^{\otimes N}| \prod_{k=1}^{N} \tilde{Q}_{10}^{eL,k} |\emptyset\rangle \tag{4.9}$$

$$\begin{aligned}
\langle\Psi_{id}| P_N |\Psi_{re}\rangle &= (-1)^N \left[\langle L^{\otimes N}| \prod_{k=1}^{N} \left(c_0c_2 \hat{A}_0^{\dagger,L,k} + c_3c_1 \hat{B}_0^{\dagger,e,k} + c_3c_2 \hat{B}_0^{\dagger,e,k} \hat{A}_0^{\dagger,L,k} \right) |\emptyset\rangle \right] \\
&= (-1)^N (c_0c_2)^N
\end{aligned}$$

In the last step of the calculation the only term that survives is $\langle L^{\otimes N}| (c_0c_2)^N \hat{A}_0^{\dagger,L,N}...\hat{A}_0^{\dagger,L,1}\hat{A}_0^{\dagger,L,0}|\emptyset\rangle$. Therefore, the nominator of the conditional fidelity is $|\langle\Psi_{Id}| P_N |\Psi_{re}\rangle|^2 = |c_0c_2|^{2N}$.

Now we will compute the denominator of the conditional fidelity $P_S = tr(P_{N\geq 1}\hat{\rho})$.

$$
\begin{aligned}
&tr(P_{N\geq 1}\hat{\rho}P_{N\geq 1}) \\
&= \frac{1}{2}tr\left[\left(\prod_{k=1}^{N}\tilde{Q}_{01}^{eL,k}|0,\emptyset\rangle + \prod_{k=1}^{N}\tilde{Q}_{01}^{eL,k}|1,\emptyset\rangle\right)\left(\prod_{k=1}^{N}\langle 0,\emptyset|\tilde{Q}_{01}^{\dagger,eL,k} + \prod_{k=1}^{N}\langle 1,\emptyset|\tilde{Q}_{01}^{\dagger,eL,k}\right)\right] \\
&= \frac{1}{2}tr\left(\prod_{k=1}^{N}\tilde{Q}_{01}^{eL,k}|0,\emptyset\rangle\prod_{k=1}^{N}\langle 0,\emptyset|\tilde{Q}_{01}^{\dagger,eL,k}\right) + \frac{1}{2}tr\left(\prod_{k=1}^{N}\tilde{Q}_{10}^{eL,k}|1,\emptyset\rangle\prod_{k=1}^{N}\langle 1,\emptyset|\tilde{Q}_{10}^{\dagger,eL,k}\right) \\
&= tr\left(\prod_{k=1}^{N}\tilde{Q}_{01}^{eL,k}|0,\emptyset\rangle\prod_{k=1}^{N}\langle 0,\emptyset|\tilde{Q}_{01}^{\dagger,eL,k}\right)
\end{aligned}
$$

Where we have again used the symmetry of $\hat{Q}_{01}^{eL}$. The trace of the density matrix containing the operator $\hat{Q}_{01}^{eL}$ and the one containing $\hat{Q}_{10}^{eL}$ must be the same, since they describe the same physical phenomenon but with the early and late parts interchanged. The sum pf the diagonal remains unchanged.

$$
\begin{aligned}
tr(P_{N\geq 1}\hat{\rho}P_{N\geq 1}N) &= \sum_S \langle 0,S|\left(\prod_{k=1}^{N}\tilde{Q}_{01}^{eL,k}|0,\emptyset\rangle\langle 0,\emptyset|\prod_{k=1}^{N}\tilde{Q}_{01}^{\dagger,eL,k}\right)|0,S\rangle \\
&= \sum_S \langle 0,S|\left(\prod_{k=1}^{N}\tilde{Q}_{01}^{eL,k}|0,\emptyset\rangle\right)(h.c.)
\end{aligned}
$$

With S being all possible combinations of $\{\hat{A}_0^{\dagger,L}, \hat{A}_0^{\dagger,e}, \hat{B}_0^{\dagger,L}, \hat{B}_0^{\dagger,e}\}$, making up to N photons. Due to this reason, the denominator part will consist on all the possible combinations of photonic excitations present in $\tilde{Q}_{01}^{eL}$, therefore:

$$tr(P_{N\geq 1}\hat{\rho}P_{N\geq 1}) = \left[|c_0c_2|^2 + |c_3c_1|^2 + |c_3c_2|^2\right]^N$$

And the conditional fidelity will be:

$$F = \frac{|c_0c_2|^{2N}}{(|c_0c_2|^2 + |c_3c_1|^2 + |c_3c_2|^2)^N} \tag{4.10}$$

4.3.2. Conditional fidelity with filter and experimental efficiency

In this subsection we will compute the conditional fidelity by taking into account the efficiency of the experimental setup and assuming that cavity frequency filters [31] are being used to get rid of the undesired photons (coming from the far-detuned transition) and allowing to pass the photons coming from the main transition. We will model the action of the frequency filters by assuming that they do not behave ideally. Equation 4.11 describes the action of the filters on the photonic excitations coming from the system.

$$
\begin{aligned}
A_0^\dagger &\to \sqrt{\eta_2}A_0^\dagger + \sqrt{1-\eta_2}\tilde{A}_0^\dagger \\
B_0^\dagger &\to \sqrt{\eta_3}B_0^\dagger + \sqrt{1-\eta_3}\tilde{B}_0^\dagger
\end{aligned} \tag{4.11}
$$

Where $\eta_2 = \eta_{f2}\eta_e$ and $\eta_3 = \eta_{f3}\eta_e$. η_e corresponds to the efficiency of the system (due to all the inconsistencies of the experimental setup) and η_{f2} and η_{f3} describe the filtering process. If we want to consider the system without filters, we will have to set $\eta_{f2} = \eta_{f3} = 1$.

The operator Q_{01}^{eL}, when taking into account the action of the filters has the form:

$$Q_{01}^{eL} = Q_0^e Q_1^L = \left(c_0 + c_3\sqrt{\eta_3}B_0^{\dagger,e} + c_3\sqrt{1-\eta_3}\tilde{B}_0^{\dagger,e}\right)\left(c_1 + c_2\sqrt{\eta_2}A_0^{\dagger,L} + c_2\sqrt{1-\eta_2}\tilde{A}_0^{\dagger,L}\right)$$

After selecting only the events containing at least one photon we end up with:

$$\begin{aligned}
&P_{N\geq 1}Q_{01}^{eL} \\
&= c_0c_2\sqrt{\eta_2}A_0^{\dagger,L} + c_3c_1\sqrt{\eta_3}B_0^{\dagger,e} + c_3c_2\sqrt{\eta_3}\sqrt{1-\eta_2}B_0^{\dagger,e}\tilde{A}_0{}^{\dagger,L} \\
&+ c_3c_2\sqrt{1-\eta_3}\sqrt{\eta_2}\tilde{B}_0^{\dagger,e}A_0^{\dagger,L} + c_3c_2\sqrt{\eta_2}\sqrt{\eta_3}B_0^{\dagger,e}A_0^{\dagger,L}
\end{aligned}$$

The wavefunction of the system after N cycles is:

$$P_{N\geq 1}\left|\Psi_{re}\right\rangle = \frac{(-1)^N}{\sqrt{2}}\left[\prod_{k=1}^{N}\tilde{Q}_{01}^{eL,k}\left|0,\emptyset\right\rangle + \prod_{k=1}^{N}\tilde{Q}_{10}^{eL,k}\left|1,\emptyset\right\rangle\right]$$

Now, before continuing the computation of the fidelity we have to trace over the lost and filtered photons. The setup behaves as a bipartite system where we can only measure the subspace that contains photons that get to the detector.

Up to this point we were using the photonic vacuum $\left|\emptyset\right\rangle$ to describe all possible photonic modes. In this case, we will have photons that get to the detector and filtered or lost photons that we can not measure. For this reason, we will split the photonic vacuum into two parts, the modes of photons that are being measured and the modes that are not measured and will be traced over $\left|\emptyset_S, \emptyset_R\right\rangle$.

It will also be interesting to split the operator $\prod_{k=1}^{N}\tilde{Q}_{01}^{eL,k} = \tilde{D}_{01}^{eL} + \tilde{R}_{01}^{eL}$. Where $\tilde{D}_{01}^{eL}$ only contains combinations of photons that get to the detector and $\tilde{R}_{01}^{eL}$ contains combinations of lost and detected photons. Then, the trace over the reservoir modes (R) will become:

$$\begin{aligned}
&tr_R\left(P_{N\geq 1}\hat{\rho}P_{N\geq 1}\right) = \sum_R \left\langle R\right| P_{N\geq 1}\left|\Psi_{re}\right\rangle (h.c.) \\
&= \frac{1}{2}\sum_R \left\langle R\right|\left((\tilde{D}_{01}^{eL} + \tilde{R}_{01}^{eL})\left|0,\emptyset_S,\emptyset_R\right\rangle + (\tilde{D}_{10}^{eL} + \tilde{R}_{10}^{eL})\left|1,\emptyset_S,\emptyset_R\right\rangle\right)(h.c.) \\
&= \frac{1}{2}\left[\tilde{D}_{01}^{eL}\left|0,\emptyset_S\right\rangle + \tilde{D}_{10}^{eL}\left|1,\emptyset_S\right\rangle\right](h.c.) + \frac{1}{2}\sum_{R\neq\emptyset_R}\left[\left\langle R\right|\tilde{R}_{01}^{eL}\left|0,\emptyset_S,\emptyset_R\right\rangle + \left\langle R\right|\tilde{R}_{10}^{eL}\left|1,\emptyset_S,\emptyset_R\right\rangle\right](h.c.)
\end{aligned} \tag{4.12}$$

Where we have traced over the part containing only photons that get to the detector. We still have to perform the sum over R, which belongs to any possible configuration containing lost or filtered photons $\{\tilde{A}_0^\dagger, \tilde{B}_0^\dagger\}$. Now we will compute the overlap $\left\langle\Psi_{id}\right| tr_R\left(P_{N\geq 1}\hat{\rho}P_{N\geq 1}\right)\left|\Psi_{id}\right\rangle$:

$$
\begin{aligned}
&\langle \Psi_{id} | \, tr_R \left(P_{N\geq 1} \hat{\rho} P_{N\geq 1} \right) | \Psi_{id} \rangle \\
&= \frac{1}{4} \left[\left(\langle 0, L^{\otimes N} | + \langle 1, e^{\otimes N} | \right) \left(\tilde{D}_{01}^{eL} | 0, \emptyset_S \rangle + \tilde{D}_{10}^{eL} | 1, \emptyset_S \rangle \right) \right] (h.c.) \\
&+ \frac{1}{4} \left[\left(\langle 0, L^{\otimes N} | + \langle 1, e^{\otimes N} | \right) \sum_{R \neq \emptyset_R} \left[\langle R | \, \tilde{R}_{01}^{eL} | 0, \emptyset_S, \emptyset_R \rangle + \langle R | \, \tilde{R}_{10}^{eL} | 1, \emptyset_S, \emptyset_R \rangle \right] \right] (h.c.) \\
&= \frac{1}{4} \left[\langle 0, L^{\otimes N} | \, \tilde{D}_{01}^{eL} | 0, \emptyset_S \rangle + \langle 1, e^{\otimes N} | \, \tilde{D}_{10}^{eL} | 1, \emptyset_S \rangle \right] (h.c.) \\
&+ \frac{1}{4} \sum_{R \neq \emptyset_R} \left[\langle 0, L^{\otimes N}, R | \, \tilde{R}_{01}^{eL} | 0, \emptyset_S, \emptyset_R \rangle + \langle 1, e^{\otimes N}, R | \, \tilde{R}_{10}^{eL} | 1, \emptyset_S, \emptyset_R \rangle \right] (h.c.) \\
&= \frac{1}{4} \left[2 \langle 0, L^{\otimes N} | \, \tilde{D}_{01}^{eL} | 0, \emptyset_S \rangle \right] (h.c.) + \frac{1}{2} \sum_{R \neq \emptyset_R} \left[\langle 0, L^{\otimes N}, R | \, \tilde{R}_{01}^{eL} | 0, \emptyset_S, \emptyset_R \rangle \right] (h.c.)
\end{aligned}
\tag{4.13}
$$

Where symmetry of the $\tilde{D}_{01}^{eL}$ and $\tilde{R}_{01}^{eL}$ operators has been used. Notice that the term of the summation with $|R\rangle = |\emptyset_R\rangle$ contains two repeated factors $\langle 0, L^{\otimes N} | \, \tilde{D}_{01}^{eL} | 0, \emptyset_S \rangle$. All other terms of the summation, with $R \neq \emptyset_R$, are repeated (half of them coming from the early part and half of them coming from the late part) but each summand only contains one factor $\langle 0, L^{\otimes N}, R | \, \tilde{R}_{01}^{eL} | 0, \emptyset_S, \emptyset_R \rangle$.

In this case, from $\langle 0, L^{\otimes N} | \, \tilde{D}_{01}^{eL} | 0, \emptyset_S \rangle$ only survives the component $\left[c_0 c_2 \sqrt{\eta_2} \right]^N$. Also, inside $\sum_{R \neq \emptyset_R} \left[\langle 0, L^{\otimes N}, R | \, \tilde{R}_{01}^{eL} | 0, \emptyset_S, \emptyset_R \rangle \right]$ there are all possible combinations of $c_0 c_2 \sqrt{\eta_2}$ and $c_3 c_2 \sqrt{\eta_2} \sqrt{1 - \eta_3}$, except the one that only contains photons that are not lost. For this reason:

$$
\begin{aligned}
&\langle \Psi_{id} | \, tr_R \left(P_{N\geq 1} \hat{\rho} P_{N\geq 1} \right) | \Psi_{id} \rangle \\
&= \eta_2^N |c_0 c_2|^2 + \frac{1}{2} \left(\eta_2 |c_0 c_2|^2 + \eta_2 (1 - \eta_3) |c_3 c_2|^2 \right)^N - \frac{1}{2} \eta_2^N |c_0 c_2|^2 \\
&= \frac{1}{2} \eta_2^N |c_0 c_2|^2 + \frac{1}{2} \left(\eta_2 |c_0 c_2|^2 + \eta_2 (1 - \eta_3) |c_3 c_2|^2 \right)^N
\end{aligned}
\tag{4.14}
$$

For the denominator part of the conditional fidelity we will have:

$$
\begin{aligned}
&tr_S \left(tr_R \left(P_{N\geq 1} \hat{\rho} P_{N\geq 1} \right) \right) = \\
&\frac{1}{2} \sum_{P=\{0,1\}, S, R} \langle P, S, R | \left((\tilde{D}_{01}^{eL} + \tilde{R}_{01}^{eL}) | 0, \emptyset_S, \emptyset_R \rangle + (\tilde{D}_{10}^{eL} + \tilde{R}_{10}^{eL}) | 1, \emptyset_S, \emptyset_R \rangle \right) (h.c.) \\
&= \frac{1}{2} \sum_{S,R} \langle 0, S, R | \left((\tilde{D}_{01}^{eL} + \tilde{R}_{01}^{eL}) | 0, \emptyset_S, \emptyset_R \rangle \right) (h.c.) \\
&+ \frac{1}{2} \sum_{S,R} \langle 1, S, R | \left((\tilde{D}_{10}^{eL} + \tilde{R}_{10}^{eL}) | 1, \emptyset_S, \emptyset_R \rangle \right) (h.c.) \\
&= \sum_{S,R} \langle 0, S, R | \left((\tilde{D}_{01}^{eL} + \tilde{R}_{01}^{eL}) | 0, \emptyset_S, \emptyset_R \rangle \right) (h.c.)
\end{aligned}
$$

Where P corresponds to the spin transition of the atom/quantum dot. Notice that in this case, for each part of the sum only one term survives. We will end up with the modulus square of each possible combinations of photons that get to the detector (modulus square of each combination of the coefficients in $\tilde{Q}_{01}^{eL}$). For this reason,

$$tr_S\left(tr_R\left(P_{N\geq 1}\hat{\rho}P_{N\geq 1}\right)\right) = \left(\eta_2|c_0c_2|^2 + \eta_3|c_3c_1|^2 + \left[\eta_2\eta_3 + \eta_2(1-\eta_3) + (1-\eta_2)\eta_3\right]|c_3c_2|^2\right)^N$$

Finally, by grouping the nominator and denominator parts, the conditional fidelity of the system taking into account the presence of a cavity filter and the efficiency of the system, for N qubits is

$$\boxed{F = \frac{\frac{1}{2}\eta_2^N|c_0c_2|^{2N} + \frac{1}{2}\left(\eta_2|c_0c_2|^2 + \eta_2(1-\eta_3)|c_3c_2|^2\right)^N}{\left(\eta_2|c_0c_2|^2 + \eta_3|c_3c_1|^2 + \left[\eta_2\eta_3 + \eta_2(1-\eta_3) + (1-\eta_2)\eta_3\right]|c_3c_2|^2\right)^N}} \quad (4.15)$$

The factor $|c_0c_2|^2$ is no longer the only one that contributes to the fidelity. The coefficient $\eta_2(1-\eta_3)|c_3c_2|^2$ describes the emission of two photons, one from the main transition and the other from the far-detuned transition, where the photon from the main transition has passed the filter (η_2) and the undesired photon has been filtered ($1-\eta_3$). The factor $\frac{1}{2}$ comes from the fact that, when we trace over the environment (removing the filtered photon), only half of the times we will end within the right state.

4.4. Square-shaped pulse coefficients

Now that we have a complete description of the state of our system and the conditional fidelity, we will derive analytical expressions for the coefficients $\{c_1, c_2, c_0, c_3\}$ in the square-pulse regime.

In equation 4.16 we have written the equations of motion for the two transitions taking into account the spontaneous emission form the two excited states and the inhomogeneous broadening.

$$\dot{c}_3(\tau) = \left(-i\tilde{\Delta} - i\tilde{\delta} - \frac{1}{2}\right)c_3(\tau) + i\frac{\tilde{\Omega}_3}{2}c_0(\tau) \qquad \dot{c}_0(\tau) = i\frac{\tilde{\Omega}_3^*}{2}c_3(\tau) \quad (4.16)$$

And:

$$\dot{c}_2(\tau) = \left(-i\tilde{\delta} - \frac{1}{2}\right)c_2(\tau) + i\frac{\tilde{\Omega}_2}{2}c_1(\tau) \qquad \dot{c}_1(\tau) = i\frac{\tilde{\Omega}_2^*}{2}c_2(\tau)$$

With $\hat{\Omega}_2 = \sqrt{(\tilde{\delta} - \frac{i}{2})^2 + \tilde{\Omega}_2^2}$ and $\hat{\Omega}_3 = \sqrt{(\tilde{\Delta} + \tilde{\delta} - \frac{i}{2})^2 + \tilde{\Omega}_3^2}$. As we have seen in section 2.4.1, the equations for the square pulse can be solved exactly. Our goal is to boil down the main dynamics of the system into a power series of $\tilde{\Delta}$.

We will set the optimal pulse length T to be the one derived in Chapter 3, where we obtained the solutions for the square pulse without broadening nor spontaneous emission in the extra energy level.

In Chapter 3, we used the relationships $\frac{T\hat{\Omega}_{02}}{2} = \frac{\pi}{2}$ and $\frac{T\hat{\Omega}_{03}}{2} = \pi$, where we have redefined the factors $\hat{\Omega}_{02} = \sqrt{\tilde{\Omega}_2^2 - \frac{1}{4}}$ and $\hat{\Omega}_{03} = \sqrt{\tilde{\Delta}^2 + \tilde{\Omega}_3^2}$. This way, there will not be any confusion between the factors containing spontaneous emission and inhomogeneous broadening ($\hat{\Omega}_2$ and $\hat{\Omega}_3$) and the ones from the previous chapter ($\hat{\Omega}_{02}$ and $\hat{\Omega}_{03}$).

Analytical expansion of c_2

By using the solution derived in section 2.4.1, we find that the solution for c_2 is:

$$c_2(T,\tilde{\delta}) = i\frac{\tilde{\Omega}_2}{\hat{\Omega}_2}e^{\frac{iT}{2}(\frac{i}{2}+\tilde{\delta})}sin\left(\frac{T\hat{\Omega}_2}{2}\right)$$

At this point, we will begin approximating each part of the analytical solution. We will start with $\hat{\Omega}_2$:

$$\hat{\Omega}_2 = \sqrt{(\tilde{\delta}-\frac{i}{2})^2+\tilde{\Omega}_2^2} = \sqrt{\tilde{\delta}^2+\frac{1}{4}-i\tilde{\delta}+\tilde{\Omega}_2^2} = \sqrt{\tilde{\delta}^2-i\tilde{\delta}+\hat{\Omega}_{02}^2} \approx \hat{\Omega}_{02}\left(1+\frac{\tilde{\delta}(\tilde{\delta}-i)}{2\hat{\Omega}_{02}^2}\right)$$

By using the restriction $T\hat{\Omega}_{02}=\pi$, we will expand the sine term:

$$sin\left(\frac{\tau\hat{\Omega}_2}{2}\right) \approx sin\left(\frac{\pi}{2}\left(1+\frac{\tilde{\delta}(\tilde{\delta}-i)}{2\hat{\Omega}_{02}^2}\right)\right) \approx 1-\frac{\pi^2}{8}\frac{\tilde{\delta}^2(\tilde{\delta}-i)^2}{4\hat{\Omega}_{02}^4} \approx 1+O(\tilde{\Delta}^{-4})$$

Now we will expand the term $\frac{\tilde{\Omega}_2}{\hat{\Omega}_2}$:

$$\frac{\tilde{\Omega}_2}{\hat{\Omega}_2} \approx \frac{\tilde{\Omega}_2}{\hat{\Omega}_{02}\left(1+\frac{\tilde{\delta}(\tilde{\delta}-i)}{2\hat{\Omega}_{02}^2}\right)} \approx \frac{1}{\left(1+\frac{\tilde{\delta}(i+\tilde{\delta})}{2\hat{\Omega}_{02}^2}\right)} \approx 1-\frac{\tilde{\delta}(\tilde{\delta}-i)}{2\hat{\Omega}_{02}^2} \approx 1-\frac{3}{2}\frac{\tilde{\delta}(\tilde{\delta}-i)}{\tilde{\Delta}^2}$$

Putting all terms together we find the analytical expansion of c_2:

$$c_2(T,\tilde{\delta}) = i\frac{\tilde{\Omega}_2}{\hat{\Omega}_2}e^{\frac{iT}{2}(\frac{i}{2}-\tilde{\delta})}sin\left(\frac{T\hat{\Omega}_2}{2}\right) \approx ie^{\frac{iT}{2}(\frac{i}{2}-\tilde{\delta})}\left(1-\frac{3}{2}\frac{\tilde{\delta}(\tilde{\delta}-i)}{\tilde{\Delta}^2}\right)$$

And the modulus square is:

$$|c_2|^2 \approx e^{-\frac{T}{2}}\left(1-3\frac{\tilde{\delta}^2}{\tilde{\Delta}^2}\right) \approx \left(1-\frac{T}{2}\right)\left(1-3\frac{\tilde{\delta}^2}{\tilde{\Delta}^2}\right) \approx 1-\frac{\sqrt{3}\pi}{2\tilde{\Delta}}-3\frac{\tilde{\delta}^2}{\tilde{\Delta}^2}$$

Analytical expansion of c_1

The analytical solution for the c_1 coefficient is:

$$c_1(T,\tilde{\delta}) = e^{\frac{iT}{2}(\frac{i}{2}-\tilde{\delta})}\left[cos\left(\frac{T\hat{\Omega}_2}{2}\right)+\frac{1+2i\tilde{\delta}}{2\hat{\Omega}_2}sin\left(\frac{T\hat{\Omega}_2}{2}\right)\right]$$

We start by expanding the cosine term:

$$cos\left(\frac{T\hat{\Omega}_2}{2}\right) \approx cos\left(\frac{\pi}{2}\left(1+\frac{\tilde{\delta}(\tilde{\delta}-i)}{2\hat{\Omega}_{02}^2}\right)\right) \approx -\frac{\pi}{2}\frac{\tilde{\delta}(\tilde{\delta}-i)}{2\hat{\Omega}_{02}^2} \approx -\frac{3\pi}{4}\frac{\tilde{\delta}(\tilde{\delta}-i)}{\tilde{\Delta}^2}$$

Now, we expand the term $\frac{1+2i\tilde{\delta}}{2\hat{\Omega}_2}$:

$$\frac{1+2i\tilde{\delta}}{2\hat{\Omega}_2} \approx \frac{1+2i\tilde{\delta}}{2\hat{\Omega}_{02}\left(1+\frac{\tilde{\delta}(\tilde{\delta}-i)}{2\hat{\Omega}_{02}^2}\right)} \approx \frac{\sqrt{3}(1+2i\tilde{\delta})}{2\tilde{\Delta}}\left(1-\frac{3}{2}\frac{\tilde{\delta}(\tilde{\delta}-i)}{\tilde{\Delta}^2}\right) \approx \frac{\sqrt{3}(1+2i\tilde{\delta})}{2\tilde{\Delta}}+O(\tilde{\Delta}^{-3})$$

Putting all terms together inside the analytical expression of c_1 we obtain:

$$c_1(T,\tilde{\delta}) \approx e^{\frac{iT}{2}(\frac{i}{2}-\tilde{\delta})}\left[-\frac{3\pi}{4}\frac{\tilde{\delta}(i-\tilde{\delta})}{\tilde{\Delta}^2} - \frac{\sqrt{3}(1+2i\tilde{\delta})}{2\tilde{\Delta}}\right]$$

Computing the modulus square:

$$|c_1|^2 \approx e^{-\frac{T}{2}}\frac{3}{4}\frac{(1+4\tilde{\delta}^2)}{\tilde{\Delta}^2} \approx \left(1-\frac{T}{2}\right)\frac{3}{4}\frac{(1+4\tilde{\delta}^2)}{\tilde{\Delta}^2} \approx \frac{3(\tilde{\delta}^2+\frac{1}{4})}{\tilde{\Delta}^2}$$

Analytical expansion of c_3

The analytical solution for the c_3 coefficient is:

$$c_3(T,\tilde{\delta}) = i\frac{\tilde{\Omega}_3}{\hat{\Omega}_3}e^{\frac{iT}{2}(\frac{i}{2}-\tilde{\Delta}-\delta)}sin\left(\frac{T\hat{\Omega}_3}{2}\right)$$

Where

$$\begin{aligned}\hat{\Omega}_3 &= \sqrt{(\tilde{\Delta}+\tilde{\delta}-\frac{i}{2})^2+\tilde{\Omega}_3^2} = \sqrt{(\tilde{\delta}-\frac{i}{2})^2+\tilde{\Delta}^2+2\tilde{\Delta}(\tilde{\delta}-\frac{i}{2})+\tilde{\Omega}_3^2} \\ &= \sqrt{(\tilde{\delta}-\frac{i}{2})^2+2\tilde{\Delta}(\tilde{\delta}-\frac{i}{2})+\hat{\Omega}_{03}^2} \approx \hat{\Omega}_{03}\left(1+\frac{(\tilde{\delta}-\frac{i}{2})^2+2\tilde{\Delta}(\tilde{\delta}-\frac{i}{2})}{2\hat{\Omega}_{03}^2}\right)\end{aligned}$$

By using the restriction $T\hat{\Omega}_{03}=2\pi$, we will expand the sine term:

$$sin\left(\frac{T\hat{\Omega}_3}{2}\right) \approx sin\left(\pi\left(1+\frac{(\tilde{\delta}-\frac{i}{2})^2+2\tilde{\Delta}(\tilde{\delta}-\frac{i}{2})}{2\hat{\Omega}_{03}^2}\right)\right) \approx -\frac{3\pi}{8}\left(\frac{2(\tilde{\delta}-\frac{i}{2})}{\tilde{\Delta}}+\frac{(\tilde{\delta}-\frac{i}{2})^2}{\tilde{\Delta}^2}\right)$$

And the expansion of $\frac{\tilde{\Omega}_3}{\hat{\Omega}_3}$ is:

$$\frac{\tilde{\Omega}_3}{\hat{\Omega}_3} \approx \frac{\tilde{\Omega}_3}{\hat{\Omega}_{03}\left(1+\frac{(\tilde{\delta}-\frac{i}{2})^2+2\tilde{\Delta}(\tilde{\delta}-\frac{i}{2})}{2\hat{\Omega}_{03}^2}\right)} \approx \frac{1}{2}+\frac{3}{16}\left(\frac{2(\tilde{\delta}-\frac{i}{2})}{\tilde{\Delta}}+\frac{(\tilde{\delta}-\frac{i}{2})^2}{\tilde{\Delta}^2}\right)$$

Plugging these expansions into c_0 we obtain:

$$\begin{aligned}c_3(T,\tilde{\delta}) &= -i\frac{\tilde{\Omega}_3}{\hat{\Omega}_3}e^{\frac{iT}{2}(\frac{i}{2}-\tilde{\Delta}-\tilde{\delta})}sin\left(\frac{T\hat{\Omega}_3}{2}\right) \\ &\approx -ie^{\frac{iT}{2}(\frac{i}{2}-\tilde{\Delta}-\tilde{\delta})}\left(\frac{1}{2}+\frac{3}{16}\left(\frac{2(\tilde{\delta}-\frac{i}{2})}{\tilde{\Delta}}+\frac{(\tilde{\delta}-\frac{i}{2})^2}{\tilde{\Delta}^2}\right)\right)\left(\frac{3\pi}{8}\left(\frac{2(\tilde{\delta}-\frac{i}{2})}{\tilde{\Delta}}+\frac{(\tilde{\delta}-\frac{i}{2})^2}{\tilde{\Delta}^2}\right)\right) \\ &\approx -ie^{\frac{iT}{2}(\frac{i}{2}-\tilde{\Delta}-\tilde{\delta})}\frac{3\pi}{16}\left(\frac{2(\tilde{\delta}-\frac{i}{2})}{\tilde{\Delta}}+\frac{(\tilde{\delta}-\frac{i}{2})^2}{\tilde{\Delta}^2}\right)\left(1+\frac{3}{4}\frac{(\tilde{\delta}-\frac{i}{2})}{\tilde{\Delta}}\right) \\ &\approx -ie^{\frac{iT}{2}(\frac{i}{2}-\tilde{\Delta}-\tilde{\delta})}\frac{3\pi}{16}\left(\frac{2(\tilde{\delta}-\frac{i}{2})}{\tilde{\Delta}}+\frac{5(\tilde{\delta}-\frac{i}{2})^2}{2\tilde{\Delta}^2}\right)\end{aligned}$$

And the modulus square is:

$$|c_3|^2 \approx e^{-\frac{T}{2}}\frac{9\pi^2}{64}\frac{(\tilde{\delta}^2+\frac{1}{4})}{\tilde{\Delta}^2} \approx \frac{9\pi^2}{64}\frac{(\tilde{\delta}^2+\frac{1}{4})}{\tilde{\Delta}^2}$$

Analytical expansion of c_0

The analytical solution for the c_0 coefficient is:

$$c_0(T,\tilde{\delta}) = e^{\frac{iT}{2}(\frac{i}{2}-\tilde{\Delta}-\tilde{\delta})}\left[cos\left(\frac{T\hat{\Omega}_3}{2}\right) + \frac{1+2i(\tilde{\Delta}+\tilde{\delta})}{2\hat{\Omega}_3}sin\left(\frac{T\hat{\Omega}_3}{2}\right)\right]$$

The expansion of the cosine term is:

$$cos\left(\frac{T\hat{\Omega}_3}{2}\right) \approx cos\left(\pi\left(1+\frac{(\tilde{\delta}-\frac{i}{2})^2+2\tilde{\Delta}(\tilde{\delta}-\frac{i}{2})}{2\hat{\Omega}_{03}^2}\right)\right)$$
$$\approx -1+\frac{\pi^2}{8}\frac{((\tilde{\delta}-\frac{i}{2})^2+2\tilde{\Delta}(\tilde{\delta}-\frac{i}{2}))^2}{\hat{\Omega}_{03}^4} \approx -1+\frac{9\pi^2(\tilde{\delta}-\frac{i}{2})^2}{32\tilde{\Delta}^2}$$

And the expansion for $\frac{1+2i(\tilde{\Delta}+\tilde{\delta})}{2\hat{\Omega}_3}$ is:

$$\frac{1+2i(\tilde{\Delta}+\tilde{\delta})}{2\hat{\Omega}_3} \approx \frac{1+2i(\tilde{\Delta}+\tilde{\delta})}{2\hat{\Omega}_{03}\left(1+\frac{(\tilde{\delta}-\frac{i}{2})^2+2\tilde{\Delta}(\tilde{\delta}-\frac{i}{2})}{2\hat{\Omega}_{03}^2}\right)} \approx \frac{\sqrt{3}}{4}\frac{(1+2i(\tilde{\Delta}+\tilde{\delta}))}{\tilde{\Delta}}\left(1-\frac{3}{8}\frac{(\tilde{\delta}-\frac{i}{2})^2+2\tilde{\Delta}(\tilde{\delta}-\frac{i}{2})}{\tilde{\Delta}^2}\right)$$

$$\approx \frac{\sqrt{3}}{4}\left(2i+\frac{(1+2i\tilde{\delta})}{\tilde{\Delta}}\right)\left(1-\frac{3}{4}\frac{(\tilde{\delta}-\frac{i}{2})}{\tilde{\Delta}}-\frac{3}{8}\frac{(\tilde{\delta}-\frac{i}{2})^2}{\tilde{\Delta}^2}\right) \approx \frac{\sqrt{3}}{4}\left(2i+\frac{(\frac{1}{2}+i\tilde{\delta})}{2\tilde{\Delta}}\right)$$

Grouping all the expansions from the analytical solution of c_0, we end with:

$$c_0(T,\tilde{\delta}) = e^{\frac{iT}{2}(\frac{i}{2}-\tilde{\Delta}-\tilde{\delta})}\left[-1+\frac{9\pi^2(\tilde{\delta}-\frac{i}{2})^2}{32\tilde{\Delta}^2}-\frac{3\sqrt{3}\pi}{32}\left(2i+\frac{(\frac{1}{2}-i\tilde{\delta})}{2\tilde{\Delta}}\right)\left(\frac{2(\tilde{\delta}+\frac{i}{2})}{\tilde{\Delta}}-\frac{(\tilde{\delta}+\frac{i}{2})^2}{\tilde{\Delta}^2}\right)\right]$$
$$\approx e^{\frac{iT}{2}(\frac{i}{2}-\tilde{\delta}-\tilde{\delta})}\left[-1-\frac{3\sqrt{3}\pi}{8\tilde{\Delta}}(i\tilde{\delta}+\frac{1}{2})-\frac{3\sqrt{3}\pi}{32\tilde{\Delta}^2}\left(\frac{\sqrt{3}\pi}{4}-\frac{3i}{4}+3\tilde{\delta}+i\sqrt{3}\pi\tilde{\delta}+3i\tilde{\delta}^2-\sqrt{3}\pi\tilde{\delta}^2\right)\right]$$

Computing the modulus square:

$$|c_0|^2 = e^{-\frac{T}{2}}\left[1+\frac{3\sqrt{3}\pi}{8\tilde{\Delta}}+\frac{3\sqrt{3}\pi}{32\tilde{\Delta}^2}\left(\frac{5\sqrt{3}\pi}{4}+6\tilde{\delta}-\frac{\sqrt{3}\pi}{2}\tilde{\delta}^2\right)\right]$$
$$\approx 1-\frac{\sqrt{3}\pi}{8\tilde{\Delta}}+\frac{3\sqrt{3}\pi}{32\tilde{\Delta}^2}\left(-\frac{3\sqrt{3}\pi}{4}+6\tilde{\delta}-\frac{\sqrt{3}\pi}{2}\tilde{\delta}^2\right)$$

Remember that we assume that for each realization of the experiment, the inhomogeneous broadening is constant, but it changes between experiments following a Gaussian distribution.

$$p_b(\delta) = \frac{1}{\sqrt{2\pi\sigma_b^2}}e^{-\frac{\delta^2}{2\sigma_b^2}}$$

We will have to convolute the analytical expressions of the coefficients $|c_i(T,\tilde{\delta})|^2$ with the inhomogeneous broadening distribution (eq. 4.17):

$$|c_i(T)|^2 = \int_{-\infty}^{\infty}|c_i(T,\tilde{\delta})|^2 p_b(\tilde{\delta})\tilde{\delta} \tag{4.17}$$

In the analytical expansions, only factors of $\tilde{\delta}$ and $\tilde{\delta}^2$ do appear. Taking them into account we end up with:

$$\boxed{|c_2|^2 \approx 1 - \frac{\sqrt{3}\pi}{2\tilde{\Delta}} - 3\frac{\sigma_b^2}{\tilde{\Delta}^2} \qquad |c_1|^2 \approx \frac{3(\sigma_b^2 + \frac{1}{4})}{\tilde{\Delta}^2}}$$

$$\boxed{|c_3|^2 \approx \frac{9\pi^2}{64}\frac{(\sigma_b^2 + \frac{1}{4})}{\tilde{\Delta}^2} \qquad |c_0|^2 \approx 1 - \frac{\sqrt{3}\pi}{8\tilde{\Delta}} + \frac{3\sqrt{3}\pi}{32\tilde{\Delta}^2}\left(-\frac{3\sqrt{3}\pi}{4} - \frac{\sqrt{3}\pi}{2}\sigma_b^2\right)} \tag{4.18}$$

Now that we have computed the analytical expansions for all the populations in the square pulse, we will be able to derive the analytical expansion of the conditional fidelity. Our results will also be useful in next section, where we will add the second-order emission coefficients.

4.5. Gaussian-shaped pulse coefficients

In this section we will compute the coefficients for the Gaussian-shaped pulse taking into account inhomogeneous broadening and spontaneous emission from the extra energy level. We will start with the differential equations that govern the dynamics of the system:

$$\dot{c}_3(\tau) = \left(-i\tilde{\Delta} - i\tilde{\delta} - \frac{1}{2}\right) c_3(\tau) + i\frac{\tilde{\Omega}_3}{2}c_0(\tau) \qquad \dot{c}_0(\tau) = i\frac{\tilde{\Omega}_3^*}{2}c_3(\tau)$$

And:

$$\dot{c}_2(\tau) = -\left(i\tilde{\delta} + \frac{1}{2}\right) c_2(\tau) + i\frac{\tilde{\Omega}_2}{2}c_1(\tau) \qquad \dot{c}_1(\tau) = i\frac{\tilde{\Omega}_2^*}{2}c_2(\tau)$$

Resonant transition $|1\rangle - |2\rangle$

We will proceed to solve the following system of coupled linear differential equations:

$$\dot{c}_2(\tau) = \kappa c_2(\tau) + i\frac{\tilde{\Omega}_2}{2}c_1(\tau) \qquad \dot{c}_1(\tau) = i\frac{\tilde{\Omega}_2^*}{2}c_2(\tau)$$

Where we have defined $\kappa = -i\tilde{\delta} - \frac{1}{2}$. Due to the fact that $\kappa << \frac{\tilde{\Omega}_3}{2}$, we can perform perturbation theory around κ. We expand c_1 and c_2 as follows:

$$\begin{aligned} c_2(\tau) &= c_2^{(0)}(\tau) + c_2^{(1)}(\tau)\kappa + c_2^{(2)}(\tau)\kappa^2 + ... \\ c_1(\tau) &= c_1^{(0)}(\tau) + c_1^{(1)}(\tau)\kappa + c_1^{(2)}(\tau)\kappa^2 + ... \end{aligned}$$

Plugging this into the differential equations we find:

$$\begin{aligned} &\left[\dot{c}_2^{(0)}(\tau) + \dot{c}_2^{(1)}(\tau)\kappa + ...\right] = \left[c_2^{(0)}(\tau)\kappa + c_2^{(1)}(\tau)\kappa^2 + ...\right] + i\frac{\tilde{\Omega}_2}{2}\left[c_1^{(0)}(\tau) + c_1^{(1)}(\tau)\kappa + ...\right] \\ &\left[\dot{c}_1^{(0)}(\tau) + \dot{c}_1^{(1)}(\tau)\kappa + ...\right] = i\frac{\tilde{\Omega}_2^*}{2}\left[c_2^{(0)}(\tau) + c_2^{(1)}(\tau)\kappa + ...\right] \end{aligned}$$

By grouping the terms with the same powers of κ we end up with the same recursive equations that we found in section 3.4.

$$\begin{aligned} \dot{c}_2^{(N)}(\tau) &= c_2^{(N-1)}(\tau) + i\frac{\tilde{\Omega}_2}{2}c_1^{(N)}(\tau) \\ \dot{c}_1^{(N)}(\tau) &= i\frac{\tilde{\Omega}_2^*}{2}c_2^{(N)}(\tau) \end{aligned}$$

We already solved these equations up to first order, therefore, we will use the results obtained in the previous sections:

$$\begin{aligned} c_2(\tau) &\simeq c_2^{(0)}(\tau) + \kappa c_2^{(1)}(\tau) \\ &\simeq i\frac{\tilde{\Omega}_2}{|\tilde{\Omega}_2|} sin\left(\frac{1}{2}\int_0^\tau |\tilde{\Omega}_2| d\tau'\right) - i\frac{\tilde{\Omega}_2}{|\tilde{\Omega}_2|}\kappa\frac{\tau}{2} \end{aligned} \tag{4.19}$$

Now, we can compute $c_2(T, \tilde{\delta})$:

$$c_2(T, \tilde{\delta}) \approx c_2^{(0)}(T) + \kappa c_2^{(1)}(T) \approx i\frac{\tilde{\Omega}_2}{|\tilde{\Omega}_2|} + i\frac{\tilde{\Omega}_2}{|\tilde{\Omega}_2|}(i\tilde{\delta} - \frac{1}{2})\frac{T}{2}$$

And the modulus square becomes:

$$|c_2(T,\tilde{\delta})|^2 \approx 1 - \frac{T}{2} + \frac{T^2}{4}\left(\tilde{\delta}^2 + \frac{1}{4}\right)$$

Far-detuned transition $|0\rangle - |3\rangle$

In this part we are interested in looking at the dynamics of the $|0\rangle - |3\rangle$ transition. The equations of motion are:

$$\dot{c}_3(\tau) = -\Lambda c_3(\tau) + i\frac{\tilde{\Omega}_3(\tau)}{2}c_0(\tau) \qquad \dot{c}_0(\tau) = i\frac{\tilde{\Omega}_3^*(\tau)}{2}c_3(\tau) \tag{4.20}$$

We we have defined $\Lambda = \frac{1}{2} + i\tilde{\Delta} + i\tilde{\delta}$. Before expanding these differential equations perturbatively, first we will perform the change of variable $d\xi = |\tilde{\Omega}_3|d\tau$. In eq.4.21 one can see the coupled differential equations after the change of variable.

$$\dot{c}_3(\xi) = -i\frac{\Lambda}{|\tilde{\Omega}_3|}c_3(\xi) + \frac{i}{2}\frac{\tilde{\Omega}_3}{|\tilde{\Omega}_3|}c_0(\xi) \qquad \dot{c}_0(\xi) = \frac{i}{2}\frac{\tilde{\Omega}_3^*}{|\tilde{\Omega}_3|}c_3(\xi) \tag{4.21}$$

Now, we can use perturbation theory and expand the coefficients around $\epsilon = \frac{i}{2}\frac{\tilde{\Omega}_3}{|\tilde{\Omega}_3|}$:

$$c_3(\xi) = c_3^{(0)}(\xi) + c_3^{(1)}(\xi)\epsilon + c_3^{(2)}(\xi)\epsilon^2 + ...$$
$$c_0(\xi) = c_0^{(0)}(\xi) + c_0^{(1)}(\xi)\epsilon + c_0^{(2)}(\xi)\epsilon^2 + ...$$

By plugging in again the expansion into equation 4.21, we get N differential equations for each term of the expansion. In our case, we will see that we only have to go to the first order. These differential equations are:

$$\dot{c}_3^{(N)}(\xi) = -i\frac{\Lambda}{|\tilde{\Omega}_3|}c_3^{(N)}(\xi) + c_0^{(N-1)}(\xi) \qquad \dot{c}_0^{(N)}(\xi) = \frac{\tilde{\Omega}_3^{*2}}{|\tilde{\Omega}_3|^2}c_3^{(N-1)}(\xi) \tag{4.22}$$

Since we already solved these differential equations in section 3.4, we will use the results obtained there, but this time changing $\tilde{\Delta}$ by Λ.

$$c_3(T,\tilde{\delta}) \simeq c_3^{(0)}(T) + \epsilon c_3^{(1)}(T) \simeq i\frac{\pi R}{4}\frac{\tilde{\Omega}_3}{|\tilde{\Omega}_3|}e^{-i\Lambda\frac{T}{2}}e^{-\frac{\Lambda^2T^2}{2\beta^2}} \tag{4.23}$$

And the modulus square will be:

$$|c_3(T,\tilde{\delta})|^2 \approx \frac{\pi^2}{16}e^{-\frac{T}{2}}e^{-\frac{T^2(\tilde{\Delta}^2+\tilde{\delta}^2+\tilde{\Delta}\tilde{\delta}-\frac{1}{4})}{\beta^2}} \tag{4.24}$$

Now, the action of the inhomogeneous broadening will be taken into account, by convolving the analytical result of $|c_3(T,\tilde{\delta})|^2$ with the broadening distribution:

$$\begin{aligned} |c_3(T)|^2 &= \int_{-\infty}^{\infty}|c_3(T,\tilde{\delta})|^2 p_b(\tilde{\delta})d\tilde{\delta} \\ &\approx \frac{\pi^2}{16\sqrt{2\pi}\sigma_b}e^{-\frac{T}{2}}\int_{-\infty}^{\infty}e^{-\frac{T^2(\tilde{\Delta}^2+\tilde{\delta}^2+\tilde{\Delta}\tilde{\delta}-\frac{1}{4})}{\beta^2}}e^{-\frac{\tilde{\delta}^2}{2\sigma_b^2}}d\tilde{\delta} \end{aligned} \tag{4.25}$$

We now perform the change of variable $u = \tilde{\delta}\left(\frac{T^2}{\beta^2} + \frac{1}{2\sigma_b^2}\right)^{\frac{1}{2}} + \frac{T^2}{2\beta^2}\left(\frac{T^2}{\beta^2} + \frac{1}{2\sigma_b^2}\right)^{-\frac{1}{2}}$ to obtain:

$$|c_3(T)|^2 \approx \frac{\pi^2}{16\sqrt{2}\sigma_b}\left(\frac{T^2}{\beta^2} + \frac{1}{2\sigma_b^2}\right)^{-\frac{1}{2}}e^{-\frac{T}{2}}e^{-\frac{T^2}{\beta^2}(\tilde{\Delta}^2+\frac{1}{4})}e^{\frac{T^4\tilde{\Delta}^2}{4\beta^4}\left(\frac{T^2}{\beta^2}+\frac{1}{2\sigma_b}\right)^{-1}} \tag{4.26}$$

Now, we will use the approximations $\tilde{\Delta}^2 >> \frac{1}{4}$ and $2\sigma_b T^2 << \beta^2$ (we are in the regime where $\beta >> 1$):

$$|c_3(T)|^2 \approx \frac{\pi^2}{16} e^{-\frac{T}{2}} e^{-\frac{T^2}{\beta^2}\tilde{\Delta}^2} \tag{4.27}$$

As one can see in equations 4.26 and 4.27, the inhomogeneous broadening does only appear weakly on the analytical expansion, and can be neglected. On the other hand, the factor $e^{-\frac{T}{2}}$ comes from spontaneous emission from the far-detuned excited state.

Notice that the first order expansion of $|c_0(T)|^2$ is zero. We will make the approximation $|c_0(T)|^2 \approx 1 - |c_3(T)|^2$. It is an approximation because on this section, we are also taking into account spontaneous emission from $|3\rangle$.

$$|c_0(T)|^2 \approx 1 - \frac{\pi^2}{16} e^{-\frac{T}{2}} e^{-\frac{T^2}{\beta^2}\tilde{\Delta}^2}$$

The analytical expansions for the Gaussian-shaped pulse are:

$$\boxed{|c_2|^2 \approx 1 - \frac{T}{2} + \frac{T^2}{4}\left(\sigma_b^2 + \frac{1}{4}\right) \qquad |c_1|^2 \approx 0}$$

$$\boxed{|c_3|^2 \approx \frac{\pi^2}{16} e^{-\frac{T}{2}} e^{-\frac{T^2}{\beta^2}\tilde{\Delta}^2} \qquad |c_0|^2 \approx 1 - \frac{\pi^2}{16} e^{-\frac{T}{2}} e^{-\frac{T^2}{\beta^2}\tilde{\Delta}^2}} \tag{4.28}$$

Notice that the coefficients from 4.28 do depend on T. We have not used the optimal time found on Chapter 3, because on next chapter we will have to derive a new optimization of T for the Gaussian regime.

4.6. Analytical expansion of the fidelity

We will use the results obtained in sections 4.4 (square-shaped pulse) and 4.5 (Gaussian-shaped pulse) to find an analytical expression of the conditional fidelity (eq. 4.15). Then, we will compare the analytical results with the numerical simulations and we will discuss the behavior of the protocol under different parameters for the Gaussian regime and the constant-pulse regime.

In order to expand the conditional fidelity (4.15), it will be useful to rewrite it in the form:

$$F_f = \frac{\frac{1}{2}D_1^N + \frac{1}{2}(D_1 + D_2)^N}{(D_1 + D_2 + D_3)^N} = \frac{1}{2}\left(\frac{1}{1 + \frac{D2+D_3}{D_1}}\right)^N + \frac{1}{2}\left(\frac{1}{1 + \frac{D_3}{D_1+D_2}}\right)^N$$

Where:

$$\begin{aligned} D_1 &= \eta_2 |c_0 c_2|^2 \\ D_2 &= \eta_2(1-\eta_3)|c_3 c_2|^2 \\ D_3 &= \eta_3 |c_3 c_1|^2 + \left[\eta_2\eta_3 + \eta_3(1-\eta_2)\right]|c_3 c_2|^2 \end{aligned}$$

Where the analytical solutions for the coefficients from the square-shaped pulse are:

$$
\begin{aligned}
|c_0c_2|^2 &\approx 1 - \frac{5\sqrt{3}\pi}{8\tilde{\Delta}} - \frac{3\sqrt{3}\pi}{32\tilde{\Delta}^2}\left(\frac{\pi}{4\sqrt{3}} + \sigma_b^2\left(\frac{\sqrt{3}\pi}{2} + \frac{32}{\sqrt{3}\pi}\right)\right) \\
|c_3c_2|^2 &\approx \frac{9\pi^2}{64\tilde{\Delta}^2}\left(\sigma_b^2 + \frac{1}{4}\right) \\
|c_3c_1|^2 &\approx 0
\end{aligned}
$$

And for the Gaussian-shaped pulse, using the optimal time derived in Chapter 3 are:

$$
\begin{aligned}
|c_0c_2|^2 &\approx 1 - \frac{\beta}{\tilde{\Delta}}\left(\frac{1}{8} + \lambda\right) + \frac{\beta^2}{4\tilde{\Delta}^2}\left(\sigma_b^2 + 3\lambda^2 + \frac{1}{4}\right) \\
|c_3c_2|^2 &\approx \frac{\beta}{8\tilde{\Delta}} - \frac{\beta^2\lambda}{8\tilde{\Delta}^2} \\
|c_3c_1|^2 &\approx 0
\end{aligned}
$$

With $\lambda = \sqrt{ln\left(\frac{\pi^2\tilde{\Delta}}{2\beta}\right)}$.

We will make the approximations $D_1 >> D_2 + D_3$ and $D_1 + D_2 >> D_3$ to further expand the conditional fidelity. We can perform this approximation expansion because $D_1 \propto \tilde{\Delta}^0$, $D_2 \propto \tilde{\Delta}^{-2}$ and $D_3 \propto \tilde{\Delta}^{-2}$.

$$
F \simeq \frac{1}{2}\left(1 - N\frac{D_2 + D_3}{D_1}\right) + \frac{1}{2}\left(1 - N\frac{D_3}{D_1 + D_2}\right) \tag{4.29}
$$

And the analytical expansion of the fidelity for the square pulse and the Gaussian pulse, respectively, are:

$$
\boxed{F_S \simeq 1 - N\frac{9\pi^2}{128\tilde{\Delta}^2}\left(\frac{1}{4} + \sigma_b^2\right)\left(1 - \eta_3 + 2\frac{\eta_3}{\eta_2}\right)} \tag{4.30}
$$

$$
\boxed{F_G \simeq 1 - N\frac{\beta}{16\tilde{\Delta}}\left(1 - \eta_3 + 2\frac{\eta_3}{\eta_2}\right)}
$$

In appendix B.2 one can find the comparison between the obtained analytical solutions and the numerical results.

As one can see in equation 4.30, the conditional fidelity for the square pulse is very close to unity, since the first term appears with the power of $O(\tilde{\Delta}^{-2})$. Due to the fact that we are conditioning the fidelity on detecting at least one photon on each cycle, the effect of spontaneous emission on the fidelity is no longer present.

4.7. Numerical and Analytical results

In figure 4.2 one can see a 2D plot of the numerical conditional fidelity as a function of the length of the pulse T and the normalized detuning $\tilde{\Delta}$, for 5 qubits (N=5).

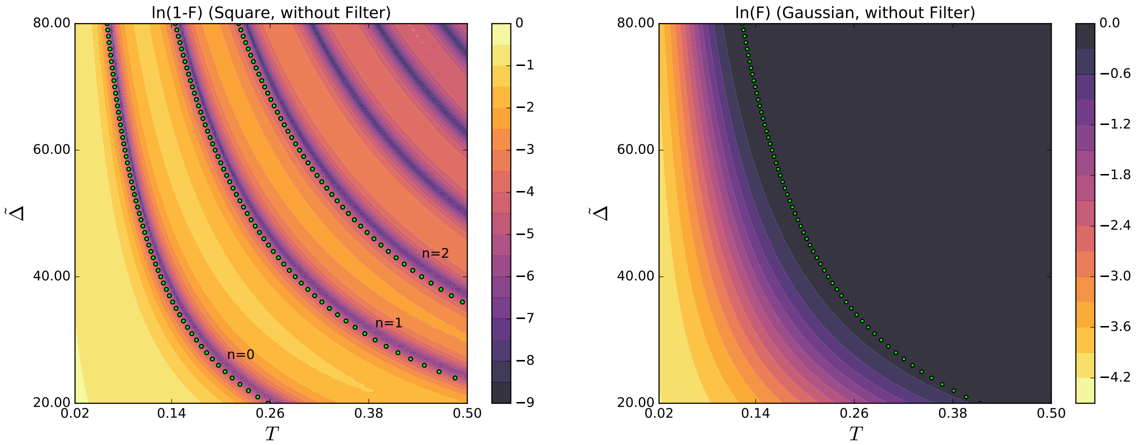

Figure 4.2.: 2D colormap of the numerical results for the $ln(1-F)$ (conditional fidelity) for the square-shaped pulse (left) and the Gaussian-shaped pulse (right), as a function of the length of the pulse T (x axis) and the dimensionless detuning $\tilde{\Delta}$ (y axis), without filtering. The green-dotted lines correspond to the analytical optimal times for the square pulse (left) and for the Gaussian pulse (right).

For the square-shaped pulse the interference pattern is still present and the optimal time derived in Chapter 3 is still a good approximation of the maximums of the fidelity. For the Gaussian-shaped pulse, one can see that there is no interference pattern. In this regime, for long enough time T, the conditional fidelity approaches unity.

In figure 4.3 the fidelity for the square pulse is plotted as a function of T for a realistic value of the detuning [32], $\tilde{\Delta} = 50$.

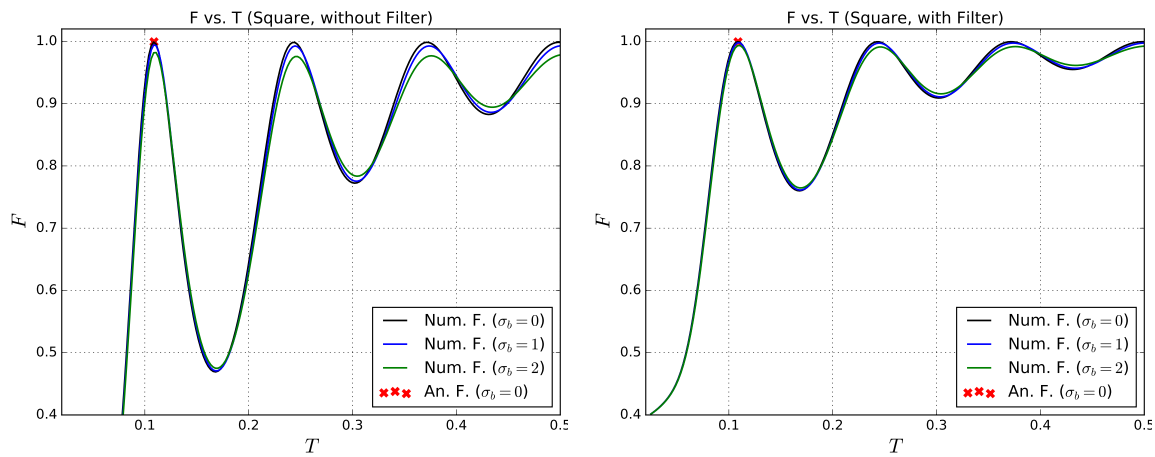

Figure 4.3.: Plots of the numerical conditional fidelity F for the square-shaped pulse as a function of the length of the pulse T without filtering (left) and frequency filters $\eta_{f2} = 0.95$, $\eta_{f3} = 0.05$ (right), with $\tilde{\Delta} = 50$ for 5 qubits ($N = 5$). The red cross corresponds to the analytical fidelity.

As one can see, the application of frequency filters does smear out the oscillations and decrease the effect of inhomogeneous broadening. Despite this, the fidelity in the optimal time (first maximum) is almost unity. Inhomogeneous broadening decreases the fidelity but not considerably.

In figure 4.3 the fidelity for the Gaussian pulse is plotted as a function of the time T, for $\tilde{\Delta} = 50$.

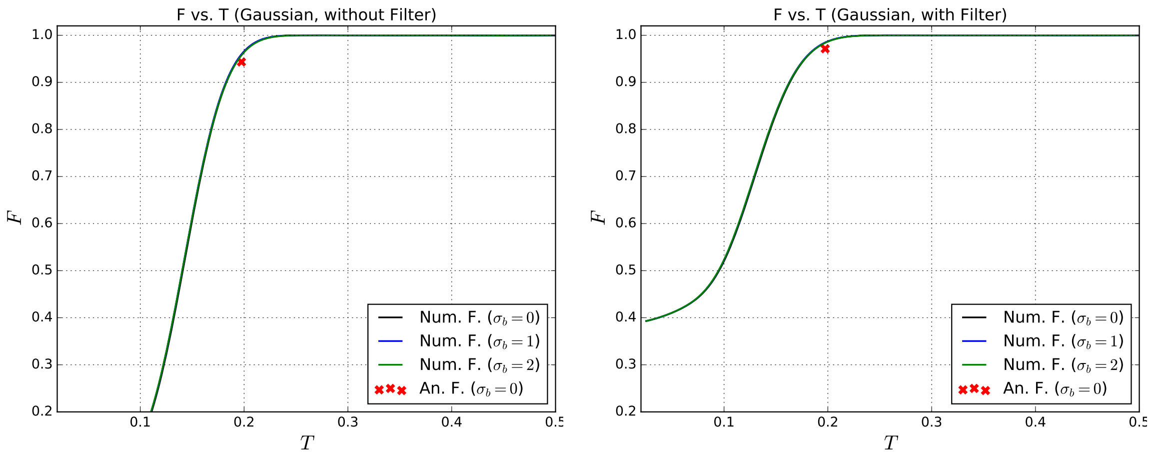

Figure 4.4.: Plots of the numerical conditional fidelity F for the Gaussian-shaped pulse as a function of the length of the pulse T without filtering (left) and frequency filters $\eta_{f2} = 0.95$, $\eta_{f3} = 0.05$ (right), with $\tilde{\Delta} = 50$ for 5 qubits ($N = 5$). The red cross corresponds to the analytical fidelity.

The conditional fidelity for the Gaussian pulse is very similar to a logistic regression. There are no oscillations present, due to this fact, for long enough times, when the far-detuned excitation is not populated, the fidelity is almost unity. As we can see, the optimal time derived in Chapter 3 does not capture the time where the fidelity is maximal. This is due to the fact that we derived the optimal time for the Gaussian pulse by taking into account the compromise between the excitation of the far-detuned transition and the spontaneous emission. On the contrary, the square-shaped pulse optimal time is still valid, since it was derived by imposing to lie on the maximum of the interference pattern of the fidelity.

We can also see that the fidelity for the Gaussian pulse is almost unaffected by the inhomogeneous broadening. Due to the shape of the conditional fidelity, it is not plausible to derive an optimal pulse-length (it resembles a threshold function, without a clear maximum). In next chapter, where we will include second-order photonic emissions, we will be able to derive a new optimal time for the Gaussian pulse.

5. Second-order emissions

5.1. Formalism description

So far we have only considered single excitations for the two transitions of our system $|1\rangle \leftrightarrow |2\rangle$ and $|0\rangle \leftrightarrow |3\rangle$. In the previous chapter photons were only retrieved during the relaxation time of the protocol, right after each pulse. We were treating spontaneous emission as an incoherent process that limited the maximum amount of population of the excited states at the end of the pulses.

Our goal is to use the protocol described in section 3.3 to generate a photonic GHZ state, which is also entangled with the spin state of the atom/quantum dot. For this reason, photon emissions while the driving transition is still active are important and should be taken into account.

In this section we will use a formalism that takes into account and keeps track of the emissions produced when the energy levels are still being driven by the laser pulse [33, 34]. From the Hamiltonian of our system, we will use an emitter-field wavefuncton ansatz to properly keep track of all photon emissions from each excitation.

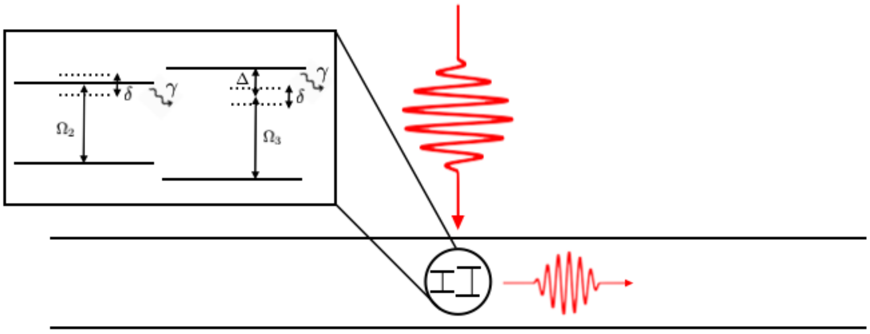

Figure 5.1.: Scheme of the excitation and emission of a quantum dot embedded in a waveguide.

For quantum dots embedded in waveguides [35], we will assume that the coherent excitation is performed from the exterior of the nanophotonioc waveguide. We also consider chiral waveguides [36], where the quantum dot can only emit into a particular direction.

The Hamiltonian of the system is:

$$\hat{H} = \hat{H}_A + \hat{H}_C + \hat{H}_F + \hat{H}_I$$

Where:

$$\begin{aligned}
\hat{H}_A &= \hbar\omega_0 \left|e\right\rangle \left\langle e\right| \\
\hat{H}_C &= -\hat{d}\vec{E} = -\left(\left|e\right\rangle \left\langle g\right| \mu_{eg} + \left|g\right\rangle \left\langle e\right| \mu_{ge}\right)\left(\frac{\varepsilon}{2}e^{-i\nu t} + \frac{\varepsilon^*}{2}e^{i\nu t}\right) \\
\hat{H}_F &= \hbar \int \omega_k \hat{a}_k^\dagger \hat{a}_k dk \\
\hat{H}_I &= -\hbar \int g_k \left(\left|e\right\rangle \left\langle g\right| \hat{a}_k + \left|g\right\rangle \left|e\right\rangle \hat{a}_k^\dagger\right) dk
\end{aligned} \tag{5.1}$$

$\hat{H}_A$ corresponds to the Hamiltonian of the two-level system without any interaction (bare spin Hamiltonian). $\hat{H}_C$ corresponds to the Hamiltonian of the classical field that we are driving from above (see fig. 5.1). $\hat{H}_F$ corresponds to the free propagating field inside the waveguide. Finally, $\hat{H}_I$ describes the interaction between the spin states of the system and the field modes inside the waveguide.

First, we will move to the interaction picture by performing the following transformation:

$$\hat{\hat{H}} = \hat{U}^\dagger(t)\left(\hat{H}_C + \hat{H}_I\right)\hat{U}(t) \tag{5.2}$$

With $\hat{U}(t) = exp[-\frac{it}{\hbar}(\hat{H}_A + \hat{H}_F)]$. In Appendix A.2 some steps of the transformation are described. The transformed Hamiltonian with the Rotation Wave Approximation (described in 2.4.1) is:

$$\hat{\hat{H}} = -\hbar \int dk g_k \left(\left|e\right\rangle \left\langle g\right| \hat{a}_k e^{i\Delta t} + \left|g\right\rangle \left\langle e\right| \hat{a}_k^\dagger e^{-i\Delta t}\right) - \hbar\left(\frac{\Omega}{2}\left|e\right\rangle \left\langle g\right| e^{i\Delta t} + \frac{\Omega^*}{2}\left|g\right\rangle \left\langle e\right| e^{-i\Delta t}\right) \tag{5.3}$$

For convenience, we will transform the annihilation and creation operators $\{\hat{a}_k, \hat{a}_k^\dagger\}$ into the real space annihilation and creation operators $\{\hat{E}(z), \hat{E}^\dagger(z)\}$.

$$\hat{E}(z) = \frac{1}{\sqrt{2\pi}}\int dk \hat{a}_k e^{i(k-k_0)z} \Rightarrow \hat{a}_k = \frac{1}{\sqrt{2\pi}}\int dz' \hat{E}(z') e^{-i(k-k_0)z'} \tag{5.4}$$

Where $k_0 = \frac{\omega_0}{vg}$ and v_g is the group velocity of the field. By performing this transformation (Fourier transformation) we are able to keep track of the position and time of emission of the photons. The commutation relation for these operators is given by:

$$[\hat{E}(z), \hat{E}^\dagger(z')] = \delta(z - z') \tag{5.5}$$

The real space Hamiltonian will be:

$$\begin{aligned}
\hat{\hat{H}} = &-\hbar\sqrt{2\pi}\int dz\delta(z)\left[e^{i\Delta t}\left|e\right\rangle \left\langle g\right| g\hat{E}(z=0) + e^{-i\Delta t}\left|g\right\rangle \left\langle e\right| g\hat{E}^\dagger(z=0)\right] \\
&- \hbar\left[e^{i\Delta t}\left|e\right\rangle \left\langle g\right| \Omega + e^{-i\Delta t}\left|g\right\rangle \left\langle e\right| \Omega^*\right]
\end{aligned}$$

We will proceed by making an Ansatz for the wave-function:

$$\begin{aligned}
\left|\Psi\right\rangle = c_g(t)\left|g, \emptyset\right\rangle &+ c_e(t)\left|e, \emptyset\right\rangle + \int dt_e \phi_g(t, t_e)\hat{E}^\dagger(v_g(t - t_e))\left|g, \emptyset\right\rangle \\
&+ \int dt_e \phi_e(t, t_e)\hat{E}^\dagger(v_g(t - t_e))\left|e, \emptyset\right\rangle \\
&+ \int dte_2 \int dte_1 \phi_{gg}(t, t_{e2}, t_{e1})\hat{E}^\dagger(v_g(t - t_{e2}))\hat{E}^\dagger(v_g(t - t_{e1}))\left|g, \emptyset\right\rangle
\end{aligned} \tag{5.6}$$

This wave-function Ansatz takes into account the usual ground state and excited state coefficients c_g and c_e but it also considers the possibility to emit one photon and end in the ground state ϕ_g, to emit a photon and end in the excited state ϕ_e and the probability to emit two photons and end in the ground state ϕ_{gg}. The coefficients are integrated in order to take into account all the possible time emissions t_e.

Now, we will use the Schrödinger equation $i\hbar\frac{d}{dt}|\Psi\rangle = \hat{\hat{H}}|\Psi\rangle$ to find the dynamic equations of the system.

We start by computing $\hat{\hat{H}}|\Psi\rangle$:

$$\begin{aligned}
&\hat{\hat{H}}|\Psi\rangle = -\hbar\sqrt{2\pi}e^{-i\Delta t}g\hat{E}^\dagger(0)|g,\emptyset\rangle c_e(t)\\
&-\hbar\sqrt{2\pi}e^{i\Delta t}g\int dt_e\phi_g(t,t_e)\hat{E}(0)\hat{E}^\dagger(v_g(t-t_e))|e,\emptyset\rangle\\
&-\hbar\sqrt{2\pi}e^{-i\Delta t}g\int dt_e\phi_e(t,t_e)\hat{E}(0)\hat{E}^\dagger(v_g(t-t_e))|g,\emptyset\rangle\\
&-\hbar\sqrt{2\pi}e^{i\Delta t}g\int dt_{e1}\int dt_{e2}\phi_{gg}(t,t_{e2},t_{e1})\hat{E}(0)\hat{E}^\dagger(v_g(t-t_{e2}))\hat{E}^\dagger(v_g(t-t_{e1}))\\
&-\hbar\frac{\Omega}{2}e^{i\Delta t}cg(t)|e,\emptyset\rangle-\hbar\frac{\Omega^*}{2}e^{-i\Delta t}ce(t)|g,\emptyset\rangle\\
&-\hbar\frac{\Omega}{2}e^{i\Delta t}\int dt_e\phi_g(t,t_e)\hat{E}^\dagger(v_g(t-t_e))|e,\emptyset\rangle\\
&-\hbar\frac{\Omega^*}{2}e^{-i\Delta t}\int dt_e\phi_g(t,t_e)\hat{E}^\dagger(v_g(t-t_e))|g,\emptyset\rangle\\
&-\hbar\frac{\Omega}{2}e^{i\Delta t}\int dt_{e1}\int dt_{e2}\phi_{gg}(t,t_{e2},t_{e1})\hat{E}(0)\hat{E}^\dagger(v_g(t-t_{e2}))\hat{E}^\dagger(v_g(t-t_{e1}))
\end{aligned}\tag{5.7}$$

To find the differential equations that govern the dynamics of the system we apply $\{\langle e,\emptyset|$, $\langle g,\emptyset|$, $\langle e,\emptyset|\hat{E}(z)$, $\langle g,\emptyset|\hat{E}(z)\}$ into eq. 5.7:

$$
\begin{aligned}
& i\hbar \langle e, \emptyset | \dot{\Psi} \rangle = \langle e, \emptyset | \hat{\tilde{H}} | \Psi \rangle \\
& \Rightarrow \dot{c}_e(t) = i\frac{\Omega}{2} e^{i\Delta t} c_g(t) + i\frac{\sqrt{2\pi}}{v_g} g e^{i\Delta t} \phi_g(t,t) \\
& \\
& i\hbar \langle g, \emptyset | \dot{\Psi} \rangle = \langle g, \emptyset | \hat{\tilde{H}} | \Psi \rangle \\
& \Rightarrow \dot{c}_g(t) = i\frac{\Omega^*}{2} e^{-i\Delta t} c_e(t) \\
& \\
& i\hbar \langle g, \emptyset | \hat{E}(z) | \dot{\Psi} \rangle = \langle g, \emptyset | \hat{E}(z) \hat{\tilde{H}} | \Psi \rangle \\
& \Rightarrow \dot{\phi}_g(t,t_e) = i\sqrt{2\pi} g e^{-i\Delta t} \delta(t-t_e) c_e(t_e) + i\frac{\Omega^*}{2} e^{-i\Delta t} \phi_e(t,t_e) \\
& \\
& i\hbar \langle e, \emptyset | \hat{E}(z) | \dot{\Psi} \rangle = \langle e, \emptyset | \hat{E}(z) \hat{\tilde{H}} | \Psi \rangle \\
& \Rightarrow \dot{\phi}_e(t,t_e) = i\frac{\sqrt{2\pi}}{v_g} g e^{i\Delta t} \left(\phi_{gg}(t,t,t_e) + \phi_{gg}(t,t_e,t)\right) + i\frac{\Omega}{2} e^{i\Delta t} \phi_g(t,t_e) \\
& \\
& i\hbar \langle g, \emptyset | \hat{E}(z)\hat{E}(z') | \dot{\Psi} \rangle = \langle e, \emptyset | \hat{E}(z)\hat{E}(z') \hat{\tilde{H}} | \Psi \rangle \\
& \Rightarrow \dot{\phi}_{gg}(t,t_{e2},t_{e1}) = ig\sqrt{2\pi} e^{i\Delta t_{e2}} \phi_e(t_{e2},t_{e1}) \delta(t-t_{e2})
\end{aligned}
\tag{5.8}
$$

By substituting $\gamma = \frac{2\pi g^2}{v_g}$, $\phi_g = \sqrt{\gamma v_g}\tilde{\phi}_g$, $\phi_e = \sqrt{\gamma v_g}\tilde{\phi}_e$ and $\phi_{gg} = \gamma v_g \tilde{\phi}_{gg}$ and using the dimensionless time $\tau = \frac{t}{\gamma}$, we obtain the following equations:

$$
\begin{aligned}
& \dot{c}_e(\tau) = i\frac{\tilde{\Omega}}{2} e^{i\tilde{\Delta} t} c_g(\tau) + i e^{i\tilde{\Delta}\tau} \tilde{\phi}_g(\tau,\tau) \\
& \\
& \dot{c}_g(\tau) = i\frac{\tilde{\Omega}^*}{2} e^{-i\tilde{\Delta}\tau} c_e(\tau) \\
& \\
& \dot{\tilde{\phi}}_g(\tau,\tau_e) = i e^{-i\tilde{\Delta}\tau} \delta(\tau-\tau_e) c_e(\tau_e) + i\frac{\tilde{\Omega}^*}{2} e^{-i\tilde{\Delta}\tau} \tilde{\phi}_e(\tau,\tau_e) \\
& \\
& \dot{\tilde{\phi}}_e(\tau,\tau_e) = i e^{i\tilde{\Delta}\tau} \delta(\tau-\tau_e) \left(\tilde{\phi}_{gg}(\tau,\tau,\tau_e) + \tilde{\phi}_{gg}(\tau,\tau_e,\tau)\right) + i\frac{\tilde{\Omega}}{2} e^{i\tilde{\Delta}\tau} \tilde{\phi}_g(\tau,\tau_e) \\
& \\
& \dot{\tilde{\phi}}_{gg}(\tau,\tau_{e2},\tau_{e1}) = i e^{i\tilde{\Delta}\tau_{e2}} \tilde{\phi}_e(\tau_{e2},\tau_{e1}) \delta(\tau-\tau_{e2})
\end{aligned}
\tag{5.9}
$$

We assume that we start in the ground state $c_g(0) = 1$. Notice that the the amplitudes that describe states with emitted photons do only get a contribution when $\tau > \tau_e$. The equations of motion for states containing emitted photons and for states before emitting any photon can be uncoupled. We will start by breaking the time in two time windows $0 < \tau < \tau_e + \epsilon$ (evolution of the system up to the emission of one photon) and $\tau_e + \epsilon < \tau < \infty$ (dynamics after the first photon emission).

For the first time window $0 < \tau < \tau_e$:

$$\begin{aligned} &\dot{\tilde{\phi}}_g(\tau,\tau_e) = ie^{-i\tilde{\Delta}\tau}\delta(\tau-\tau_e)c_e(\tau_e) \\ &\Rightarrow \tilde{\phi}_g(\tau,\tau_e) = ie^{-i\tilde{\Delta}\tau}\theta(\tau-\tau_e)c_e(\tau_e) \end{aligned} \tag{5.10}$$

Using 5.10 into 5.9 the differential equation of $\dot{c}_e(\tau)$ can be decoupled:

$$\begin{aligned} \dot{c}_e(\tau) &= i\frac{\tilde{\Omega}}{2}e^{i\tilde{\Delta}\tau}c_g(\tau) - \frac{1}{2}c_e(\tau) \\ \dot{c}_g(\tau) &= i\frac{\tilde{\Omega}^*}{2}e^{-i\tilde{\Delta}\tau}c_e(\tau) \end{aligned} \tag{5.11}$$

By following the same procedure for the time interval $\tau_e + \epsilon < \tau < \infty$, we get:

$$\begin{aligned} &\dot{\tilde{\phi}}_{gg}(\tau,\tau_{e2},\tau_{e1}) = ie^{-i\tilde{\Delta}\tau_{e_2}}\tilde{\phi}_e(\tau_{e2},\tau_{e1})\delta(\tau-\tau_{e2}) \\ &\Rightarrow \tilde{\phi}_g g(\tau,\tau_{e2},\tau_{e1}) = ie^{-i\tilde{\Delta}\tau_{e_2}}\tilde{\phi}_e(\tau_{e2},\tau_{e1})\theta(\tau-\tau_{e2}) \end{aligned} \tag{5.12}$$

And by using 5.12 into 5.9 the differential of equation of $\dot{\tilde{\phi}}_e(\tau,\tau_e)$ can be decoupled:

$$\begin{aligned} \dot{\tilde{\phi}}_e(\tau,\tau_e) &= i\frac{\tilde{\Omega}}{2}e^{i\tilde{\Delta}\tau}\tilde{\phi}_g(\tau,\tau_e) - \frac{1}{2}\tilde{\phi}_e(\tau,\tau_e) \\ \dot{c}_g(\tau) &= i\frac{\tilde{\Omega}^*}{2}e^{-i\tilde{\Delta}\tau}\tilde{\phi}_e(\tau,\tau_e) \end{aligned} \tag{5.13}$$

With the initial conditions $c_g(0) = 1$, and $\tilde{\phi}_g(\tau_e,\tau_e) = i\theta(\tau_e,\tau_e)c_e(\tau_e)$.

Finally, to see that we have obtained the same equations from 2.29 we will apply the change $\breve{c}_e(\tau) = e^{i\tilde{\Delta}\tau}c_e(\tau)$ and $\breve{\phi}_e(\tau) = e^{i\tilde{\Delta}\tau}\tilde{\phi}_e(\tau)$:

$$\begin{aligned} \dot{\breve{c}}_e(\tau) &= i\frac{\tilde{\Omega}}{2}c_g(\tau) - \left(\frac{1}{2} + i\tilde{\Delta}\right)\breve{c}_e(\tau) \\ \dot{c}_g(\tau) &= i\frac{\tilde{\Omega}^*}{2}\breve{c}_e(\tau) \\ \dot{\breve{\phi}}_e(\tau,\tau_e) &= i\frac{\tilde{\Omega}}{2}\breve{\phi}_g(\tau,\tau_e) - \left(\frac{1}{2} + i\tilde{\Delta}\right)\breve{\phi}_e(\tau,\tau_e) \\ \dot{\breve{\phi}}_g(\tau) &= i\frac{\tilde{\Omega}^*}{2}\breve{\phi}_e(\tau,\tau_e) \end{aligned} \tag{5.14}$$

For simplicity, in next section the tildes on the coefficients will be omitted.

5.2. System wave-function

Now that we have a formalism to explain the state of the system before and after field excitations, we are interested in using it to obtain a formal description of the creation and annihilation operators, while the laser field is driving the system (from $\tau = 0$ to $\tau = T$) and when the pulse is not active and the system relaxes from the excited state to the ground state (from $\tau = T$ to $\tau = \infty$).

The second-order photon coefficients are not normalized so we will have to impose normalization to re-define the creation operators corresponding to the generation of photons through this mechanism. We start computing the modulus square of each term:

$$\left(\sqrt{v_g}\int \phi^*_{g(e)}(\tau,\tau_e)E(v_g(\tau-\tau_e))d\tau_e\right)\left(\sqrt{v_g}\int \phi_{g(e)}(\tau,\tau_e)E^\dagger(v_g(\tau-\tau_e))d\tau_e\right)$$
$$= v_g\int\int d\tau_e d\tau'_e|\phi_{g(e)}(\tau,\tau_e)|^2\delta(z-z') = \int d\tau_e|\phi_{g(e)}(\tau,\tau_e)|^2 = |\Phi_{g(e)}|^2 \tag{5.15}$$

With the normalization factor $|\Phi_{g(e)}|^2$ we can re-define the photon creation and annihilation operators:

$$\sqrt{v_g}\int \phi_{g(e)}(\tau,\tau_e)E^\dagger(v_g(\tau-\tau_e))d\tau_e$$
$$= \frac{|\Phi_{g(e)}|}{|\Phi_{g(e)}|}\sqrt{v_g}\int \phi_{g(e)}(\tau,\tau_e)E^\dagger(v_g(\tau-\tau_e))d\tau_e = |\Phi_{g(e)}|A^\dagger_{g(e)} \tag{5.16}$$

The commutation relation of the operators $A^\dagger_{g(e)}, A_{g(e)}$ is given by:

$$[A_{g(e)}, A^\dagger_{g(e)}] =$$
$$\frac{v_g}{|\Phi_{g(e)}|^2}\int\int d\tau_e d\tau'_e\left[|\phi_{g(e)}|^2 E(v_g(\tau-\tau_e))E^\dagger(v_g(\tau-\tau'_e)) - |\phi_{g(e)}|^2 E^\dagger(v_g(\tau-\tau_e)E(v_g(\tau-\tau'_e)))\right]$$
$$= \frac{v_g}{|\Phi_{g(e)}|^2}\int\int d\tau_e d\tau'_e|\phi_{g(e)}|^2\left[E(v_g(\tau-\tau_e)), E^\dagger(v_g(\tau-\tau'_e))\right]$$
$$= \frac{v_g}{|\Phi_{g(e)}|^2}\int\int d\tau_e d\tau'_e|\phi_{g(e)}|^2\delta(v_g(\tau-\tau_e)-v_g(\tau-\tau'_e))$$
$$= \frac{\int|\phi_{g(e)}|^2 d\tau_e}{|\Phi_{g(e)}|^2} = 1 \tag{5.17}$$

We will start by formally characterizing the photon emissions in the relaxation time (from $\tau = T$ to $\tau = \infty$). Since in this part we wait enough time for all the population on the excited state to relax, setting the final time $\tau = \infty$ is a good approximation. In the relaxation window there is no laser field driving the transitions, for this reason, we will use the equations from 5.14 but setting $\tilde{\Omega} = 0$. If we wait enough time, the only nonzero coefficient at the end of this window will be $\phi_g(\tau,\tau_e)$, which corresponds to emitting one photon and staying in the ground state.

$$c_e(\tau) = c_e(T)e^{(\tau-T)(\frac{1}{2}+i\tilde{\Delta})} \Rightarrow \phi_g(\tau_e,\tau_e) = ic_e(T)e^{(\tau_e-T)(\frac{1}{2}+i\tilde{\Delta})} \tag{5.18}$$

Therefore,

$$|e,\emptyset\rangle\,(\tau=T) \rightarrow$$
$$i\sqrt{v_g}e^{i\tilde{\Delta}T}c_e(T)\int_T^\infty e^{-(\tau_e-T)(\frac{1}{2}+i\tilde{\Delta})}\hat{E}^\dagger(v_g(\tau-\tau_e))\,|g,\emptyset\rangle\,d\tau_e$$
$$= c_e(T)\hat{A}^\dagger_0\,|g,\emptyset\rangle \tag{5.19}$$

Remember that we are dealing with two transitions. The first transition $|1\rangle - |2\rangle$, is resonant with the field and has spontaneous emission. The second transition $|0\rangle - |3\rangle$ is far-detuned and also has spontaneous emission:

$$\hat{A}^\dagger_0 \equiv i\sqrt{v_g}\int_T^\infty d\tau_e e^{-\frac{1}{2}(\tau_e-T)}\hat{E}^\dagger(v_g(\tau-\tau_e)) \tag{5.20}$$

$$\hat{B}_0^\dagger \equiv i\sqrt{v_g}\int_T^\infty d\tau_e e^{-\frac{1}{2}(\tau_e - T)} e^{-i\tilde{\Delta}\tau_e}\hat{E}^\dagger(v_g(\tau-\tau_e)) \tag{5.21}$$

Where the subindex 0 corresponds to photons emitted during the relaxation time. It is interesting to look at the commutation relationship $[\hat{A}_0^\dagger, \hat{B}_0]$:

$$\begin{aligned}
&[\hat{A}_0, \hat{B}_0^\dagger] \\
&= v_g \int_T^\infty \int_T^\infty d\tau_e d\tau_e' e^{-\frac{1}{2}(\tau_e+\tau_e'-2T)} e^{-i\tilde{\Delta}\tau_e'} \left(\hat{E}(v_g(\tau-\tau_e))\hat{E}^\dagger(v_g(\tau-\tau_e')) - \hat{E}^\dagger(v_g(\tau-\tau_e'))\hat{E}(v_g(\tau-\tau_e))\right) \\
&= v_g \int_T^\infty \int_T^\infty d\tau_e d\tau_e' e^{-\frac{1}{2}(\tau_e+\tau_e'-2T)} e^{-i\tilde{\Delta}\tau_e'}[\hat{E}(v_g(\tau-\tau_e)), \hat{E}^\dagger(v_g(\tau-\tau_e'))] \\
&= \int_T^\infty \int_T^\infty d\tau_e d\tau_e' e^{-\frac{1}{2}(\tau_e+\tau_e'-2T)} e^{-i\tilde{\Delta}\tau_e'} \delta\left(\tau_e' - \tau_e\right) \\
&= e^T \int_T^\infty d\tau_e e^{-\tau_e(1+i\tilde{\Delta})} = e^{-iT\tilde{\Delta}} \frac{1}{1+i\tilde{\Delta}}
\end{aligned} \tag{5.22}$$

Since $\tilde{\Delta} >> 1$ we can approximate $[\hat{A}_0^\dagger, \hat{B}_0] \simeq 0$.

For the time window $0 < \tau < T$, when the laser pulse is driving the transitions $|1\rangle - |2\rangle$ and $|0\rangle - |3\rangle$ we will define:

$$\hat{A}_{p1}^\dagger \equiv \sqrt{v_g}\int_0^T d\tau_e \frac{\phi_1(T,\tau_e)}{|\Phi_1|}\hat{E}^\dagger(v_g(T-\tau_e)) \tag{5.23}$$

$$\hat{A}_{p2}^\dagger \equiv \sqrt{v_g}\int_0^T d\tau_e \frac{\phi_2(T,\tau_e)}{|\Phi_2|}\hat{E}^\dagger(v_g(T-\tau_e)) \tag{5.24}$$

$$\hat{B}_{p1}^\dagger \equiv \sqrt{v_g}e^{-i\tilde{\Delta}T}\int_0^T d\tau_e \frac{\phi_0(T,\tau_e)}{|\Phi_0|}\hat{E}^\dagger(v_g(T-\tau_e)) \tag{5.25}$$

$$\hat{B}_{p2}^\dagger \equiv \sqrt{v_g}e^{-i\tilde{\Delta}T}\int_0^T d\tau_e \frac{\phi_3(T,\tau_e)}{|\Phi_3|}\hat{E}^\dagger(v_g(T-\tau_e)) \tag{5.26}$$

Where the subindex p indicates that the photon emission happens inside the pulse. The coefficients $\phi_1(T,\tau_e), \phi_2(T,\tau_e), \phi_0(T,\tau_e), \phi_3(T,\tau_e)$ will be solved in the following sections by using the differential equations from 5.14 for each particular shape of the pulse $\tilde{\Omega}(\tau)$.

Now that we have well defined operators, we can work out an expression for the wave-function of our system after applying the protocol to create a GHZ state. In order to keep the equations simple, we will drop the time-dependency of the coefficients and the modulus square $|\Phi_i(T)| \rightarrow \Phi_i$. The system wave-function for the early part of the protocol, taking into account the second-order emissions is given by:

$$\begin{aligned}
&\frac{1}{\sqrt{2}}\left(|0,\emptyset\rangle + |1,\emptyset\rangle\right) \xrightarrow{\pi_{1-2}} \frac{1}{\sqrt{2}}\Big(c_0\,|0,\emptyset\rangle + c_3\,|3,\emptyset\rangle + \Phi_0 \hat{B}^{\dagger,e}_{p1}\,|0,\emptyset\rangle + \Phi_3 \hat{B}^{\dagger,e}_{p2}\,|3,\emptyset\rangle + c_1\,|1,\emptyset\rangle \\
&\quad + c_2\,|2,\emptyset\rangle + \Phi_1 \hat{A}^{\dagger,e}_{p1}\,|1,\emptyset\rangle + \Phi_2 \hat{A}^{\dagger}_{p2}\,|2,\emptyset\rangle\Big) \xrightarrow{s.e.} \frac{1}{\sqrt{2}}\Big(c_0\,|0,\emptyset\rangle + c_3 \hat{B}^{\dagger,e}_{0}\,|0,\emptyset\rangle + \Phi_0 \hat{B}^{\dagger,e}_{p1}\,|0,\emptyset\rangle \\
&\quad + \Phi_3 \hat{B}^{\dagger,e}_{p2} \hat{B}^{\dagger,e}_{0}\,|0,\emptyset\rangle + c_1\,|1,\emptyset\rangle + c_2 \hat{A}^{\dagger,e}_{0}\,|1,\emptyset\rangle + \Phi_1 \hat{A}^{\dagger,e}_{p1}\,|1,\emptyset\rangle + \Phi_2 \hat{A}^{\dagger,e}_{p2} \hat{A}^{\dagger,e}_{0}\,|1,\emptyset\rangle\Big) \\
&\quad = \frac{1}{\sqrt{2}}\Big(c_0 + c_3 \hat{B}^{\dagger,e}_{0} + \Phi_0 \hat{B}^{\dagger,e}_{p1} + \Phi_3 \hat{B}^{\dagger,e}_{p2} \hat{B}^{\dagger,e}_{0}\Big)\,|0,\emptyset\rangle \\
&\quad\quad + \frac{1}{\sqrt{2}}\Big(c_1 + c_2 \hat{A}^{\dagger,e}_{0} + \Phi_1 \hat{A}^{\dagger,e}_{p1} + \Phi_2 \hat{A}^{\dagger,e}_{p2} \hat{A}^{\dagger,e}_{0}\Big)\,|1,\emptyset\rangle \\
&\quad = \frac{1}{\sqrt{2}}\left(Q^e_0\,|0,\emptyset\rangle + Q^e_1\,|1,\emptyset\rangle\right)
\end{aligned}$$

We can compress the action of the laser pulse and the spontaneous emission into two operators, Q^e_0 and Q^e_1 (redefining the operators derived in section 4.2). After applying the late part of the protocol, the state of the system will be given by:

$$M\,|\Psi\rangle = \frac{-1}{\sqrt{2}}\left(Q^{eL}_{01}\,|0,\emptyset\rangle + Q^{eL}_{10}\,|1,\emptyset\rangle\right) \tag{5.27}$$

For the generation of N entangled photons, the same operators will be applied N times:

$$M^N\,|\Psi\rangle = \frac{(-1)^N}{\sqrt{2}}\left(\prod_{k=1}^{N} Q^{eL,k}_{01}\,|0,\emptyset\rangle + \prod_{k=1}^{N} Q^{eL,k}_{10}\,|1,\emptyset\rangle\right) \tag{5.28}$$

5.3. Conditional fidelity with second-order emissions

In this section we will compute the conditional fidelity taking into account the presence of the extra energy level with spontaneous emission and keeping track of the emissions of photons during the pulse and in the relaxation time.

When computing the fidelity for our system there are many variables that we have to take into account and we will have to make some assumptions on the system we are working with. To start, we will assume that the photons generated during the pulse are blocked, therefore, will never be detected. Despite the fact that we will not measure these photons, they will contribute to the fidelity of the system, since we will have to trace over them.

It is realistic to think that experimentally we could get rid of these photons, because for some setups, the background light from the laser may be relevant and it may be necessary to prevent the detector to measure during the pulse, to avoid leaking light being detected.

As seen in the previous section, the operators that describe the wave-function of the system when taking into account second-order emissions of photons are:

$$\begin{aligned}
&Q^L_1 Q^e_0 \\
&= \Big(c_0 + c_3 B^{\dagger,L}_0 + \Phi_0 B^{\dagger,L}_{p1} + \Phi_3 B^{\dagger,L}_{p2} B^{\dagger,L}_0\Big)\Big(c_1 + c_2 A^{\dagger,e}_0 + \Phi_1 A^{\dagger,e}_{p1} + \Phi_2 A^{\dagger,e}_{p2} A^{\dagger,e}_0\Big)
\end{aligned} \tag{5.29}$$

We are interested in taking into account the action of the cavity filters and the efficiency of the system. With these considerations, the operators can be expressed as:

$$
\begin{aligned}
&Q_1^L Q_0^e = \\
&\left(c_1 + c_2\sqrt{\eta_2}A_0^{\dagger,L} + c_2\sqrt{1-\eta_2}\tilde{A}_0^{\dagger,L} + \Phi_1 A_{p1}^{\dagger,L} + \Phi_2\sqrt{\eta_2}A_{p2}^{\dagger,L}A_0^{\dagger,L} + \Phi_2\sqrt{1-\eta_2}A_{p2}^{\dagger,L}\tilde{A}_0^{\dagger,L}\right) \\
&\left(c_0 + c_3\sqrt{\eta_3}B_0^{\dagger,e} + c_3\sqrt{1-\eta_3}\tilde{B}_0^{\dagger,e} + \Phi_0 B_{p1}^{\dagger,e} + \Phi_3\sqrt{\eta_3}B_{p2}^{\dagger,e}B_0^{\dagger,e} + \Phi_3\sqrt{1-\eta_3}B_{p2}^{\dagger,e}\tilde{B}_0^{\dagger,e}\right)
\end{aligned}
\tag{5.30}
$$

Now we apply the projector $P_{N\geq 1}$ on $Q_0^L Q_1^e$ by keeping only the terms that correspond to receiving at least one photon in the detector (for one cycle of the protocol).

$$
\begin{aligned}
&P_{N\geq 1}Q_0^L Q_1^e = \tilde{Q}_{01}^{Le} = \\
&c_1c_3\sqrt{\eta_3}B_0^{\dagger,e} + c_1\Phi_3\sqrt{\eta_3}B_{p_2}^{\dagger,e}B_0^{\dagger,e} + c_2c_0\sqrt{\eta_2}A_0^{\dagger,L} + c_2c_3\sqrt{\eta_2}\sqrt{\eta_3}A_0^{\dagger,L}B_0^{\dagger,e} \\
&c_2c_3\sqrt{\eta_2}\sqrt{1-\eta_3}A_0^{\dagger,L}\tilde{B}_0^{\dagger,e} + c_2\Phi_0\sqrt{\eta_2}A_0^{\dagger,L}B_{p_1}^{\dagger,e} + c_2\Phi_3\sqrt{\eta_2}\sqrt{\eta_3}A_0^{\dagger,L}B_{p_2}^{\dagger,e}B_0^{\dagger,e} \\
&+ c_2\Phi_3\sqrt{\eta_2}\sqrt{1-\eta_3}A_0^{\dagger,L}B_{p_2}^{\dagger,e}\tilde{B}_0^{\dagger,e} + c_2c_3\sqrt{1-\eta_2}\sqrt{\eta_3}\tilde{A}_0^{\dagger,L}B_0^{\dagger,e} + c_2\Phi_3\sqrt{1-\eta_2}\sqrt{\eta_3}\tilde{A}_0^{\dagger,L}B_{p_2}^{\dagger,e}B_0^{\dagger,e} \\
&+ \Phi_1c_3\sqrt{\eta_3}A_{p_1}^{\dagger,L}B_0^{\dagger,e} + \Phi_1\Phi_3\sqrt{\eta_3}A_{p_1}^{\dagger,L}B_{p_2}^{\dagger,e}B_0^{\dagger,e} + \Phi_2c_0\sqrt{\eta_2}A_{p_2}^{\dagger,L}A_0^{\dagger,L} \\
&\Phi_2c_3\sqrt{\eta_2}\sqrt{\eta_3}A_{p_2}^{\dagger,L}A_0^{\dagger,L}B_0^{\dagger,e} + \Phi_2c_3\sqrt{\eta_2}\sqrt{1-\eta_3}A_{p_2}^{\dagger,L}A_0^{\dagger,L}\tilde{B}_0^{\dagger,e} + \Phi_2\Phi_0\sqrt{\eta_2}A_{p_2}^{\dagger,L}A_0^{\dagger,L}B_{p_1}^{\dagger,e} \\
&\Phi_2\Phi_3\sqrt{\eta_2}\sqrt{\eta_3}A_{p_2}^{\dagger,L}A_0^{\dagger,L}B_{p_2}^{\dagger,e}B_0^{\dagger,e} + \Phi_2\Phi_3\sqrt{\eta_2}\sqrt{1-\eta_3}A_{p_2}^{\dagger,L}A_0^{\dagger,L}B_{p_2}^{\dagger,e}\tilde{B}_0^{\dagger,e} \\
&\Phi_2c_3\sqrt{1-\eta_2}\sqrt{\eta_3}A_{p_2}^{\dagger,L}\tilde{A}_0^{\dagger,L}B_0^{\dagger,e} + \Phi_2\Phi_3\sqrt{1-\eta_2}\sqrt{\eta_3}A_{p_2}^{\dagger,L}\tilde{A}_0^{\dagger,L}B_{p_2}^{\dagger,e}B_0^{\dagger,e}
\end{aligned}
\tag{5.31}
$$

The wavefunction of the system projected onto the subspace where at least one photon is measured on each cycle of the protocol is:

$$
P_{N\geq 1}\left|\Psi_{re}\right\rangle = \frac{(-1)^N}{\sqrt{2}}\left[\prod_{k=1}^{N}\tilde{Q}_{01}^{eL,k}\left|0,\emptyset\right\rangle + \prod_{k=1}^{N}\tilde{Q}_{10}^{eL,k}\left|1,\emptyset\right\rangle\right]
$$

Now, before continuing the computation of the fidelity we have to trace over the lost and filtered photons. Similar to the conditional fidelity computed in section 4.3, we will have photons that get to the detector, filtered or lost photons that we can not measure and we will also have photons emitted during the pulse that also will not be measured. For this reason, we will split the photonic vacuum in two parts, the modes of photons that are being measured and the modes that are not measured and will be traced over $\left|\emptyset_S,\emptyset_R\right\rangle$.

It will also be interesting to split the operator $\prod_{k=1}^{N}\tilde{Q}_{01}^{eL,k} = \tilde{D}_{01}^{eL} + \tilde{R}_{01}^{eL}$. Where $\tilde{D}_{01}^{eL}$ only contains combinations of photons that get to the detector and $\tilde{R}_{01}^{eL}$, that contains combinations of lost and detected photons. Then, the trace over the reservoir can be expressed as:

$$
\begin{aligned}
&tr_R\left(P_{N\geq 1}\hat{\rho}P_{N\geq 1}\right) = \sum_R \left\langle R\right| P_{N\geq 1}\left|\Psi_{re}\right\rangle (h.c.) \\
&= \frac{1}{2}\sum_R \left\langle R\right| \left((\tilde{D}_{01}^{eL} + \tilde{R}_{01}^{eL})\left|0,\emptyset_S,\emptyset_R\right\rangle + (\tilde{D}_{10}^{eL} + \tilde{R}_{10}^{eL})\left|1,\emptyset_S,\emptyset_R\right\rangle\right)(h.c.) \\
&= \frac{1}{2}\left[\tilde{D}_{01}^{eL}\left|0,\emptyset_S\right\rangle + \tilde{D}_{10}^{eL}\left|1,\emptyset_S\right\rangle\right](h.c.) + \frac{1}{2}\sum_{R\neq\emptyset_R}\left[\left\langle R\right|\tilde{R}_{01}^{eL}\left|0,\emptyset_S,\emptyset_R\right\rangle + \left\langle R\right|\tilde{R}_{10}^{eL}\left|1,\emptyset_S,\emptyset_R\right\rangle\right](h.c.)
\end{aligned}
\tag{5.32}
$$

Where we have traced over the part containing only photons that get to the detector. We still have to perform the sum over R, which belongs to any possible configuration containing lost photons, filtered photons or photons emitted during the pulse $\{\tilde{A}_0^{\dagger,e}, \tilde{B}_0^{\dagger}, A_{p1}^{\dagger}, B_{p1}^{\dagger}, A_{p2}^{\dagger}, B_{p2}^{\dagger}\}$. Now we will compute the overlap $\langle\Psi_{id}|\, tr_R\left(P_{N\geq 1}\hat{\rho}P_{N\geq 1}\right)|\Psi_{id}\rangle$:

$$
\begin{aligned}
&\langle\Psi_{id}|\, tr_R\left(P_{N\geq 1}\hat{\rho}P_{N\geq 1}\right)|\Psi_{id}\rangle \\
&= \frac{1}{4}\left[\left(\langle 0, L^{\otimes N}| + \langle 1, e^{\otimes N}|\right)\left(\tilde{D}_{01}^{eL}|0,\emptyset_S\rangle + \tilde{D}_{10}^{eL}|1,\emptyset_S\rangle\right)\right](h.c.) \\
&+ \frac{1}{4}\left[\left(\langle 0, L^{\otimes N}| + \langle 1, e^{\otimes N}|\right)\sum_{R\neq\emptyset_R}\left[\langle R|\,\tilde{R}_{01}^{eL}|0,\emptyset_S,\emptyset_R\rangle + \langle R|\,\tilde{R}_{10}^{eL}|1,\emptyset_S,\emptyset_R\rangle\right]\right](h.c.) \\
&= \frac{1}{4}\left[\langle 0, L^{\otimes N}|\,\tilde{D}_{01}^{eL}|0,\emptyset_S\rangle + \langle 1, e^{\otimes N}|\,\tilde{D}_{10}^{eL}|1,\emptyset_S\rangle\right](h.c.) \\
&+ \frac{1}{4}\sum_{R\neq\emptyset_R}\left[\langle 0, L^{\otimes N}, R|\,\tilde{R}_{01}^{eL}|0,\emptyset_S,\emptyset_R\rangle + \langle 1, e^{\otimes N}, R|\,\tilde{R}_{10}^{eL}|1,\emptyset_S,\emptyset_R\rangle\right](h.c.) \\
&= \frac{1}{4}\left[2\langle 0, L^{\otimes N}|\,\tilde{D}_{01}^{eL}|0,\emptyset_S\rangle\right](h.c.) + \frac{1}{2}\sum_{R\neq\emptyset_R}\left[\langle 0, L^{\otimes N}, R|\,\tilde{R}_{01}^{eL}|0,\emptyset_S,\emptyset_R\rangle\right](h.c.)
\end{aligned}
\tag{5.33}
$$

Where symmetry of the $\tilde{D}_{01}^{eL}$ and $\tilde{R}_{01}^{eL}$ operators has been used (the exact same procedure described in section 4.3).

Again, the only component from $\langle 0, L^{\otimes N}|\,\tilde{D}_{01}^{eL}|0,\emptyset_S\rangle$ that survives is $\left[c_0c_2\sqrt{\eta_2}\right]^N$. Also, $\sum_{R\neq\emptyset_R}\left[\langle 0, L^{\otimes N}, R|\,\tilde{R}_{01}^{eL}|0,\emptyset_S,\emptyset_R\rangle\right]$ contains all possible combinations of $c_0c_2\sqrt{\eta_2}$, $\Phi_0c_2\sqrt{\eta_2}$, $\Phi_0\Phi_2\sqrt{\eta_2}$, $c_3c_2\sqrt{\eta_2}\sqrt{1-\eta_3}$, $c_3\Phi_2\sqrt{\eta_2}\sqrt{1-\eta_3}$, $\Phi_3c_2\sqrt{\eta_2}\sqrt{1-\eta_3}$ and $\Phi_3\Phi_2\sqrt{\eta_2}\sqrt{1-\eta_3}$ except the one that only contains photons that are not lost. For this reason:

$$
\begin{aligned}
&\langle\Psi_{id}|\, tr_R\left(P_{N\geq 1}\hat{\rho}P_{N\geq 1}\right)|\Psi_{id}\rangle \\
&= \frac{1}{2}\eta_2^N|c_0c_2|^{2N} + \frac{1}{2}\left[\eta_2\left(|c_0c_2|^2+|\Phi_0c_2|^2+|\Phi_0\Phi_2|^2\right) + \eta_2(1-\eta_3)\left(|c_3c_2|^2+|c_3\Phi_2|^2+|\Phi_3c_2|^2+|\Phi_3\Phi_2|^2\right)\right]^N
\end{aligned}
\tag{5.34}
$$

The denominator part of the conditional fidelity can be expressed as:

$$
\begin{aligned}
&tr_S\left(tr_R\left(P_{N\geq 1}\hat{\rho}P_{N\geq 1}\right)\right) = \\
&\frac{1}{2}\sum_{P=\{0,1\},S,R}\langle P,S,R|\left((\tilde{D}_{01}^{eL}+\tilde{R}_{01}^{eL})|0,\emptyset_S,\emptyset_R\rangle + (\tilde{D}_{10}^{eL}+\tilde{R}_{10}^{eL})|1,\emptyset_S,\emptyset_R\rangle\right)(h.c.) \\
&= \frac{1}{2}\sum_{S,R}\langle 0,S,R|\left((\tilde{D}_{01}^{eL}+\tilde{R}_{01}^{eL})|0,\emptyset_S,\emptyset_R\rangle\right)(h.c.) \\
&+ \frac{1}{2}\sum_{S,R}\langle 1,S,R|\left((\tilde{D}_{10}^{eL}+\tilde{R}_{10}^{eL})|1,\emptyset_S,\emptyset_R\rangle\right)(h.c.) \\
&= \sum_{S,R}\langle 0,S,R|\left((\tilde{D}_{01}^{eL}+\tilde{R}_{01}^{eL})|0,\emptyset_S,\emptyset_R\rangle\right)(h.c.)
\end{aligned}
$$

Where P corresponds to the spin transition of the atom/quantum dot. Notice that in this case, for each part of the sum only one term survives. We will end up with the modulus square of each possible combinations of photons that get to the detector (modulus square of each combination of the coefficients in $\tilde{Q}_{01}^{eL}$). For this reason,

$$
\begin{aligned}
& tr_S\left(tr_R\left(P_{N\geq 1}\hat{\rho}P_{N\geq 1}\right)\right) \\
& = \left[\eta_2\left(|c_0c_2|^2+|c_0\Phi_2|^2+|\Phi_0c_2|^2+|\Phi_0\Phi_2|^2\right)+\eta_3\left(|c_3c_1|^2+|c_3\Phi_1|^2+|\Phi_3c_1|^2+|\Phi_3\Phi_1|^2\right)\right. \\
& \qquad \left.+\left(\eta_3(1-\eta_2)+\eta_2(1-\eta_3)\right)\left(|c_3c_2|^2+|c_3\Phi_2|^2+|\Phi_3c_2|^2+|\Phi_3\Phi_2|^2\right)\right]^N
\end{aligned}
\tag{5.35}
$$

The conditional fidelity for N qubits including the second-order emissions can be expressed as:

$$
\boxed{
\begin{aligned}
& F=\frac{\frac{1}{2}D_1^N+\frac{1}{2}\left(D_1+D_2\right)^N}{\left(D_1+D_2+D_3\right)^N} \\
& D_1=\eta_2|c_0c_2|^2 \\
& D_2=\eta_2\left(|c_0\Phi_2|^2+|\Phi_0c_2|^2+|\Phi_0\Phi_2|^2\right)+\eta_2(1-\eta_3)\left(|c_3c_2|^2+|c_3\Phi_2|^2+|\Phi_3c_2|^2+|\Phi_3\Phi_2|^2\right) \\
& D_3=\eta_3\left(|c_3c_1|^2+|c_3\Phi_1|^2+|\Phi_3c_1|^2+|\Phi_3\Phi_1|^2\right) \\
& \quad+\left(\eta_2\eta_3+\eta_3(1-\eta_2)\right)\left(|c_3c_2|^2+|c_3\Phi_2|^2+|\Phi_3c_2|^2+|\Phi_3\Phi_2|^2\right)
\end{aligned}
}
\tag{5.36}
$$

For convenience, the result of the conditional fidelity has been split in several parts.

For one round of the protocol, D_1 corresponds to the emission of only one photon from the main transition. D_2 contains two types of terms, the terms with the factor η_2, tracing over the photons inside the pulse, and the terms with $\eta_2(1-\eta_3)$, containing terms with two or more photons emitted, but only being detected the photon from the transition we are interested. The factor $\frac{1}{2}$ in front of (D_1+D_2) comes from the trace over the reservoir.

D_3 contains all the rest of combinations of photons that arrive to the detector but come from the far-detuned transition.

5.4. Second-order coefficients of the square pulse

In this section we will use the results derived in 5.1 to obtain the analytical solutions of the second excitation coefficients for the square pulse $\{\Phi_1, \Phi_2, \Phi_0, \Phi_3\}$. The differential equations that describe the dynamics of the second-order coefficients are the same as the equations derived an solved in 2.4.1, but with the initial conditions given by $\phi_g(\tau_e, \tau_e) = i\theta(\tau_e, \tau_e)c_e(\tau_e)$. For this reason, a general solution for the second-order coefficients can be expressed as:

$$\phi_e(\tau, \tau_e) = -i\frac{\tilde{\Omega}_e^2}{\hat{\Omega}_e^2} e^{\frac{i\tau}{2}(\frac{i}{2}-\tilde{\Delta})} sin\left(\frac{\tau_e}{2}\hat{\Omega}_e\right) sin\left(\frac{\tau - \tau_e}{2}\hat{\Omega}_e\right) \tag{5.37}$$

$$\phi_g(\tau, \tau_e) = \frac{\tilde{\Omega}_e}{\hat{\Omega}_e} e^{\frac{i\tau}{2}(\frac{i}{2}-\tilde{\Delta})} sin\left(\frac{\tau_e}{2}\hat{\Omega}_e\right) \left[i\frac{(i-2\tilde{\Delta})}{2\hat{\Omega}} sin\left(\frac{\tau - \tau_e}{2}\hat{\Omega}_e\right) - cos\left(\frac{\tau - \tau_e}{2}\hat{\Omega}_e\right)\right] \tag{5.38}$$

Before computing the analytical expressions for the coefficients we will see that there is no need to take into account the presence of inhomogeneous broadening in the expansion. So far, what we have seen is that the broadening appears in the analytical expansions with powers of $(\tilde{\Delta}^{-2})$. We know that the second order coefficients will be proportional to the spontaneous emission of the system, which is proportional to $|\Phi_e|^2 \propto 1 - |c_e|^2 \propto T \propto \tilde{\Delta}^{-1}$. For this reason, we expect the inhomogeneous broadening to appear at least with powers of $\propto \tilde{\Delta}^{-3}$. Since we will only expand the analytical solutions up to $\tilde{\Delta}^{-2}$ we will neglect the inhomogeneous broadening in the second excitation coefficients.

Analytical expansion of Φ_2

We start by expanding the solution of $|\Phi_2|^2$:

$$\begin{aligned}
|\Phi_2|^2 &= \int_0^T |\phi_2(T, \tau_e)|^2 d\tau_e = -i\frac{\tilde{\Omega}_2^2}{\hat{\Omega}_2^2} e^{-\frac{T}{2}} \int_0^T |sin\left(\frac{\tau_e}{2}\hat{\Omega}_2\right) sin\left(\frac{\tau - \tau_e}{2}\hat{\Omega}_2\right)|^2 \\
&= e^{-\frac{T}{2}} \int_0^T |sin\left(\frac{\tau_e}{2}\hat{\Omega}_2\right) \left[sin\left(\frac{T}{2}\hat{\Omega}_2\right) cos\left(\frac{\tau_e}{2}\hat{\Omega}_2\right) - cos\left(\frac{T}{2}\hat{\Omega}_2\right) sin\left(\frac{\tau_e}{2}\hat{\Omega}_2\right)\right]|^2
\end{aligned}$$

Where in the first step we have used the property $sin(A-B) = sin(A)cos(B) - cos(A)sin(B)$. Remember that we have defined our pulse to fulfill $\frac{T}{2}\hat{\Omega}_2 = \frac{\pi}{2}$:

$$\begin{aligned}
|\Phi_2|^2 &= e^{-\frac{T}{2}} \int_0^T |sin\left(\frac{\tau_e}{2}\hat{\Omega}_2\right) cos\left(\frac{\tau_e}{2}\hat{\Omega}_2\right)|^2 = \frac{1}{4}e^{-\frac{T}{2}} \int_0^T |sin\left(\frac{\tau_e}{2}\hat{\Omega}_2\right)|^2 \\
&= \frac{1}{4}e^{-\frac{T}{2}} \left(\frac{T}{2} - \frac{sin(2T\hat{\Omega}_2)}{4\hat{\Omega}_2}\right) \approx \frac{T}{8} - \frac{T^2}{16} \\
&\approx \frac{\sqrt{3}\pi}{8\tilde{\Delta}} \left(1 - \frac{\sqrt{3}\pi}{2\tilde{\Delta}}\right)
\end{aligned}$$

Analytical expansion of Φ_1

For the $|\Phi_1|^2$ coefficient we will have:

$$\begin{aligned}
&|\Phi_1|^2 = \int_0^T |\phi_1(T, \tau_e)|^2 d\tau_e = \\
&\frac{\tilde{\Omega}_2}{\hat{\Omega}_2} e^{-\frac{T}{2}} \int_0^T |sin\left(\frac{\tau_e}{2}\hat{\Omega}_2\right) \left[\frac{1}{2\hat{\Omega}_2} sin\left(\frac{T - \tau_e}{2}\hat{\Omega}_2\right) + cos\left(\frac{T - \tau_e}{2}\hat{\Omega}_2\right)\right]|^2
\end{aligned} \tag{5.39}$$

We will use $sin(A-B) = sin(A)cos(B)-cos(A)sin(B)$, and also $cos(A-B) = cos(A)cos(B)+ sin(A)sin(B)$:

$$|\Phi_1|^2 = \frac{\tilde{\Omega}_2}{\hat{\Omega}_2}e^{-\frac{T}{2}}\int_0^T |sin\left(\frac{\tau_e}{2}\hat{\Omega}_2\right)\left[\frac{1}{2\hat{\Omega}_2}sin\left(\frac{T}{2}\hat{\Omega}_2\right)cos\left(\frac{\tau_e}{2}\hat{\Omega}_2\right) - \frac{1}{2\hat{\Omega}_2}cos\left(\frac{T}{2}\hat{\Omega}_2\right)sin\left(\frac{\tau_e}{2}\hat{\Omega}_2\right)\right.$$
$$\left. + cos\left(\frac{T}{2}\hat{\Omega}_2\right)cos\left(\frac{\tau_e}{2}\hat{\Omega}_2\right) + sin\left(\frac{T}{2}\hat{\Omega}_2\right)sin\left(\frac{\tau_e}{2}\hat{\Omega}_2\right)\right]|^2$$

Now, we apply the constrain $\frac{T}{2}\hat{\Omega}_2 = \frac{\pi}{2}$ and we use $\frac{1}{2\hat{\Omega}_2} \approx \frac{\sqrt{3}}{2\tilde{\Delta}}$:

$$\begin{aligned}
|\Phi_1|^2 &= \frac{\tilde{\Omega}_2}{\hat{\Omega}_2}e^{-\frac{T}{2}}\int_0^T |sin\left(\frac{\tau_e}{2}\hat{\Omega}_2\right)\left[\frac{1}{2\hat{\Omega}_2}cos\left(\frac{\tau_e}{2}\hat{\Omega}_2\right) + sin\left(\frac{\tau_e}{2}\hat{\Omega}_2\right)\right]|^2 \\
&\approx e^{-\frac{T}{2}}\int_0^T sin^2\left(\frac{\tau_e}{2}\hat{\Omega}_2\right)\left(\frac{3}{4\tilde{\Delta}^2}cos^2\left(\frac{\tau_e}{2}\hat{\Omega}_2\right) + sin^2\left(\frac{\tau_e}{2}\hat{\Omega}_2\right) + \frac{\sqrt{3}}{\tilde{\Delta}}cos\left(\frac{\tau_e}{2}\hat{\Omega}_2\right)sin\left(\frac{\tau_e}{2}\hat{\Omega}_2\right)\right) \\
&= e^{-\frac{T}{2}}\frac{3}{4\tilde{\Delta}^2}\int_0^T sin^2\left(\frac{\tau_e}{2}\hat{\Omega}_2\right)cos^2\left(\frac{\tau_e}{2}\hat{\Omega}_2\right) + e^{-\frac{T}{2}}\int_0^T sin^4\left(\frac{\tau_e}{2}\hat{\Omega}_2\right) \\
&+ e^{-\frac{T}{2}}\frac{\sqrt{3}}{\tilde{\Delta}}\int_0^T cos\left(\frac{\tau_e}{2}\hat{\Omega}_2\right)sin^3\left(\frac{\tau_e}{2}\hat{\Omega}_2\right) \\
&= e^{-\frac{T}{2}}\left[\frac{1}{16\hat{\Omega}_2}\left(6\hat{\Omega}_2 - 8sin\left(T\hat{\Omega}_2\right) + sin\left(2T\hat{\Omega}_2\right)\right) + \frac{3}{4\tilde{\Delta}^2}\left(\frac{T}{8} - \frac{1}{16\hat{\Omega}_2}sin\left(2T\hat{\Omega}_2\right)\right)\right] \\
&+ e^{-\frac{T}{2}}\left[+\frac{3}{4\tilde{\Delta}^2}\left(\frac{T}{8} - \frac{1}{16\hat{\Omega}_2}sin\left(2T\hat{\Omega}_2\right)\right) - \frac{\sqrt{3}}{\tilde{\Delta}}sin^4\left(\frac{T}{2}\hat{\Omega}_2\right)\right] \\
&\approx \frac{3T}{8} - \frac{T^2}{2}\left(\frac{3}{8} - \frac{1}{\pi^2}\right) \approx \frac{3\sqrt{3}\pi}{8\tilde{\Delta}} - \frac{3\pi^2}{2\tilde{\Delta}^2}\left(\frac{3}{8} - \frac{1}{\pi^2}\right)
\end{aligned} \tag{5.40}$$

Analytical expansion of Φ_3

For the $|\Phi_3|^2$ coefficient we will have:

$$\begin{aligned}
\int_0^T |\phi_3(T,\tau_e)|^2 d\tau_e &= |\frac{\tilde{\Omega}_3^2}{\hat{\Omega}_3^2}|^2 e^{-\frac{T}{2}}\int_0^T |sin\left(\frac{\tau_e}{2}\hat{\Omega}_3\right)sin\left(\frac{\tau-\tau_e}{2}\hat{\Omega}_3\right)|^2 \\
&= e^{-\frac{T}{2}}|\frac{\tilde{\Omega}_3^2}{\hat{\Omega}_3^2}|^2\int_0^T |sin\left(\frac{\tau_e}{2}\hat{\Omega}_3\right)\left[sin\left(\frac{T}{2}\hat{\Omega}_3\right)cos\left(\frac{\tau_e}{2}\hat{\Omega}_3\right) - cos\left(\frac{T}{2}\hat{\Omega}_3\right)sin\left(\frac{\tau_e}{2}\hat{\Omega}_3\right)\right]|^2 \\
&\approx e^{-\frac{T}{2}}|\frac{\tilde{\Omega}_3^2}{\hat{\Omega}_3^2}|^2\int_0^T |sin^2\left(\frac{\tau_e}{2}\hat{\Omega}_3\right)|^2 \approx \left(1-\frac{T}{2}\right)\frac{1}{16}\frac{3T}{8} \\
&\approx \frac{3}{16}\left(\frac{\sqrt{3}\pi}{8\tilde{\Delta}} - \frac{3\pi^2}{16\tilde{\Delta}^2}\right)
\end{aligned}$$

Analytical expansion of Φ_0

Finally, the expansion of $|\Phi_0|^2$ is:

$$\int_0^T |\phi_0(T,\tau_e)|^2 d\tau_e = |\frac{\tilde{\Omega}_3}{\hat{\Omega}_3}|^2 e^{-\frac{T}{2}} \int_0^T |sin\left(\frac{\tau_e}{2}\hat{\Omega}_3\right)\left[\frac{1+2\tilde{\Delta}}{2\hat{\Omega}_3} sin\left(\frac{T-\tau_e}{2}\hat{\Omega}_3\right) + cos\left(\frac{T-\tau_e}{2}\hat{\Omega}_3\right)\right]|^2$$

$$= |\frac{\tilde{\Omega}_3}{\hat{\Omega}_3}|^2 e^{-\frac{T}{2}} \int_0^T |sin\left(\frac{\tau_e}{2}\hat{\Omega}_3\right)\left[\frac{1+2\tilde{\Delta}}{2\hat{\Omega}_3} sin\left(\frac{T}{2}\hat{\Omega}_3\right) cos\left(\frac{\tau_e}{2}\hat{\Omega}_3\right) - \frac{1+2\tilde{\Delta}}{2\hat{\Omega}_3} cos\left(\frac{T}{2}\hat{\Omega}_3\right) sin\left(\frac{\tau_e}{2}\hat{\Omega}_3\right)\right.$$

$$\left. + cos\left(\frac{T}{2}\hat{\Omega}_3\right) cos\left(\frac{\tau_e}{2}\hat{\Omega}_3\right) + sin\left(\frac{T}{2}\hat{\Omega}_3\right) sin\left(\frac{\tau_e}{2}\hat{\Omega}_3\right)\right]|^2$$

$$\approx |\frac{\tilde{\Omega}_3}{\hat{\Omega}_3}|^2 e^{-\frac{T}{2}} \int_0^T |\left[\frac{1+2\tilde{\Delta}}{2\hat{\Omega}_3} sin^2\left(\frac{\tau_e}{2}\hat{\Omega}_3\right) - cos\left(\frac{\tau_e}{2}\hat{\Omega}_3\right) sin\left(\frac{\tau_e}{2}\hat{\Omega}_3\right)\right]|^2$$

$$\approx |\frac{\tilde{\Omega}_3}{\hat{\Omega}_3}|^2 e^{-\frac{T}{2}} \int_0^T \left[cos^2\left(\frac{\tau_e}{2}\hat{\Omega}_3\right) sin^2\left(\frac{\tau_e}{2}\hat{\Omega}_3\right) + \frac{3}{4} sin^4\left(\frac{\tau_e}{2}\hat{\Omega}_3\right)\right.$$

$$\left. - \sqrt{3}(\frac{1}{2} + \tilde{\Delta}) cos\left(\frac{\tau_e}{2}\hat{\Omega}_3\right) sin^3\left(\frac{\tau_e}{2}\hat{\Omega}_3\right)\right]$$

$$= \frac{1}{4} e^{-\frac{T}{2}} \left[\frac{3}{64\hat{\Omega}_3}\left(6\hat{\Omega}_3 - 8 sin\left(T\hat{\Omega}_3\right) + sin\left(2T\hat{\Omega}_3\right)\right) + \frac{T}{8} - \frac{1}{16\hat{\Omega}_3} sin\left(2T\hat{\Omega}_3\right)\right.$$

$$\left. - \frac{\sqrt{3}}{2\hat{\Omega}_3} sin^4\left(\frac{T}{2}\hat{\Omega}_3\right)\right] \approx \left(1 - \frac{T}{2}\right)\frac{13T}{128}$$

$$\approx \left(1 - \frac{\sqrt{3}\pi}{2\tilde{\Delta}}\right)\frac{13\sqrt{3}\pi}{128\tilde{\Delta}}$$

The second-order coefficients for the square-shaped pulse with the optimal time derived in Chapter 3 are:

$$|\Phi_2|^2 \approx \frac{\sqrt{3}\pi}{8\tilde{\Delta}}\left(1 - \frac{\sqrt{3}\pi}{2\tilde{\Delta}}\right) \qquad |\Phi_1|^2 \approx \frac{3\sqrt{3}\pi}{8\tilde{\Delta}} - \frac{3\pi^2}{2\tilde{\Delta}^2}\left(\frac{3}{8} - \frac{1}{\pi^2}\right) \tag{5.41}$$

$$|\Phi_3|^2 \approx \frac{3}{16}\left(\frac{\sqrt{3}\pi}{8\tilde{\Delta}} - \frac{3\pi^2}{16\tilde{\Delta}^2}\right) \qquad |\Phi_0|^2 \approx \left(1 - \frac{\sqrt{3}\pi}{2\tilde{\Delta}}\right)\frac{13\sqrt{3}\pi}{128\tilde{\Delta}} \tag{5.42}$$

For the square pulse we have used the optimal time derived on first chapter because, as we will see in the numerical results, it will still be a valid approximation.

5.5. Second-order coefficients of the Gaussian pulse

In this section we will use the results derived in 5.1 to obtain the analytical solutions of the second excitation coefficients. For the Gaussian pulse we use as initial conditions $\phi_g(\tau_e,\tau_e) = i\theta(\tau_e,\tau_e)c_e^{(0)}(\tau_e)$, the zeroth order perturbative expansions (derived in section 3.4) of the coefficients c_3 and c_2.

For the main transition $|1\rangle - |2\rangle$, the solution of the second-order coefficients can be obtained by solving the equation described in appendix A.1, but with the initial conditions $\phi_1(\tau_e,\tau_e) = i\theta(\tau_e,\tau_e)c_2^{(0)}(\tau_e)$. For the transition $|0\rangle - |3\rangle$, the solution of the second-order coefficients can be obtained up to zeroth order by imposing the initial conditions $\phi_0(\tau_e,\tau_e) =$

$i\theta(\tau_e,\tau_e)c_3^{(0)}(\tau_e)$. With these considerations, the analytical solutions for the second-order coefficients can be described as:

$$\begin{aligned}
\phi_1(\tau,\tau_e) &\approx -\frac{\tilde{\Omega}_2}{|\tilde{\Omega}_3|} sin\left(\frac{1}{2}\int_0^{\tau_e}|\tilde{\Omega}_2|d\tau'\right) cos\left(\frac{1}{2}\int_0^{\tau}|\tilde{\Omega}_2|d\tau' - \frac{1}{2}\int_0^{\tau_e}|\tilde{\Omega}_3|d\tau'\right)\\
\phi_2(\tau,\tau_e) &\approx -isin\left(\frac{1}{2}\int_0^{\tau_e}|\tilde{\Omega}_2|d\tau'\right) sin\left(\frac{1}{2}\int_0^{\tau}|\tilde{\Omega}_2|d\tau' - \frac{1}{2}\int_0^{\tau_e}|\tilde{\Omega}_2|d\tau'\right)\\
\phi_0(\tau,\tau_e) &\approx \frac{\pi^2}{64}e^{-\frac{\tilde{\Delta}^2\tau_e^2}{\beta^2}}\\
\phi_3(\tau,\tau_e) &\approx 0
\end{aligned}$$

Now, we set $\tau = T$ and since we have tailored the length of our pulse to fulfill $\pi = \int_0^T |\tilde{\Omega}_2|d\tau'$, we have:

$$\begin{aligned}
\phi_1(\tau,\tau_e) &\approx -\frac{\tilde{\Omega}_3}{|\tilde{\Omega}_3|} sin^2\left(\frac{1}{2}\int_0^{\tau_e}|\tilde{\Omega}_3|d\tau'\right)\\
\phi_2(\tau,\tau_e) &\approx -isin\left(\frac{1}{2}\int_0^{\tau_e}|\tilde{\Omega}_2|d\tau'\right) cos\left(\frac{1}{2}\int_0^{\tau_e}|\tilde{\Omega}_2|d\tau'\right)\\
\phi_0(\tau,\tau_e) &\approx \frac{\pi^2}{64}e^{-\frac{\tilde{\Delta}^2\tau_e^2}{\beta^2}}\\
\phi_3(\tau,\tau_e) &\approx 0
\end{aligned}$$

Analytical expansion of Φ_1

Now we will compute the integral of $|\Phi_1|^2$:

$$\begin{aligned}
|\Phi_1|^2 &= \int_0^T |\phi_1(T,\tau_e)|^2 d\tau_e = \int_0^T sin^4\left(\frac{1}{2}\int_0^{\tau_e}|\tilde{\Omega}_2|d\tau'\right) d\tau_e\\
&= \frac{1}{8}\int_0^T \left(3 - 4cos\left(\int_0^{\tau_e}|\tilde{\Omega}_2|d\tau'\right) + cos\left(2\int_0^{\tau_e}|\tilde{\Omega}_2|d\tau'\right)\right)\\
&= \frac{3T}{8} - \frac{1}{2}\int_0^T cos\left(\frac{\pi}{2}\left(erf\left(\frac{\tau_e-\mu}{\sqrt{2}\sigma}\right) + erf\left(\frac{\mu}{\sqrt{2}\sigma}\right)\right)\right) d\tau_e\\
&+ \frac{1}{8}\int_0^T cos\left(\pi\left(erf\left(\frac{\tau_e-\mu}{\sqrt{2}\sigma}\right) + erf\left(\frac{\mu}{\sqrt{2}\sigma}\right)\right)\right) d\tau_e
\end{aligned} \tag{5.43}$$

Notice that $\sigma = \frac{T}{\beta}$, $\mu = \frac{T}{2}$. Also, in the Gaussian regime we are exploring, $erf(\frac{\beta}{2\sqrt{2}}) \approx 1$.

$$\int_0^T |\phi_1(T,\tau_e)|^2 d\tau_e = \frac{3T}{8} + \frac{1}{2}\int_0^T sin\left(\frac{\pi}{2}erf\left(\frac{\tau_e-\mu}{\sqrt{2}\sigma}\right)\right) d\tau_e - \frac{1}{8}\int_0^T cos\left(\pi erf\left(\frac{\tau_e-\mu}{\sqrt{2}\sigma}\right)\right) d\tau_e \tag{5.44}$$

Notice that $\int_0^T erf\left(\frac{\tau_e-\mu}{\sqrt{2}\sigma}\right) = 0$ because the function is odd with respect to $\tau_e = \frac{T}{2}$, for this reason, the sine integral will vanish:

$$\int_0^T |\phi_1(T,\tau_e)|^2 d\tau_e = \frac{3T}{8} - \frac{1}{8}\int_0^T cos\left(\pi erf\left(\frac{\tau_e-\mu}{\sqrt{2}\sigma}\right)\right) d\tau_e \tag{5.45}$$

Now, we will expand $erf\left(\frac{\tau_e-\mu}{\sqrt{2}\sigma}\right)$. In order to be able to do it, we will have to break the integral in three regimes. As we can see in figure 5.2, in the regime where τ_e is close to $\frac{T}{2}$, one can approximate:

$$cos\left(\pi erf\left(\frac{\tau_e-\mu}{\sqrt{2}\sigma}\right)\right) \approx cos\left(\pi\frac{\tau_e-\mu}{\sqrt{2}\sigma}\right) \tag{5.46}$$

In the regime where $|\frac{T}{2}-\tau_e|$ is not small enough, we will be able to approximate the function with:

$$cos\left(\pi erf\left(\frac{\tau_e-\mu}{\sqrt{2}\sigma}\right)\right) \approx erf\left(\frac{\tau_e-\mu}{\sqrt{2}\sigma}\right) \tag{5.47}$$

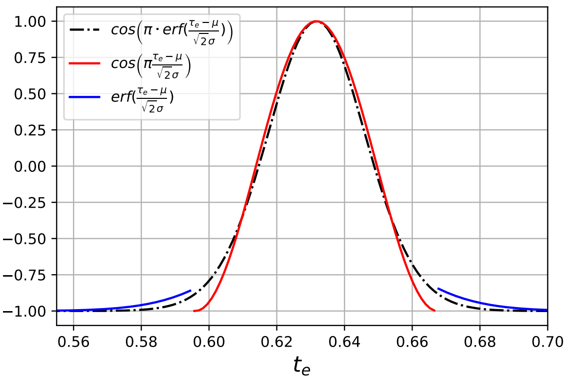

Figure 5.2.: Plot of the coefficients and time regimes used in the approximation.

In order to find the transition points τ_t where we will stop using the approximation from 5.46 to use 5.47, we will impose:

$$cos\left(\pi\frac{\tau-\mu}{\sqrt{2}\sigma}\right) = 0 \Rightarrow \tau_{t\pm} = \frac{T}{2} \pm \frac{\sqrt{2}}{\beta}$$

In the regime where $|\frac{T}{2}-\tau_e| \leq \frac{T}{2} \pm \frac{\sqrt{2}}{\beta}$ we will use the approximation described in 5.46 and outside the interval we will use 5.47.

$$\begin{aligned}
&\int_0^T |\phi_1(T,\tau_e)|^2 d\tau_e = \\
&\frac{3T}{8} - \frac{1}{8}\int_0^{\tau_{t-}} cos\left(\pi erf\left(\frac{\tau_e-\mu}{\sqrt{2}\sigma}\right)\right) d\tau_e - \frac{1}{8}\int_{\tau_{t-}}^{\tau_{t+}} cos\left(\pi erf\left(\frac{\tau_e-\mu}{\sqrt{2}\sigma}\right)\right) d\tau_e \\
&-\frac{1}{8}\int_{\tau_{t+}}^{T} cos\left(\pi erf\left(\frac{\tau_e-\mu}{\sqrt{2}\sigma}\right)\right) d\tau_e \\
&= \frac{3T}{8} - \frac{1}{4}\int_0^{\tau_{t-}} cos\left(\pi erf\left(\frac{\tau_e-\mu}{\sqrt{2}\sigma}\right)\right) d\tau_e - \frac{1}{8}\int_{\tau_{t-}}^{\tau_{t+}} cos\left(\pi erf\left(\frac{\tau_e-\mu}{\sqrt{2}\sigma}\right)\right) d\tau_e \\
&\approx \frac{3T}{8} - \frac{\sqrt{2}T}{4\beta}\left(erf(1) + \frac{e^{-1}}{\sqrt{\pi}} - \frac{\beta}{2\sqrt{2}} - \frac{e^{-\frac{\beta^2}{8}}}{\sqrt{\pi}}\right) \\
&\approx \frac{T}{2}\left(1-\frac{\sqrt{2}}{2\beta}\right)
\end{aligned} \tag{5.48}$$

Analytical expansion of Φ_2

Now we are going to work on the expansion of $|\Phi_2|^2$:

$$\int_0^T |\phi_2(T,\tau_e)|^2 d\tau_e =$$
$$= \int_0^T sin^2\left(\frac{1}{2}\int_0^{\tau_e}|\tilde{\Omega}_2|d\tau'\right) cos^2\left(\frac{1}{2}\int_0^{\tau_e}|\tilde{\Omega}_2|d\tau'\right) d\tau_e$$
$$= \frac{1}{4}\int_0^T sin^2\left(\int_0^{\tau_e}|\tilde{\Omega}_2|d\tau'\right) d\tau_e \approx \frac{1}{4}\int_0^T sin^2\left(\frac{\pi}{2}\left(erf\left(\frac{\tau_e-\mu}{\sqrt{2}\sigma}\right) + erf\left(\frac{\mu}{\sqrt{2}\sigma}\right)\right)\right) d\tau_e$$
$$\approx \frac{1}{4}\int_0^T sin^2\left(\frac{\pi}{2}erf\left(\frac{\tau_e-\mu}{\sqrt{2}\sigma}\right) + \frac{\pi}{2}\right) d\tau_e = \frac{1}{8}\int_0^T\left(1 + cos\left(\pi erf\left(\frac{\tau_e-\mu}{\sqrt{2}\sigma}\right)\right)\right) d\tau_e$$
$$= \frac{T}{8} + \frac{1}{8}\int_0^T cos\left(\pi erf\left(\frac{\tau_e-\mu}{\sqrt{2}\sigma}\right)\right) d\tau_e$$

Notice that we have ended with the integral that we already solved when computing $|\Phi_1(T,\tau_e)|^2$, for this reason:

$$\int_0^T |\Phi_2(T,\tau_e)|^2 d\tau_e \approx \frac{\sqrt{2}T}{4\beta}$$

Analytical expansion of Φ_0

For the coefficient $|\Phi_0|^2$ we will have:

$$\int_0^T |\phi_0(T,\tau_e)|^2 d\tau_e \approx \frac{\pi^2}{64}\int_0^T e^{-\frac{\tilde{\Delta}^2\tau_e^2}{\beta^2}} d\tau_e = \frac{\pi^2}{64}\left(\frac{\sqrt{\pi}\beta}{2\tilde{\Delta}}erf\left(\frac{T\tilde{\Delta}}{\sqrt{2}\beta}\right)\right)$$
$$\approx \frac{\pi^2\sqrt{\pi}T}{256}$$

Where we used $T \propto 2\frac{\beta}{\tilde{\Delta}}$ and also $erf\left(\frac{T\tilde{\Delta}}{\sqrt{2}\beta}\right) \approx erf\left(\frac{2}{\sqrt{2}}\right) \approx 1$.

The second-order coefficients for the Gaussian, as a function of the length of the pulse T are:

$$\boxed{|\Phi_2|^2 \approx \frac{\sqrt{2}T}{4\beta} \qquad |\Phi_1|^2 \approx \frac{T}{2}\left(1 - \frac{\sqrt{2}}{2\beta}\right)} \tag{5.49}$$

$$\boxed{|\Phi_3|^2 \approx 0 \qquad |\Phi_0|^2 \approx \frac{\pi^2\sqrt{\pi}T}{256}} \tag{5.50}$$

5.6. Analytical expansion of the conditional Fidelity

We will use the results obtained in sections 5.4 (square-shaped pulse) and 5.5 (Gaussian-shaped pulse) to find an analytical expression of the conditional fidelity (eq. 4.15) taking into account the second order emission coefficients. Then, we will compare the analytical results with the numerical simulations and we will discuss the behavior of the protocol under different parameters for the Gaussian regime and the constant-pulse regime.

As performed in section 4.6, it will be useful to rewrite the conditional fidelity from 5.36, in the form:

$$F = \frac{\frac{1}{2}D_1^N + \frac{1}{2}\left(D_1 + D_2\right)^N}{\left(D_1 + D_2 + D_3\right)^N} = \frac{1}{2}\left(\frac{1}{1 + \frac{D2 + D_3}{D_1}}\right)^N + \frac{1}{2}\left(\frac{1}{1 + \frac{D_3}{D_1 + D_2}}\right)^N$$

Where:

$$D_1 = \eta_2 |c_0 c_2|^2$$
$$D_2 = \eta_2 \left(|c_0\Phi_2|^2 + |\Phi_0 c_2|^2 + |\Phi_0\Phi_2|^2\right) + \eta_2(1-\eta_3)\left(|c_3 c_2|^2 + |c_3\Phi_2|^2 + |\Phi_3 c_2|^2 + |\Phi_3\Phi_2|^2\right)$$
$$D_3 = \eta_3 \left(|c_3 c_1|^2 + |c_3\Phi_1|^2 + |\Phi_3 c_1|^2 + |\Phi_3\Phi_1|^2\right) + \left(\eta_2\eta_3 + \eta_3(1-\eta_2)\right)\left(|c_3 c_2|^2 + |c_3\Phi_2|^2 + |\Phi_3 c_2|^2 + |\Phi_3\Phi_2|^2\right)$$

The analytical solutions for the coefficient from the square-shaped pulse are:

$$|c_0 c_2|^2 \approx 1 - \frac{5\sqrt{3}\pi}{8\tilde{\Delta}} - \frac{3\sqrt{3}\pi}{32\tilde{\Delta}}\left(\frac{\pi}{4\sqrt{3}} + \sigma_b^2\left(\frac{\sqrt{3}\pi}{2} + \frac{32}{\sqrt{3}\pi}\right)\right)$$
$$|c_3 c_2|^2 \approx \frac{9\pi^2}{64\tilde{\Delta}^2}\left(\sigma_b^2 + \frac{1}{4}\right)$$
$$|\Phi_0 c_2|^2 \approx \frac{13\sqrt{3}\pi}{128\tilde{\Delta}} - \frac{39\pi^2}{128\tilde{\Delta}^2}$$
$$|\Phi_0\Phi_2|^2 \approx \frac{39\pi^2}{1024\tilde{\Delta}^2}$$
$$|\Phi_3 c_2|^2 \approx \frac{3\sqrt{3}\pi}{128\tilde{\Delta}} - \frac{9\pi^2}{128\tilde{\Delta}^2}$$
$$|\Phi_3\Phi_2|^2 \approx \frac{9\pi^2}{1024\tilde{\Delta}^2}$$
$$|c_0\Phi_2|^2 \approx \frac{\sqrt{3}\pi}{8\tilde{\Delta}} - \frac{15\pi^2}{64\tilde{\Delta}^2}$$
$$|\Phi_3\Phi_1|^2 \approx \frac{27\pi^2}{1024\tilde{\Delta}^2}$$
$$|c_3 c_1|^2 = |c_3\Phi_2|^2 = |c_3\Phi_1|^2 = |\Phi_3 c_1|^2 \approx 0$$

For the analytical solutions of the Gaussian coefficients we have:

$$
\begin{aligned}
|c_0c_2|^2 &\approx 1-\frac{T}{2}-\frac{\pi^2}{16}e^{-\frac{\tilde{\Delta}^2T^2}{\beta^2}}\left(1+\frac{T}{2}\right)^2+\frac{T^2}{4}\left(\frac{1}{4}+\sigma_b^2\right)\\
|c_3c_2|^2 &\approx \frac{\pi^2}{16}e^{-\frac{\tilde{\Delta}^2T^2}{\beta^2}}\left(1+\frac{T}{2}\right)^2\\
|\Phi_0c_2|^2 &\approx \frac{\pi^2\sqrt{\pi}\beta T}{256}\left(1-\frac{T}{2}\right)\\
|\Phi_0\Phi_2|^2 &\approx \frac{\pi^2\sqrt{2\pi}T^2}{1024}\\
|c_0\Phi_2|^2 &\approx \frac{\sqrt{2}T}{4\beta}\left(1-\frac{\pi^2}{16}\left(1-\frac{T}{2}\right)e^{-\frac{\tilde{\Delta}^2T^2}{\beta^2}}\right)\\
|c_3\Phi_2|^2 &\approx \frac{\sqrt{2}T\pi^2}{64\beta}\left(1-\frac{T}{2}\right)e^{-\frac{\tilde{\Delta}^2T^2}{\beta^2}}\\
|\Phi_3\Phi_1|^2 &= |\Phi_3\Phi_2|^2=|\Phi_3c_2|^2=|c_3c_1|^2=|c_3\Phi_1|^2=|\Phi_3c_1|^2\approx 0
\end{aligned}
\tag{5.51}
$$

As we will see in the numerical results, for the Gaussian pulse, the optimal time derived in Chapter 3 is no longer a good approximation. For this reason, we will perform an optimization of the length of the pulse T by performing the derivative of the fidelity for the Gaussian pulse (F_G) and solving the equation:

$$
\frac{dF_G}{dT}=0 \Rightarrow T\approx\frac{\beta}{\tilde{\Delta}}\sqrt{ln\left(\frac{\pi^2T\tilde{\Delta}^2}{2\sqrt{2}\beta}\right)} \tag{5.52}
$$

Where, to simplify the calculations, we have used the conditional fidelity from 5.36 without filters $\eta_2=\eta_3=1$ and we have kept only the term that contributes the most in the expansion of the optimal time. In order to solve equation 5.52, we will perform the same approximation as in section 3.4.1, by substituting $T\approx 2\frac{\beta}{\tilde{\Delta}}$:

$$
T\approx\frac{\beta}{\tilde{\Delta}}\sqrt{ln\left(\frac{\pi^2\tilde{\Delta}}{\sqrt{2}}\right)} \tag{5.53}
$$

Finally, by using $D_1>>D_2+D_3$ and $D_1+D_2>>D_3$ we obtain:

$$
F\simeq\frac{1}{2}\left(1-N\frac{D_2+D_3}{D_1}\right)+\frac{1}{2}\left(1-N\frac{D_3}{D_1+D_2}\right) \tag{5.54}
$$

The conditional fidelity for the square pulse, taking into account the second-order emissions is:

$$
\boxed{F_S\approx 1-\frac{N\sqrt{3}\pi}{256\tilde{\Delta}}\left(29+3\left(1-\eta_3+2\frac{\eta_2}{\eta_3}\right)\right)-\frac{9N\pi^2}{128\tilde{\Delta}^2}\left(\frac{\eta_3}{\eta_2}\left(2\sigma_b^2+\frac{15}{16}\right)-\frac{5}{4}\right)}
$$

The conditional fidelity for the Gaussian pulse, taking into account the second-order emissions, the optimal time from 5.52 and defining $\lambda=\sqrt{ln\left(\frac{\pi^2\tilde{\Delta}}{\sqrt{2}}\right)}$ is:

$$
\boxed{F_G\approx 1-\frac{N}{8\tilde{\Delta}}\left(\frac{\sqrt{2}}{4}\left(1-\eta_3+2\frac{\eta_3}{\eta_2}\right)+\lambda\left(\sqrt{2}+\frac{\pi^2\sqrt{\pi}\beta}{64}\right)\right)}
$$

5.7. Numerical and Analytical results

In this section the numerical results, taking into account all the inconsistencies studied in this thesis will be presented. In figure 5.3 a 2D map of the numerical fidelities for the square pulse (left) and Gaussian pulse (right) is displayed.

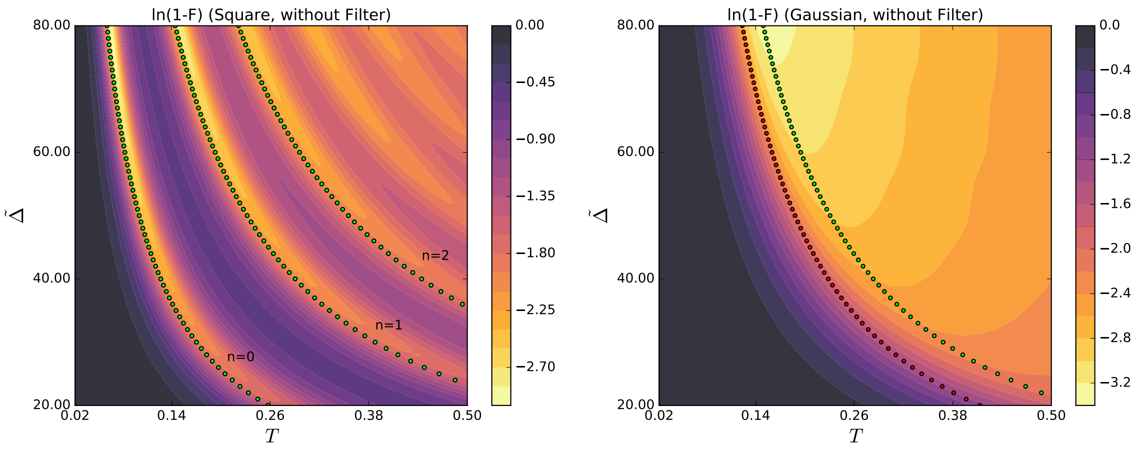

Figure 5.3.: 2D colormap of the numerical results for the $ln(1-F)$ (conditional fidelity) for the square-shaped pulse (left) and the Gaussian-shaped pulse (right) as a function of the length of the pulse T (x axis) and the dimensionless detuning $\tilde{\Delta}$ (y axis), without filtering. The green-dotted lines correspond to the analytical optimal times for the square pulse (left). The red line corresponds to the optimal time derived in chapter 3 and the green line corresponds to the optimal time derived in this chapter for the Gaussian pulse (right).

As we can see, for the square pulse, the optimal times derived in Chapter 3 are still valid. For the Gaussian pulse, the optimal time derived in Chapter 3 is displayed (red dots) and the optimal time derived in this chapter is also represented (green dots). As it can be seen, the second optimization of the time represents more accurately the numerical results.

In figure 5.4 two plots of the conditional fidelities for the square pulse with and without filters are shown. We can see that the analytical expansion of the conditional fidelity for the square pulse agrees very well with the numerical results. Similar to the section 4.7, the fidelity does show the interference pattern explained in previous chapters. The presence of the second order emissions has decreased the fidelity, this time the maximum of the oscillating fidelity do not get close to unity. When applying the frequency filter we can see that the interference pattern smears out and the effect of the inhomogeneous broadening is less present.

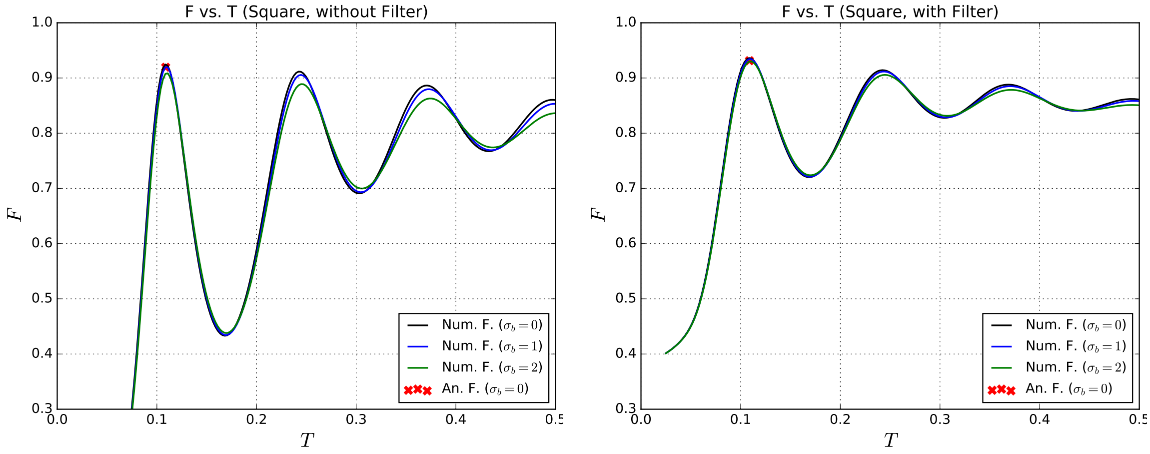

Figure 5.4.: Plots of the numerical conditional fidelity F for the square-shaped pulse as a function of the length of the pulse T without filtering (left) and with filtering (right), with $\tilde{\Delta} = 50$ for 5 qubits ($N = 5$). The red cross corresponds to the analytical fidelity.

In figure 5.5 two plots for the conditional fidelity for the Gaussian pulse are displayed. As we can see, there is no interference pattern. The fidelity only has one maximum, that arises from the compromise between the excitation of the far-detuned transition (short times T) and the presence of the second-order coefficients (long times T). The conditional fidelity gets rid of the effect of the spontaneous emission, as we saw in section 4.7. Despite this fact, the emissions of undetected photons during the excitation window do play a role in the conditional fidelity.

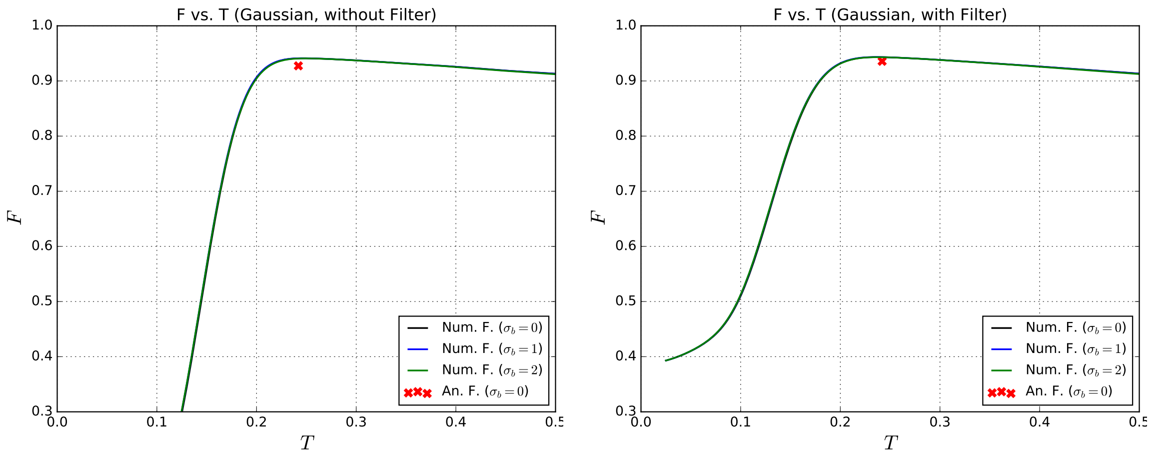

Figure 5.5.: Plots of the numerical conditional fidelity F for the Gaussian-shaped pulse as a function of the length of the pulse T without filtering (left) and with filtering (right), with $\tilde{\Delta} = 50$ for 5 qubits ($N = 5$). The red cross corresponds to the analytical fidelity.

In figure 5.6 the conditional fidelity for the square pulse as a function of the number of photons (N) is displayed for several values of the detuning $\tilde{\Delta}$ and broadening σ_b. As one can see, for small $\tilde{\Delta}$, the square pulse fidelity does strongly depend on the inhomogeneous broadening. The application of the frequency filters does correct most of the inhomogeneous broadening and also increases the fidelity globally. Due to this reason, for the square-pulse regime substantial improvements can be obtained by using frequency filters.

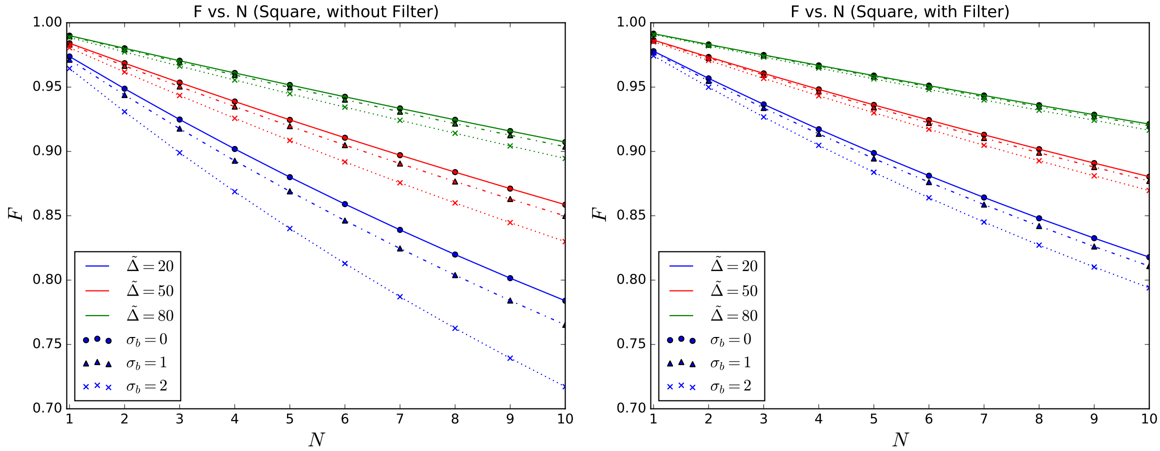

Figure 5.6.: Plots of the numerical conditional Fidelity F for the square-shaped pulse as a function of the number of qubits N, with $\sigma_b = \{0, 1, 2\}$, $\eta_e = 0.03$ without filtering (left) and frequency filters $\eta_{f2} = 0.95$, $\eta_{f3} = 0.05$ (right).

Adding cavity frequency filters on the protocol performed with Gaussian pulses do not improve the fidelity as much as with the square pulse. Also, in figure 5.7 it can clearly be seen that the Gaussian pulse is almost unaffected by inhomogeneous broadening.

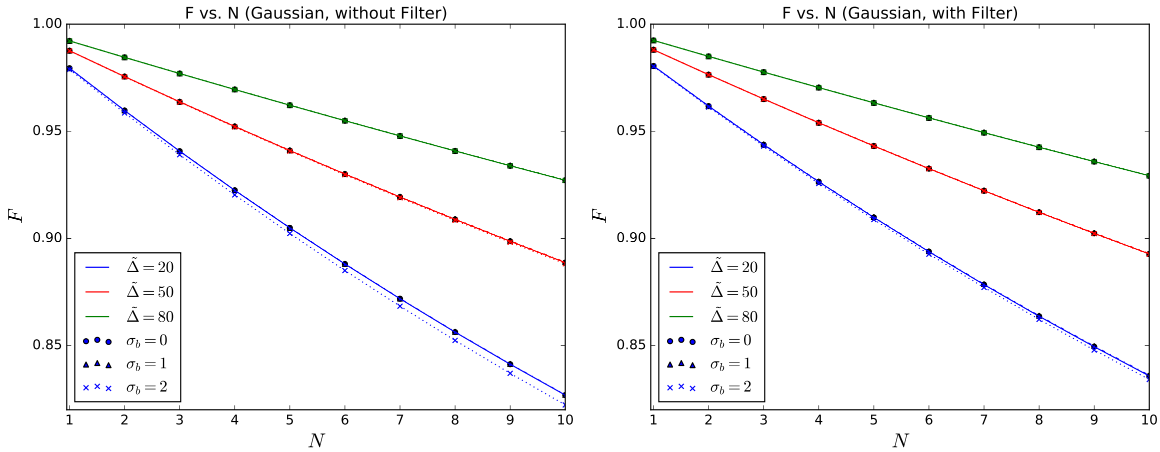

Figure 5.7.: Plots of the numerical conditional Fidelity F for the Gaussian-shaped pulse as a function of the number of qubits N, with $\sigma_b = \{0, 1, 2\}$ without filtering (left) and frequency filters $\eta_{f2} = 0.95$, $\eta_{f3} = 0.05$ (right).

We know that the experimental efficiency of the system η_e is not unity. For the quantum dots embedded in waveguides the maximum efficiency obtainable in the experimental setup, at the moment is $\eta_e = 0.03$ (if we take into account the fact that the interferometer used to perform measurements on the x basis decreases the system efficiency by a factor of 2, a realistic result would be $\eta_e = 0.015$, we will omit this part). On the other hand, if we look at the maximum efficiency for each component of the system separately, we may be able to obtain an much better and optimistic result. By assuming that a coupling of the quantum dot and the waveguide can be achieved with efficiency ~ 0.98, the coupling of the waveguide with the detector ~ 0.85, and efficiency of the superconducting nanowire detector ~ 0.93, we would obtain an efficiency of $\eta_e = 0.73$. It is important to remark that this is a highly optimistic efficiency, assuming the best performances for each part of the experimental setup and omitting any additional source of loss from the system.

In figure 5.8 a plot of the probability of success for the square pulse as a function of the number of qubits N is displayed.

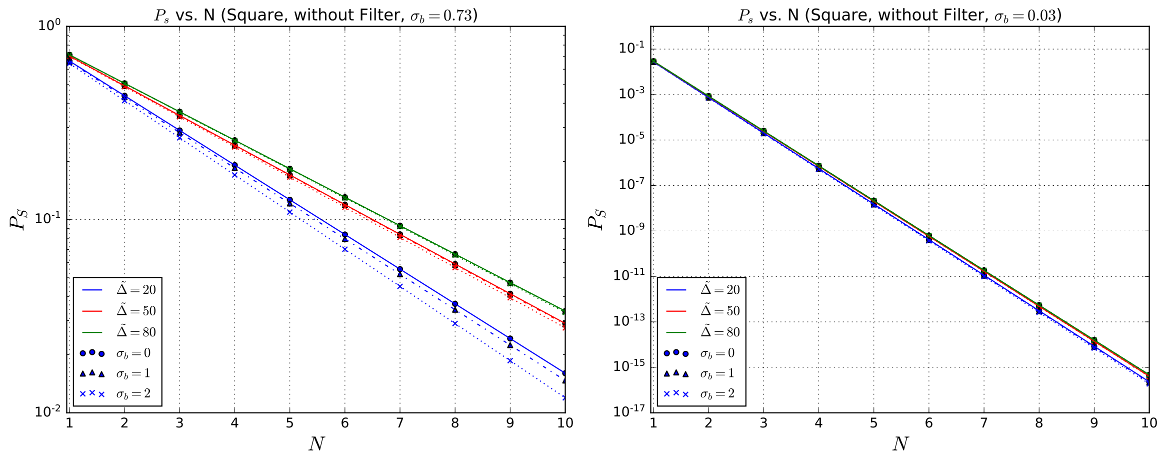

Figure 5.8.: Plots of the numerical probability of success P_s for the square-shaped pulse as a function of the number of qubits N, with $\sigma_b = \{0, 1, 2\}$, $\eta_e = 0.73$ (left) and $\eta_e = 0.03$ (right), without filtering.

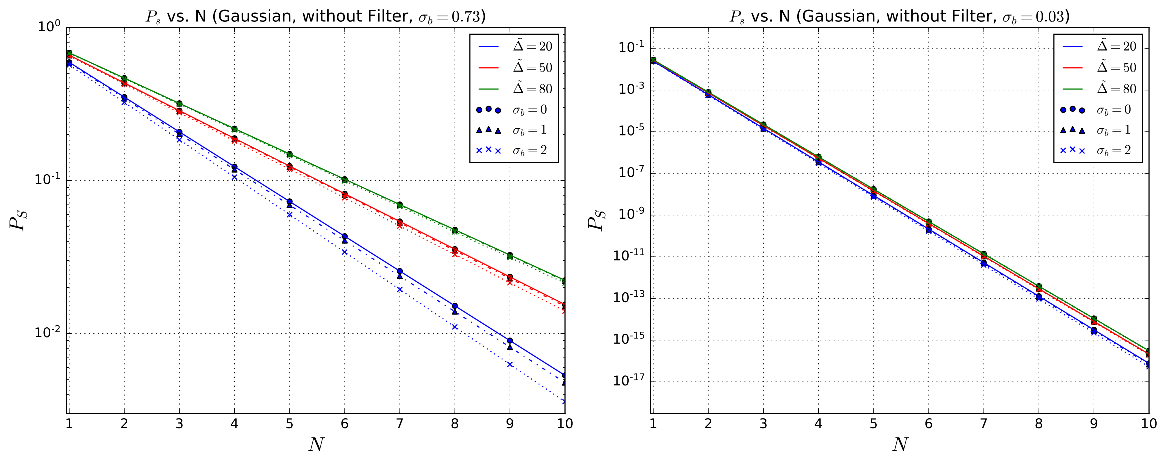

Figure 5.9.: Plots of the numerical probability of success P_s for the Gaussian-shaped pulse as a function of the number of qubits N, with $\sigma_b = \{0, 1, 2\}$, $\eta_e = 0.73$ (left) and $\eta_e = 0.03$ (right), without filtering.

Figures 5.8 and 5.9 show that the realizations with the square-shaped pulse present a higher probability of success P_s. For a robust and consistent generation of GHZ states with five photons, the ratio of success for the current experimental setup should be improved.

Finally, In table 5.1, numerical values of the conditional fidelity, probability of success and optimal time for the generation of five photons $N = 5$, are displayed. They have been computed using realistic experimental parameters ($\tilde{\Delta} = 50$, $\eta_e = 0.03$, $\sigma_b = 1$).

	F (Square)	F (Gaussian)	P_s (Square)	P_s (Gaussian)	T (Square)	T (Gaussian)
Without Filter	0.920	0.941	$2.008 \cdot 10^{-8}$	$1.441 \cdot 10^{-8}$	0.109	0.242
With Filter	0.934	0.943	$1.530 \cdot 10^{-8}$	$1.112 \cdot 10^{-8}$	0.109	0.242

Table 5.1.: Numerical values of the conditional fidelity, probability of success and length of the pulse for realistic parameters.

6. Conclusions and Outlook

6.1. Conclusions

In this thesis we have studied imperfections on the generation of spin-photon entangled GHZ states using a time-bin encoding. We have taken into account square and Gaussian shapes of the input field.

First, to study the dynamics of the system, we have performed a time optimization, only taking into account the presence of the far-detuned transition. For the square pulse we have seen constructive and destructive interferences, dependent on the length of the pulse. By exploiting these interferences we have been able to find the optimal duration of the pulse, lying on the first maximum. For the Gaussian pulse regime we have seen that the interferences are no longer present. We have optimized the duration of the pulse by finding a compromise between the excitation of the off-resonant transition and the spontaneous emission of the main excited state.

After understanding the main dynamics of the system in both regimes, inhomogeneous broadening and spontaneous emission from the off-resonant level have been taken into account. It has been seen that the fidelity for the square pulse is more sensitive on the inhomogeneous broadening. We have seen that the Gaussian pulse solutions are almost unaffected by broadening.

By applying frequency filters, we have seen notable improvements on the correction of the broadening for the square pulse, and a general increase of the fidelity, both for the square and Gaussian pulses.

The second-order emissions of photons have been taken into account. When considering these inconsistencies it has not been necessary to find a new optimal time for the square pulse but a new optimal time for the Gaussian pulse has been derived. We have seen that the second-order emissions are the dominant term inside the conditional fidelity.

The final results show higher fidelity values for the Gaussian regime. On the contrary, the probability of success is smaller for the Gaussian pulse. The optimal time for the square-shape regime may be achievable with the current experimental setup, but it remains a challenge to generate pulses long enough to match the optimal time for the Gaussian pulse.

6.2. Outlook

First, the expansion that we have made for the Gaussian pulse for the far-detuned transition is not optimal because the populations of the states do not remain constant. For this reason, a better expansion to improve the analytical results for the Gaussian pulse could be performed. An interesting approach could consist on performing perturbation theory on the derivatives of the Rabi frequency, in the dressed-states frame.

We have considered that the photons emitted during the pulse are not detected. It would be interesting to derive the conditional fidelity by assuming that all emitted photons are measured.

Finally, it would also be interesting to look at the inefficiencies studied on this thesis in the generation of a linear cluster state. As we have discussed, the protocol used to generate a linear cluster state is very similar to the one used to generate the GHZ state, but it is much more involved, since the compactness and symmetry of the GHZ state would no longer be present.

A. Analytical computations

A.1. Solution of the 1-2 transition

We are interested in solving:

$$\dot{c}_2^{(0)}(\tau) = i\frac{\tilde{\Omega}_2(\tau)}{2}c_1^{(0)}(\tau)$$
$$\dot{c}_1^{(0)}(\tau) = i\frac{\tilde{\Omega}_2^*(\tau)}{2}c_2^{(0)}(\tau)$$

With $c_1^{(0)}(0) = 1$ and $c_2^{(0)}(0) = 0$. Since the pulse is not constant we will make the change $d\xi = |\tilde{\Omega}_3|d\tau$ and our system will be rewritten as:

$$\dot{c}_2^{(0)}(\xi) = i\frac{\tilde{\Omega}_2}{2|\tilde{\Omega}_2|}c_1^{(0)}(\xi)$$
$$\dot{c}_1^{(0)}(\xi) = i\frac{\tilde{\Omega}_2^*}{2|\tilde{\Omega}_2|}c_2^{(0)}(\xi)$$

Notice that $\frac{\tilde{\Omega}_2^*}{|\tilde{\Omega}_2|}$ does not depend on time. Now we decouple the system of differential equations:

$$\ddot{c}_2^{(0)}(\xi) + \frac{1}{4}c_2^{(0)}(\xi) = 0$$
$$\ddot{c}_1^{(0)}(\xi) + \frac{1}{4}c_1^{(0)}(\xi) = 0$$

We have exactly the same differential equations for c_2 and c_1. These differential equations correspond to the dynamics of the Harmonic Oscillator. By imposing the initial conditions explained above, we the solutions are:

$$c_2^{(0)}(\tau) = i\frac{\tilde{\Omega}_2}{|\tilde{\Omega}_2|}sin\left(\frac{1}{2}\int_0^T|\tilde{\Omega}_2|d\tau\right)$$
$$c_2^{(0)}(\tau) = cos\left(\frac{1}{2}\int_0^T|\tilde{\Omega}_2|d\tau\right)$$

A.2. Interaction picture transformation

We will transform the hamiltonian $\hat{H}$ by applying:

$$\hat{\tilde{H}} = \hat{U}^\dagger(t)\left(\hat{H}_C + \hat{H}_I\right)\hat{U}(t) = \hat{U}^\dagger(t)\hat{H}_C\hat{U}(t) + \hat{U}^\dagger(t)\hat{H}_I\hat{U}(t)$$

For this, we will use the Baker–Campbell–Hausdorff formula [16]:

$$e^{i\hat{B}\lambda}\hat{A}e^{-i\hat{B}\lambda} = \hat{A} + i\lambda[\hat{B},\hat{A}] + \left(\frac{i^2\lambda^2}{2!}\right)[\hat{B},[\hat{B},\hat{A}]] + ... + \left(\frac{i^n\lambda^n}{n!}\right)[\hat{B},[\hat{B},...[\hat{B},\hat{A}]]]$$

For the $\hat{U}^\dagger(t)\hat{H}_C\hat{U}(t)$ term we have:

$$\hat{U}^{\dagger}(t)\hat{H}_C\hat{U}(t) = -e^{\frac{i}{\hbar}\left(\hat{H}_A+\hat{H}_F\right)t}\vec{E}\left(\sigma_{eg}\mu_{eg}+\sigma_{ge}\mu_{ge}\right)e^{-\frac{i}{\hbar}\left(\hat{H}_A+\hat{H}_F\right)t} =$$

$$= \left(\sigma_{eg}\mu_{eg}+\sigma_{ge}\mu_{ge}\right)\vec{E} + it\omega_0\vec{E}\left(|e\rangle\langle g|\,\mu_{eg} - |g\rangle\langle e|\,\mu_{ge}\right) + \ldots + \vec{E}\frac{(it\omega_0)^n}{n!}\left(\sigma_{eg}\mu_{eg}+(-1)^n\sigma_{ge}\mu_{ge}\right)$$

$$= \vec{E}\sum_{k=0}^{\infty}\frac{(it\omega_0)^k}{k!}\left(\sigma_{eg}\mu_{eg}+(-1)^k\sigma_{ge}\mu_{ge}\right) = \vec{E}\left(e^{it\omega_0}\sigma_{eg}\mu_{eg}+e^{-it\omega_0}\sigma_{ge}\mu_{ge}\right)$$

$$= \left(\frac{\epsilon}{2}e^{-i\nu t}+\frac{\epsilon^*}{2}e^{i\nu t}\right)\left(e^{it\omega_0}\sigma_{eg}\mu_{eg}+e^{-it\omega_0}\sigma_{ge}\mu_{ge}\right)$$

Finally, by performing the Rotating Wave Approximation and defining the Rabi frequency to be $\Omega \equiv \frac{\varepsilon\mu_{eg}}{\hbar}$, we obtaqin:

$$\hat{\hat{H}}_C = -\hbar\left(\frac{\Omega}{2}\sigma_{eg}e^{i\Delta t}+\frac{\Omega^*}{2}\sigma_{ge}e^{-i\Delta t}\right)$$

The transformation $\hat{U}^{\dagger}(t)\hat{H}_I\hat{U}(t)$ is described in detail in [34].

$$\hat{\hat{H}}_I = -\hbar\int dk g_k\left(\sigma_{eg}\hat{a}_k e^{i\Delta t}+\hat{a}_k^{\dagger}\sigma_{ge}e^{-i\Delta t}\right)$$

B. Comparison between Numerical and Analytical results

B.1. Stric fidelity

In figure B.1 we can see the comparison between the numerical and analytical strict fidelities for the square pulse (left) and the Gaussian-shaped pulse (right):

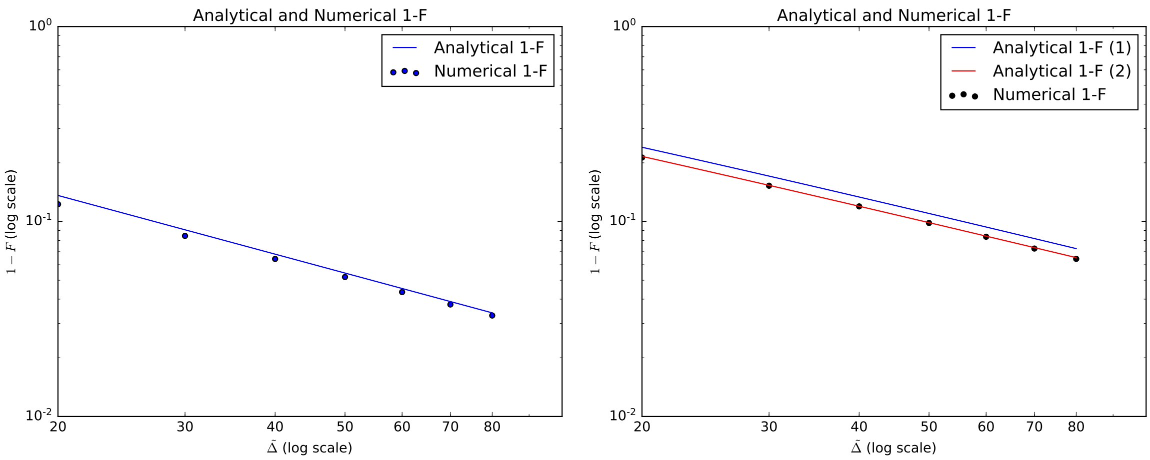

Figure B.1.: Numerical and analytical comparison of the strict fidelity as a function of the detuning $\tilde{\Delta}$. For the square-shaped pulse (left) and for the Gaussian-shaped pulse (right). (1) corresponds to the fidelity derived in 3.35 and (2) corresponds to the analytical fidelity obtained by assuming that $|c_0| \approx 1$

B.2. Conditional fidelity with broadening

In figure B.2 we can see the comparison between the numerical and analytical conditional fidelities for the square pulse (left) and the Gaussian-shaped pulse (right):

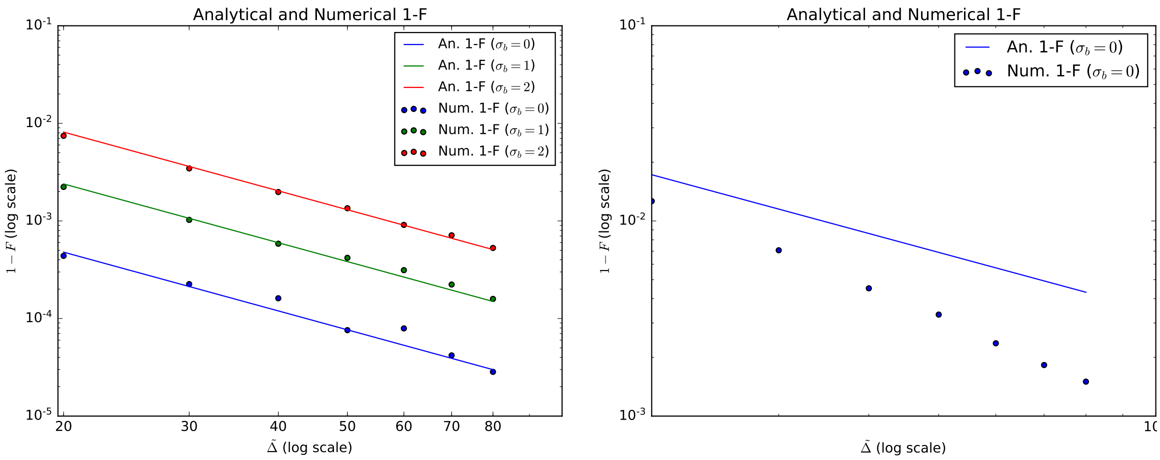

Figure B.2.: Numerical and analytical comparison of the conditional fidelity as a function of the detuning $\tilde{\Delta}$. For the square-shaped pulse (left) and for the Gaussian-shaped pulse (right), without taking into account second-order emissions.

As we can see in B.2, the analytical approximation for the Gaussian pulse does not fully converge to the numerical solution. This may be caused due to the approximation made in Chapter 3 to correct the perturbation expansion of the equations of the Gaussian-shaped pulse.

B.3. Conditional fidelity with second-order emissions

In figure B.3 we can see the comparison between the numerical and analytical conditional fidelities for the square pulse (left) and the Gaussian-shaped pulse (right):

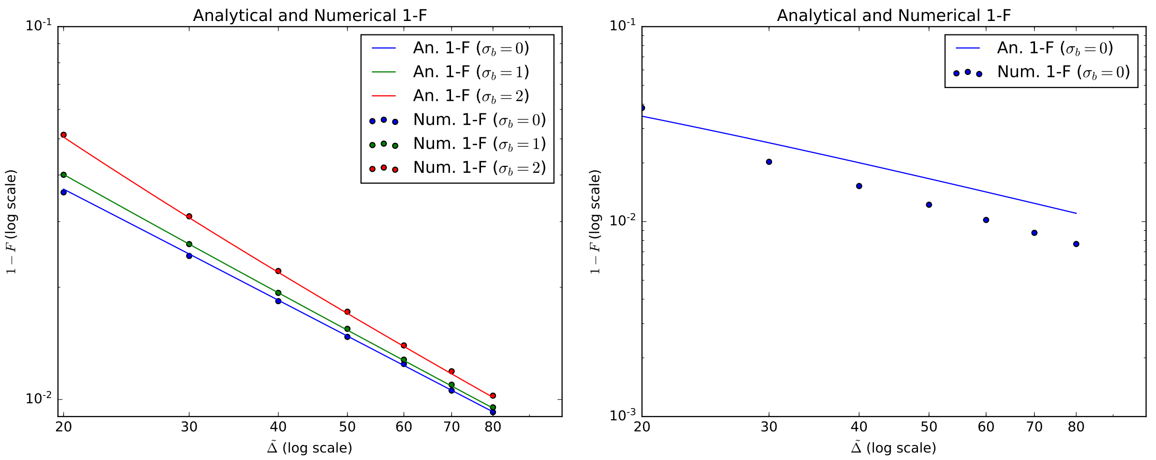

Figure B.3.: Numerical and analytical comparison of the conditional fidelity as a function of the detuning $\tilde{\Delta}$. For the square-shaped pulse (left) and for the Gaussian-shaped pulse (right), taking into account second-order emissions.

Bibliography

[1] Jonathan P Dowling and Gerard J Milburn. Quantum technology: the second quantum revolution. *Philosophical Transactions of the Royal Society of London. Series A: Mathematical, Physical and Engineering Sciences*, 361(1809):1655–1674, 2003.

[2] Charles H Bennett and Gilles Brassard. Quantum cryptography: public key distribution and coin tossing. *Theor. Comput. Sci.*, 560(12):7–11, 2014.

[3] Lov K Grover. A fast quantum mechanical algorithm for database search. *arXiv preprint quant-ph/9605043*, 1996.

[4] Peter W Shor. Algorithms for quantum computation: Discrete logarithms and factoring. In *Proceedings 35th annual symposium on foundations of computer science*, pages 124–134. Ieee, 1994.

[5] Johannes Borregaard, Anders Søndberg Sørensen, and Peter Lodahl. Quantum networks with deterministic spin–photon interfaces. *Advanced Quantum Technologies*, page 1800091, 2019.

[6] JP Lee, B Villa, AJ Bennett, RM Stevenson, DJP Ellis, I Farrer, DA Ritchie, and AJ Shields. Towards a source of multi-photon entangled states for linear optical quantum computing. *arXiv preprint arXiv:1804.11311*, 2018.

[7] Ivan Marcikic, Hugues de Riedmatten, Valerio Scarani, Hugo Zbinden, Nicolas Gisin, et al. Femtosecond time-bin entangled qubits for quantum communication. *arXiv preprint quant-ph/0205144*, 2002.

[8] Jürgen Brendel, Nicolas Gisin, Wolfgang Tittel, and Hugo Zbinden. Pulsed energy-time entangled twin-photon source for quantum communication. *Physical Review Letters*, 82(12):2594, 1999.

[9] Alisa Javadi, Dapeng Ding, Martin Hayhurst Appel, Sahand Mahmoodian, Matthias Christian Löbl, Immo Söllner, Rüdiger Schott, Camille Papon, Tommaso Pregnolato, Søren Stobbe, et al. Spin–photon interface and spin-controlled photon switching in a nanobeam waveguide. *Nature nanotechnology*, 13(5):398, 2018.

[10] Dapeng Ding, Martin Hayhurst Appel, Alisa Javadi, Xiaoyan Zhou, Matthias Christian Löbl, Immo Söllner, Rüdiger Schott, Camille Papon, Tommaso Pregnolato, Leonardo Midolo, et al. Coherent optical control of a quantum-dot spin-qubit in a waveguide-based spin-photon interface. *Physical Review Applied*, 11(3):031002, 2019.

[11] EA Chekhovich, MN Makhonin, AI Tartakovskii, Amir Yacoby, H Bluhm, KC Nowack, and LMK Vandersypen. Nuclear spin effects in semiconductor quantum dots. *Nature materials*, 12(6):494, 2013.

[12] M Grundmann, NN Ledentsov, O Stier, J Böhrer, D Bimberg, VM Ustinov, PS Kop'ev, and Zh I Alferov. Nature of optical transitions in self-organized inas/gaas quantum dots. *Physical Review B*, 53(16):R10509, 1996.

[13] Emili Bagan. Lecture notes on quantum information. *Autonomous University of Barcelona*, 2007.

[14] John Preskill. Lecture notes on quantum information. *Caltech*, 1998.

[15] Mikhail Lukin. Lecture notes on quantum optics 2. *Harvard University*, 2016.

[16] J. J. Sakurai and Jim Napolitano. *Modern quantum mechanics.* Pearson new International Edition, 2018.

[17] Michael A. Nielsen and Isaac L. Chuang. *Quantum computation and quantum information.* Cambridge University Press, 2019.

[18] Charles H Bennett, Gilles Brassard, Claude Crépeau, Richard Jozsa, Asher Peres, and William K Wootters. Teleporting an unknown quantum state via dual classical and einstein-podolsky-rosen channels. *Physical review letters*, 70(13):1895, 1993.

[19] Robert Raussendorf. Measurement-based quantum computation with cluster states. *International Journal of Quantum Information*, 7(06):1053–1203, 2009.

[20] Daniel M Greenberger, Michael A Horne, and Anton Zeilinger. Going beyond bell's theorem. In *Bell's theorem, quantum theory and conceptions of the universe*, pages 69–72. Springer, 1989.

[21] Dik Bouwmeester, Jian-Wei Pan, Matthew Daniell, Harald Weinfurter, and Anton Zeilinger. Observation of three-photon greenberger-horne-zeilinger entanglement. *Physical Review Letters*, 82(7):1345, 1999.

[22] Pierre Meystre and Murray Sargent. *Elements of quantum optics.* Springer-Verlag, 1990.

[23] Netanel H Lindner and Terry Rudolph. Proposal for pulsed on-demand sources of photonic cluster state strings. *Physical review letters*, 103(11):113602, 2009.

[24] Chandra M Natarajan, Michael G Tanner, and Robert H Hadfield. Superconducting nanowire single-photon detectors: physics and applications. *Superconductor science and technology*, 25(6):063001, 2012.

[25] Detectors, photon spot: http://www.photonspot.com/detectors.

[26] Optics of spectroscopy tutorial: http://www.horiba.com/us/en/scientific/products/optics-tutorial/.

[27] M. D. Raisinghania. *Advanced differential equations.* S Chand, 2012.

[28] Alisa Javadi, Dapeng Ding, Martin Hayhurst Appel, Sahand Mahmoodian, Matthias Christian Löbl, Immo Söllner, Rüdiger Schott, Camille Papon, Tommaso Pregnolato, Søren Stobbe, et al. Spin–photon interface and spin-controlled photon switching in a nanobeam waveguide. *Nature nanotechnology*, 13(5):398, 2018.

[29] John J Bollinger, Wayne M Itano, David J Wineland, and DJ Heinzen. Optimal frequency measurements with maximally correlated states. *Physical Review A*, 54(6):R4649, 1996.

[30] Cass A Sackett, David Kielpinski, Brian E King, Christopher Langer, Volker Meyer, Christopher J Myatt, M Rowe, QA Turchette, Wayne M Itano, David J Wineland, et al. Experimental entanglement of four particles. *Nature*, 404(6775):256, 2000.

[31] Bing Yu, Gary Pickrell, and Anbo Wang. Thermally tunable extrinsic fabry-perot filter. *IEEE Photonics Technology Letters*, 16(10):2296–2298, 2004.

[32] Richard J Warburton. Single spins in self-assembled quantum dots. *Nature materials*, 12(6):483, 2013.

[33] Liang Zhai Alisa Javadi Sahand Mahmoodian Peter Lodahl Anders S. Sørensen Sumanta Das, Mantas Cepulskovski. Wave-function ansatz method for the study of photon-photon interaction in a one dimensional waveguide coupled to two level emitters. 2018.

[34] Mantas Cepulkovskis. Nonlinear photon interactions in waveguides.

[35] Peter Lodahl, Sahand Mahmoodian, and Søren Stobbe. Interfacing single photons and single quantum dots with photonic nanostructures. *Reviews of Modern Physics*, 87(2):347, 2015.

[36] RJ Coles, DM Price, JE Dixon, B Royall, E Clarke, P Kok, MS Skolnick, AM Fox, and MN Makhonin. Chirality of nanophotonic waveguide with embedded quantum emitter for unidirectional spin transfer. *Nature communications*, 7:11183, 2016.